REPORT DOCUMENTATION PAGE

Form Approved
OMB No. 0704-0188

1. AGENCY USE ONLY *(Leave blank)*	2. REPORT DATE	3. REPORT TYPE AND DATES COVERED
	1996	

4. TITLE AND SUBTITLE
An Observational And Modeling Study of Two Gulf of California Surge

5. FUNDING NUMBERS

6. AUTHOR(S)
David Scott Andrus

7. PERFORMING ORGANIZATION NAME(S) AND ADDRESS(ES)
AFIT Student Attending:
University of Oklahoma

8. PERFORMING ORGANIZATION REPORT NUMBER
96-038

9. SPONSORING / MONITORING AGENCY NAME(S) AND ADDRESS(ES)
DEPARTMENT OF THE AIR FORCE
AFIT/CI
2950 P STEET, BLDG 125
WRIGHT-PATTERSON AFB OH 45433-7765

10. SPONSORING / MONITORING AGENCY REPORT NUMBER

11. SUPPLEMENTARY NOTES

12a. DISTRIBUTION / AVAILABILITY STATEMENT
Approved for Public Release IAW 190-1
Distribution Unlimited
BRIAN D. GAUTHIER, MSgt, USAF
Chief Administration

12b. DISTRIBUTION CODE

13. ABSTRACT *(Maximum 200 words)*

14. SUBJECT TERMS	15. NUMBER OF PAGES
	139
	16. PRICE CODE

17. SECURITY CLASSIFICATION OF REPORT	18. SECURITY CLASSIFICATION OF THIS PAGE	19. SECURITY CLASSIFICATION OF ABSTRACT	20. LIMITATION OF ABSTRACT

GENERAL INSTRUCTIONS FOR COMPLETING SF 298

The Report Documentation Page (RDP) is used in announcing and cataloging reports. It is important that this information be consistent with the rest of the report, particularly the cover and title page. Instructions for filling in each block of the form follow. It is important to ***stay within the lines*** to meet ***optical scanning requirements***.

Block 1. Agency Use Only *(Leave blank)*.

Block 2. Report Date. Full publication date including day, month, and year, if available (e.g. 1 Jan 88). Must cite at least the year.

Block 3. Type of Report and Dates Covered. State whether report is interim, final, etc. If applicable, enter inclusive report dates (e.g. 10 Jun 87 - 30 Jun 88).

Block 4. Title and Subtitle. A title is taken from the part of the report that provides the most meaningful and complete information. When a report is prepared in more than one volume, repeat the primary title, add volume number, and include subtitle for the specific volume. On classified documents enter the title classification in parentheses.

Block 5. Funding Numbers. To include contract and grant numbers; may include program element number(s), project number(s), task number(s), and work unit number(s). Use the following labels:

C	- Contract	**PR**	- Project
G	- Grant	**TA**	- Task
PE	- Program Element	**WU**	- Work Unit Accession No.

Block 6. Author(s). Name(s) of person(s) responsible for writing the report, performing the research, or credited with the content of the report. If editor or compiler, this should follow the name(s).

Block 7. Performing Organization Name(s) and Address(es). Self-explanatory.

Block 8. Performing Organization Report Number. Enter the unique alphanumeric report number(s) assigned by the organization performing the report.

Block 9. Sponsoring/Monitoring Agency Name(s) and Address(es). Self-explanatory.

Block 10. Sponsoring/Monitoring Agency Report Number. *(If known)*

Block 11. Supplementary Notes. Enter information not included elsewhere such as: Prepared in cooperation with...; Trans. of...; To be published in.... When a report is revised, include a statement whether the new report supersedes or supplements the older report.

Block 12a. Distribution/Availability Statement. Denotes public availability or limitations. Cite any availability to the public. Enter additional limitations or special markings in all capitals (e.g. NOFORN, REL, ITAR).

- **DOD** - See DoDD 5230.24, "Distribution Statements on Technical Documents."
- **DOE** - See authorities.
- **NASA** - See Handbook NHB 2200.2.
- **NTIS** - Leave blank.

Block 12b. Distribution Code.

- **DOD** - Leave blank.
- **DOE** - Enter DOE distribution categories from the Standard Distribution for Unclassified Scientific and Technical Reports.
- **NASA** - Leave blank.
- **NTIS** - Leave blank.

Block 13. Abstract. Include a brief *(Maximum 200 words)* factual summary of the most significant information contained in the report.

Block 14. Subject Terms. Keywords or phrases identifying major subjects in the report.

Block 15. Number of Pages. Enter the total number of pages.

Block 16. Price Code. Enter appropriate price code *(NTIS only)*.

Blocks 17. - 19. Security Classifications. Self-explanatory. Enter U.S. Security Classification in accordance with U.S. Security Regulations (i.e., UNCLASSIFIED). If form contains classified information, stamp classification on the top and bottom of the page.

Block 20. Limitation of Abstract. This block must be completed to assign a limitation to the abstract. Enter either UL (unlimited) or SAR (same as report). An entry in this block is necessary if the abstract is to be limited. If blank, the abstract is assumed to be unlimited.

★U.S.GPO:1990-0-273-271

UNIVERSITY OF OKLAHOMA

GRADUATE COLLEGE

AN OBSERVATIONAL AND MODELING STUDY OF TWO GULF OF CALIFORNIA SURGE EVENTS

A THESIS

SUBMITTED TO THE GRADUATE FACULTY

in partial fulfillment of the requirements for the

degree of

MASTER OF SCIENCE IN METEOROLOGY

By

DAVID SCOTT ANDRUS

Norman, Oklahoma

1996

AN OBSERVATIONAL AND MODELING STUDY OF TWO GULF OF CALIFORNIA SURGE EVENTS

A THESIS APPROVED FOR THE
SCHOOL OF METEOROLOGY

BY

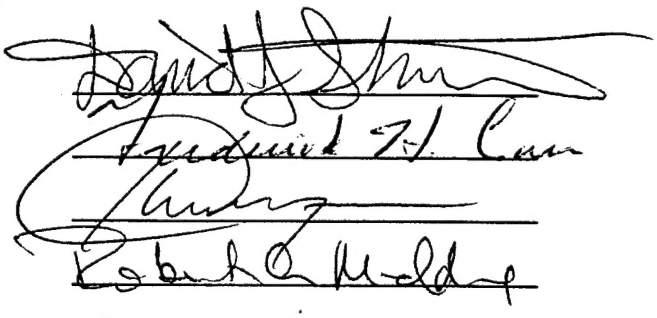

Acknowledgments:

Many people contributed to this project, and I offer my sincere thanks for all of their assistance. Special thanks go to my advisor Dr. Dave Stensrud from the National Severe Storms Laboratory (NSSL) who provided continuous support and information regarding models and gulf surge events. I also thank my committee members, Dr. Bob Maddox, Director of NSSL, Dr. Kelvin Droegemeier, Director of the Center for the Analysis and Prediction of Storms (CAPS), and Dr. Fred Carr (CAPS) for spending the time to review my thesis and for providing support. Dr. Mike Douglas (NSSL) was instrumental in obtaining data from EMVER-93 and Ken Howard provided data from SWAMP-93, plus I thank Dr. Bob Maddox for developing and supporting both of these programs. I would also like to thank Mr. Gayno and Dr. Kain who provided me with information about their modeling schemes necessary for their incorporation into MM5. Further assistance from Danny Mitchell, Tom Condo, J.J. Gourley, and Karen Winston regarding computer support and in the retrieval of satellite imagery was of great help. Additionally, I would like to thank the U.S. Air Force for allowing me to participate in this program and my program manager Major Tom Neu who did an outstanding job of keeping me current on Air Force requirements and policies.

Most importantly I thank my wife, Kathleen, and daughters Elizabeth and Heidi Rose who provided me with emotional support despite the pressures I put on them. I could not have done it without them. Finally I wish to acknowledge the one who made this all possible. I give all praise and honor to my Lord and Savior, Jesus Christ, for leading me here and helping me everyday of my life.

Table of Contents

List of Figures

Figure 27a) MM5 nested grid sigma level 0.978 potential temperature contours (K) and winds at 0300 UTC 8 July. Full barb is 5 ms-1. Dashed line indicates position of leading edge of gulf surge.

Figure 27b) Same as figure 27a, except at 0600 UTC 8 July.

Figure 27c) Same as figure 27a, except at 0900 UTC 8 July. Additionally, thick lines indicate locations of cross-sections A-A' (figure 33), and B-B' (figure 34), and the location of a model sounding, C (figure 35).

Figure 27d) Same as figure 27a, except at 1200 UTC 8 July.

Figure 28a) MM5 coarse grid surface pressure reduced to sea-level (mb) and 980 mb winds at 0300 UTC 8 July. Full barb is 5 ms-1. Dashed line indicates position of leading edge of gulf surge.

Figure 28b) Same as figure 28a, except at 0600 UTC 8 July.

Figure 28c) Same as figure 28a, except at 0900 UTC 8 July. Thick lines indicate locations of model cross-sections, A-A' (figure 36), and B-B' (figure 37), and the location of a model sounding, C (figure 38).

Figure 28d) Same as figure 28a, except at 1200 UTC 8 July.

Figure 31b) Same as figure 31a, excpet at 0600 UTC 12 August.

Figure 31c) Same as figure 31a, except at 0900 UTC 12 August. Thick lines indicate locations of model cross-sections, A-A' (figure 39), and B-B' (figure 40), and the location of a model sounding, C (figure 41).

Figure 31d) Same as figure 31a, except at 1200 UTC 12 August.

Figure 32) Isochrone analysis of leading edge of model surge on 12 August.

Figure 33) 0900 UTC 8 July MM5 nested grid cross-section along the central Gulf of California (location of cross-section shown as A-A' on figure 27c). Vertical coordinate is pressure (mb). Solid contours are wind speeds parallel to the coast (ms-1) with positive values from left to right (northwesterly). Dashed contours are mixing ratios (g kg-1).

Figure 34) 0900 UTC 8 July MM5 nested grid cross-section perpendicular to the central Gulf of California (location of cross-section shown as B-B' on figure 27c). Vertical coordinate is pressure (mb). Solid contours are wind speeds parallel to the coast (ms-1) with positive values into the figure (southeasterly). Dashed contours are mixing ratios (g kg-1).

Figure 35) 0900 UTC 8 July MM5 nested grid sounding northwest of the southern mesoscale model surge (location of sounding shown as C on figure 27c). Full barb is 5 ms-1.

Figure 36) 0900 UTC 8 July MM5 coarse grid cross-section along the northern and central Gulf of California (location of cross-section shown as A-A' on figure 28c). Vertical coordinate is pressure (mb). Solid contours are wind speeds parallel to the coast (ms-1) with positive values from left to right (northwesterly). Dashed contours are mixing ratios (g kg-1).

Figure 37) 0900 UTC 8 July MM5 coarse grid cross-section perpendicular to the northern Gulf of California (location of cross-section shown as B-B' on figure 28c). Vertical coordinate is pressure (mb). Solid contours are wind speeds parallel to the coast (ms-1) with positive values into the figure (southeasterly). Dashed contours are mixing ratios (g kg-1).

Figure 38) 0900 UTC 8 July MM5 coarse grid sounding northwest of the northern mesoscale model surge (location of sounding shown as C on figure 28c). Full barb is 5 ms-1.

Figure 39) 0900 UTC 12 August MM5 cross-section along the northern and central Gulf of California (location of cross-section shown on figure 31c). Vertical coordinate is pressure (mb). Solid contours are wind speeds parallel to the coast (ms-1) with positive values from left to right (northwesterly). Dashed contours are mixing ratios (g kg-1).

Figure 40) 0900 UTC 12 August MM5 cross-section perpendicular to the northern Gulf of California (location of cross-section shown on figure 31c). Solid contours are wind

Abstract

An observational and numerical study of two Gulf of California surges is undertaken to determine the mechanisms of surge development and evolution. While in each case the observations indicate that a boundary propagates northward over the Gulf of California, the sparcity of observations precludes the determination of a propagation mechanism. In contrast, the high resolution mesoscale model simulations provide a dynamically-consistent data set that can be used to evaluate gulf surge mechanisms. In each case the mesoscale model develops surges that move to the north-northwest along the Gulf of California consistent with the conceptual model proposed by Stensrud et al. (1996) although not predicted by the conceptual model. The stable air in the gulf region serves to allow the development and propagation of Kelvin waves northwestward along the Gulf of California and into Arizona in the mesoscale model. Results also show that the mesoscale model is overly sensitive to convection within the gulf region and produces earlier and greater precipitation than suggested in observations, indicating a possible deficiency in either the convective parameterization scheme, model initialization, or both. Nonetheless, the success of the model in reproducing the gross features of these two surge events is a significant improvement over present operational models.

CHAPTER 1

Introduction

The Mexican monsoon is a significant meteorological phenomenon that is responsible for the majority of precipitation over Mexico and the southwestern United States during the summer months (Douglas et al. 1993). The monsoon season is characterized by a shift in the synoptic weather pattern over southwestern North America as the United States becomes dominated by mid-level high pressure. This subtropical ridge, typically centered over the eastern New Mexico and north Texas, causes a predominant southerly flow over the southwestern United States that is markedly different from the westerlies observed throughout the rest of the year. Over Mexico, the midtropospheric winds shift from westerly to easterly as the subtropical convergence zone moves northward. In 1993, Douglas et al. analyzed 1200 UTC rawinsonde data from 1979 through 1989 to show that a distinct shift in mean monthly mid-tropospheric winds occurs over northern Mexico and the southwestern United States between June and July (figures 1 and 2). This seasonal wind reversal has been termed the Mexican monsoon (Douglas et al. 1993).

Accompanying this seasonal wind change over southwestern North America is a distinct change in the amount and distribution of precipitation in the southwestern United States and Mexico. The annual precipitation in Arizona and northwestern Mexico is influenced greatly by the monsoon, which typically occurs during July through September. Precipitation during the monsoon contributes more than 40% of the annual precipitation throughout Arizona (Jurwitz 1953) and more than 50% in Tucson, Arizona (Adang and Gall 1989). The monsoon precipitation pattern in

northwestern Mexico is even more dramatic with 60% to 80% of the annual rainfall occurring from July through September (figure 3) with mean monthly amounts measured in excess of 30 cm (Douglas et al. 1993). In some locations along the western slopes of the Sierra Madre Occidental, the total rainfall during the monsoon months of July through September is in excess of 65 cm. This indicates that Arizona is just the northern extent of a much larger phenomenon that is more pronounced over northwestern Mexico.

The large amount of regional-scale convection over the typically dry deserts of the southwestern United States, particularly southwest Arizona, during the monsoon season causes many hazards to life and property (Brenner 1974; Dunn and Horel 1994a; McCollum et al. 1995). The most common of these are flash floods resulting from locally heavy rains on the hard desert floor, dust storms, frequent lightning, and dry microbursts. Additionally, large hail and weak tornadoes occasionally are observed. All of these phenomena pose a serious threat to persons on the ground and for civilian and military aircraft that routinely fly over the desert southwest. Because of this, an increased understanding of the processes that lead to convection during the monsoon is of importance. Since low-level moisture often is the one ingredient lacking for convective development in the desert southwest (McCollum 1995 et al.), the sources of moisture and processes that transport moisture are of great practical interest.

Although Hales (1972) first suggested the Gulf of California as the important source of low-level moisture for Arizona, it is not until recently that more quantitative studies have examined the role of the Gulf of California. Previous studies by Jurwitz (1953), Bryson and Lowry (1955), and Sellers and Hill (1974) have argued that the

change in the midtropospheric winds associated with the monsoon serve to advect moisture from the Gulf of Mexico and the Caribbean into the southwestern United States. Despite the early arguments of Jurwitz (1953) and Bryson and Lowry (1955), Reitan (1957) began to question the veracity of whether the amount of low-level moisture observed in the Arizona deserts could be attributed to the Gulf of Mexico. More recent studies (Hales 1972; Hales 1974; Brenner 1974; Carleton 1986; Douglas et al. 1993; Stensrud et al. 1995) have led to the further investigation of the role of the Gulf of California as a moisture source during the monsoon. This shallow body of warm water bounded to the west by the mountainous Baja California peninsula and to the east by the higher mountains of the Sierra Madre Occidental is a regional source of low-level moisture that can be orographically lifted to cause precipitation. Furthermore, the monsoonal precipitation pattern shown by Douglas et al. (1993) (figure 3) indicates that the majority of the precipitation is along the eastern Gulf of California and western slopes of the Sierra Madre Occidental. These studies clearly show that the most significant moisture source for the Mexican monsoon is the Gulf of California.

While the monsoon season is associated with a seasonal change in the general precipitation pattern over southwestern North America, the actual precipitation varies greatly from day to day. Over Arizona there are typically periods of several days or weeks during which there is little or no precipitation, termed monsoon "breaks", which can rapidly be followed by an extensive period of strong thunderstorms and heavy rains, termed monsoon "bursts" (Carleton 1986; Adang and Gall 1989). This change can be rapid and often is difficult to forecast due to the current state of operational numerical models and the sparse observations over the region (Dunn and Horel 1994a).

Monsoon "breaks" often occur in response to relatively strong upper and mid-level troughs which move over the southwestern United States and serve to change the flow to northwesterly or westerly and cause drying throughout Arizona. During and following the trough passage the moisture within the region of the Gulf of California is effectively shut off from reaching Arizona and monsoon convection is limited to the western slopes of the Sierra Madre Occidental. Once the trough has sufficiently passed the region, the more climatological southerly flow of the monsoon season can redevelop and moisture from the gulf region can return to Arizona and serves to reinitiate convection. One mechanism for producing a return this southerly flow is a gulf surge which is a low-level northward or northwestward surge of moist tropical air along the Gulf of California that is preceded by extensive low-level northerly or northwesterly flow throughout the gulf.

Gulf surges are events in which the predominant surface and low-level flow over the Gulf of California abruptly changes from northwesterly to southeasterly, causing the advection of low-level moisture up the gulf and often into southern Arizona. These events typically are associated with slightly cooler surface and low-level temperatures behind the surge (Hales 1972; Brenner 1974). Since a lack of moisture often is the only inhibitor to desert convection, the advection of moisture by a gulf surge provides a crucial ingredient in the development of strong convection (McCollum et al. 1995). Although gulf surges occur every monsoon season, their frequency varies greatly each year (Brenner 1974). Hales (1972) and Brenner (1974) have studied many gulf surges using conventional upper-air and surface data and have described some common characteristics of surge events:

1) Surface conditions following the surge indicate a drop in temperature, a rise in dewpoint temperature, a windshift with an increased southerly wind component, lower visibility, a rise in sea level pressure, and increasing low-level cloudiness.

2) The low-level cooling and moistening produced by a surge are at a maximum just above the surface and decrease in intensity with height.

3) The amount of low-level cooling and sharpness of the temperature change behind the surge decrease as the surge spreads out across the low desert after moving into Arizona.

4) Thunderstorm activity in Arizona often increases markedly when strong surges occur.

Hales (1972) also observed that strong surges occur in association with large areas of cloud cover in the southern Gulf of California and warmer Mojave Desert surface temperatures. The relationship between gulf surges and deep convection over the southern gulf was further explored by Stensrud et al. (1996).

In an effort to determine the ability of operational numerical models to forecast monsoon precipitation, Dunn and Horel (1994a,b) examined the ability of the ETA model to forecast precipitation in Arizona during the monsoon. For the cases studied, the ETA model was unable to forecast the typical afternoon convection over the Mogollon Rim of northern Arizona. As discussed by Dunn and Horel, monsoon convection in the Phoenix area is often preceded by convection over the mountains of the Mogollon Rim

which extend throughout northern through eastern Arizona with an elevation of 4000 to 6000 ft. In fact, the terrain within the 81 km ETA model does not even include the Mogollon Rim and therefore neglects a significant regional feature which affects precipitation throughout most of Arizona. Additionally, the model failed to produce any significant precipitation in central Arizona despite observations of heavy rain and flooding during several cases. Dunn and Horel even note that the one case in which the ETA model produced precipitation in central Arizona, no rainfall was reported. This lack of useful guidance from operational numerical models makes providing meteorological forecasts for the local community and aircraft operations extremely difficult.

Stensrud et al. (1995) investigated whether or not a suitably constructed and initialized mesoscale model could reproduce the general characteristics of the Mexican monsoon. By using data from the Southwest Area Monsoon Project (SWAMP) of 1990 (SWAMP-90), they were able to verify many of the mesoscale features found in the model simulations over the 32 days investigated. Stensrud et al. also noted sources of error in the current National Center for Environmental Prediction (NCEP) models and identified the advection of low-level moisture from the Gulf of California as a primary factor in the initiation of deep convection over Arizona and northwestern Mexico. The first source of error noted by Stensrud et al. (1995) is in the NCEP global data in which the low-level winds east of Baja California are more than 90 degrees out of phase with observations. Secondly, they noted that the horizontal resolution of NCEP models was unable to resolve for the dramatic warming of the sea surface temperatures of the Gulf of California during the summer.

While in it may be difficult to incorporate changes in current operational models to account for these errors, understanding the role of the Gulf of California in advecting moisture into Arizona is even more challenging. Although precipitation along the western slopes of the Sierra Madre Occidental is a routine afternoon occurrence, the initiation of deep convection in central Arizona is intermittent. To determine the large-scale features associated with the development of gulf surges, one possible source of moisture transport into Arizona, Stensrud et al. (1996) examined 32 days of mesoscale model output and extracted a conceptual model for strong surge events. This included:

1) Prior to the surge, a mid-latitude disturbance passes through western North America, producing a shift in the low-level winds from southerly to northerly in the southwestern United States and northwestern Mexico. Enhanced subsidence occurs over the Gulf of California as this disturbance passes to the east, producing an anomalously strong low-level stable layer over the gulf. This stable layer provides the background thermodynamic environment necessary for the development of a strong surge.

2) A day or two later an easterly wave moves across Central America, and the convergence and upward motion associated with the passage of the wave trough south of the Gulf of California often initiates convection either south of the gulf or in the southern or central gulf.

3) Low-level, cold outflows caused by deep convection over the gulf region perturb the low-level stable layer, and this intrusion develops into a Kelvin wave as it

moves northward along the Gulf of California. The leading portion of the Kelvin wave is located along the shore, just to the east of the Gulf of California.

4) The Kelvin wave moves northward and steepens into a gravity-current like phenomena, possibly owing to the destruction of the low-level inversion upon which the Kelvin wave propagates during the late afternoon. After sunset this low-level inversion is reestablished and a new Kelvin wave may once again be initiated along the northern edge of the gravity current, or the gravity current may just propagate northward into Arizona cohesively.

5) As the surge moves into Arizona, the terrain bends sharply east, causing the disturbance to separate from the terrain and lose its identity.

This conceptual model describes one mechanism for the development of a gulf surge and its propagation into Arizona. Once the surge reaches central Arizona, the increased moisture is the primary ingredient needed for convection over the elevated terrain. Thunderstorms then typically occur over the low desert in association with outflows that move into the low desert from outside regions such as the Mogollon Rim.

Results from Stensrud et al. (1996) indicate that in order for a numerical model to accurately simulate convection over the southwestern United States during the Mexican monsoon season, it must be able to properly develop convection over the Gulf of California and western Mexico. Correspondingly, current NCEP operational models that are not accurately initialized as shown by Stensrud et al. (1995) are unable to predict the convection associated with the monsoon in Arizona (Dunn and Horel 1994a,b).

In an effort to extend the observational database collected during SWAMP-90, another field program was conducted in 1993 (SWAMP-93). The Mexican component for the 1993 study was called the Experimento Meteorologico del Verano (EMVER-93). These two programs provided the necessary observations for further study of gulf surges. In particular, data from EMVER-93 indicate two possible cases of gulf surges. The first case is 8 July 1993 when observations suggest a strong boundary rapidly moves up the Gulf of California. The second case occurred on 13 August 1993 when a more gradual surge is indicated in the observations. Both of the events suggest that a surge moves up the entire length of the Gulf of California, a much longer distance than seen in the SWAMP-90 data examined by Stensrud et al. (1996). These cases provide an excellent opportunity to examine the ability of a numerical model to discern between the two different events, to independently test the conceptual model of surge development by Stensrud et al. (1996), and to evaluate the mechanisms of surge development and evolution.

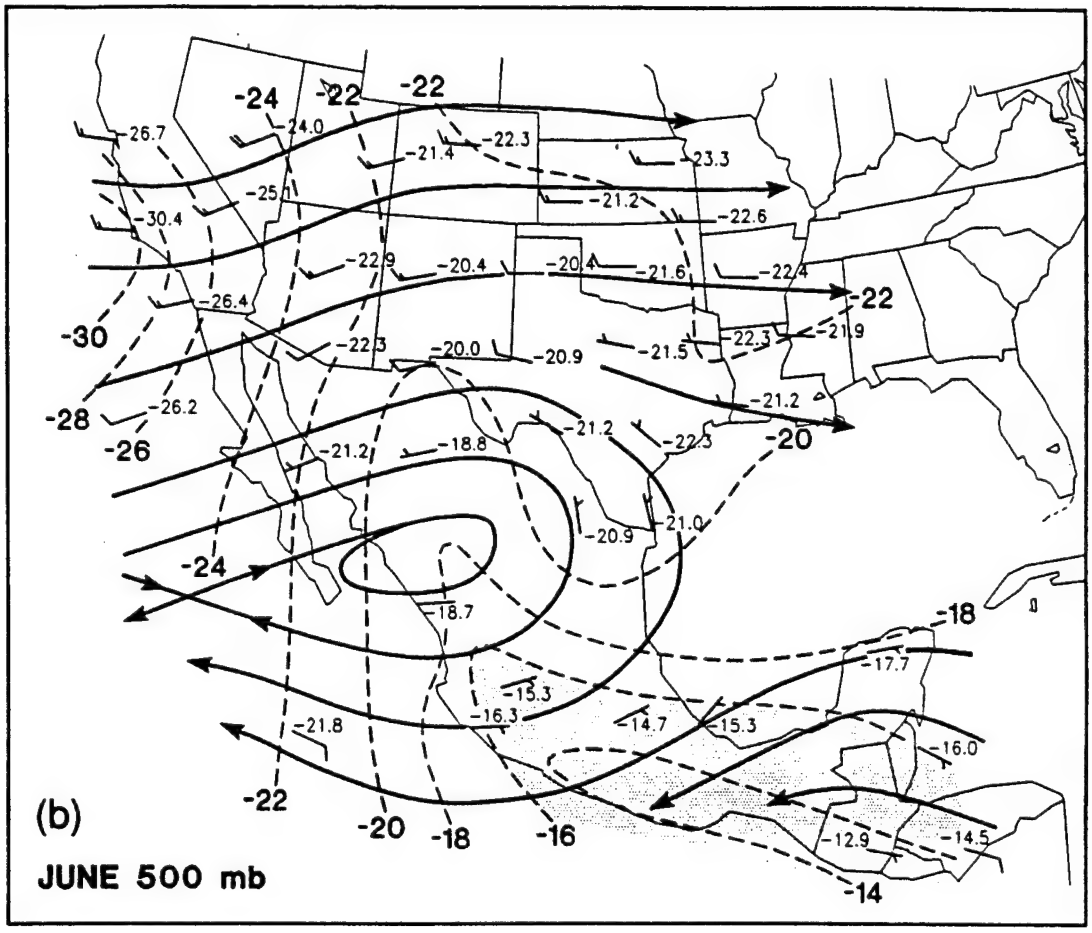

Figure 1) Mean winds, streamlines, and dewpoint (°C) analysis at 500 mb for June. Means are for 1200 UTC data for the 11-year interval 1979-1989. From Douglas et al. 1993, courtesy of M. Douglas, National Severe Storms Laboratory.

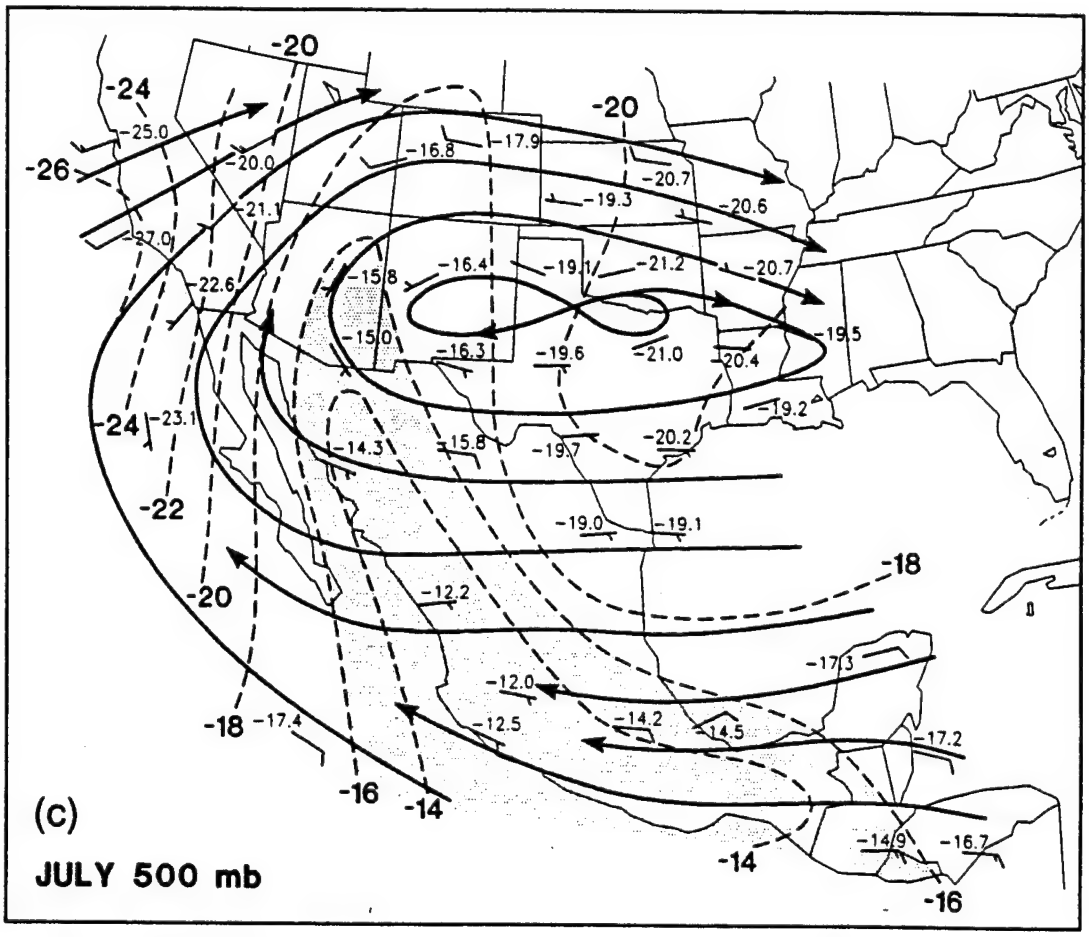

Figure 2) Mean winds, streamlines, and dewpoint (°C) analysis at 500 mb for July. Means are for 1200 UTC data for the 11-year interval 1979-1989. From Douglas et al. 1993, courtesy of M. Douglas, National Severe Storms Laboratory.

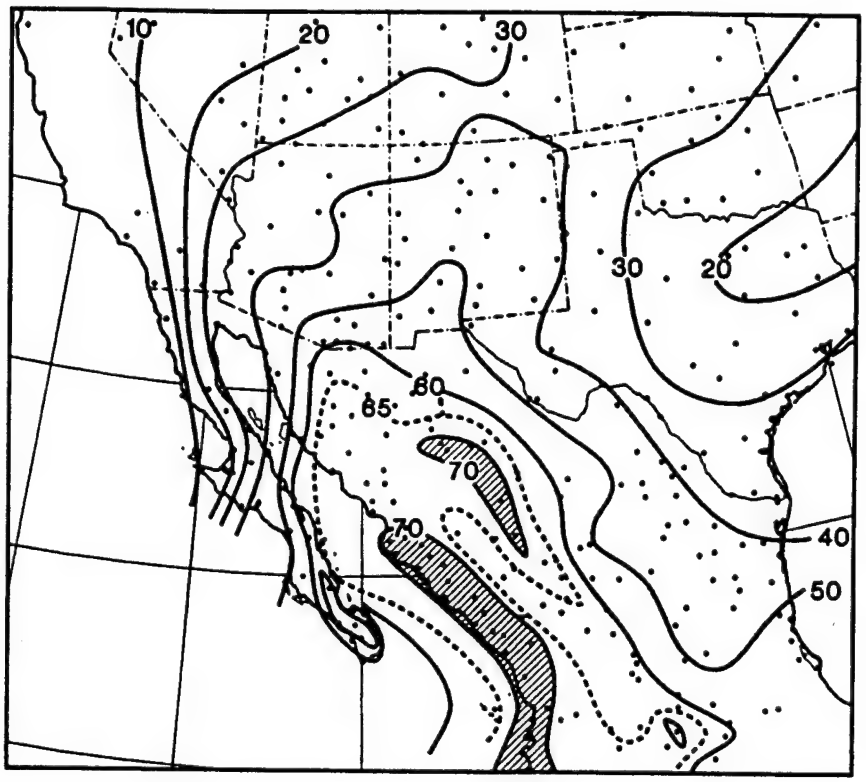

Figure 3) Analysis of the contribution of the precipitation during July, August, and September to the annual total, expressed in percent. Greater than 70% is crosshatched. Stations used in the analysis are shown as dots. From Douglas et al. 1993, courtesy of M. Douglas, National Severe Storms Laboratory.

CHAPTER 2

Observations

All observations from the SWAMP-93, the EMVER-93, the NCEP upper-air and surface analysis databases, and satellite imagery are used to evaluate the two suggested surge events. A significant portion of Mexico is not depicted on either the upper-air charts or the surface analyses available from NCEP, making the special observations particularly valuable. The SWAMP-93 and EMVER-93 data sets include additional rawinsondes, pibal data, and surface observations from select locations along the northwest coast of Mexico (figure 4). When combined, these data describe the basic regime and provide a depiction of surge evolution. Unfortunately, while these observations can be used to describe the general evolution of the surges, the data density in both time and space is not sufficient for a thorough evaluation of the mechanisms of surge development and evolution.

2.1 8 July 1993

At 1200 UTC 7 July a long-wave mid and upper-level trough is present over the western United States. A jet streak with wind speeds in excess of 50 ms-1 stretches from Washington state to western Nebraska (figure 5a). Over Arizona, the 300 mb winds are west-northwest at speeds of 8-15 ms-1. At 850 mb, two weak low centers are present in southern Nevada, and northern New Mexico (figure 6a). Associated with these lows, winds at Tucson are northwesterly, a flow pattern that typical means clear skies for Arizona. Indeed, limited moisture is evident at Tucson with a 850 mb dewpoint of 9 °C, and a surface dewpoint of 10 °C. The nearest area

of convection is in the central gulf where residual clouds are evident. These appear to be the remnants of extensive evening convection over the Sierra Madre Occidental that were advected to the west (figure 7a). A large, organized area of deep convection is seen well to the south of the Gulf of California, associated with an intensifying tropical storm. Rawinsonde, pibal and surface observations in the gulf indicate weak and variable winds are prevalent throughout the entire gulf (figure 8a) in opposition to the more climatological southeasterly flow (Douglas 1995).

By 1800 UTC 7 July the most significant feature on the surface analysis and satellite imagery is Hurricane Calvin depicted at 19.3N, 104.9W on the NCEP surface chart (not shown). Along the central and northern gulf coast typical onshore and upslope flow is evident in the surface data and there is no indication of surge activity at this time (not shown). The hurricane, positioned more than 250 km southeast of the Gulf of California, proceeds slowly north-northwest along the coast during the following six hours before it weakens.

The upper-level trough continues over the western United States and the jet streak with winds in excess of 50 ms-1 extends from Oregon to Nebraska on 0000 UTC 8 July (not shown). Over Arizona the 300 mb winds are still from the northwest at speeds of 8-18 ms-1 (not shown). The 850 mb wind speed at Tucson increases to 8 ms-1 from the northwest at this time and the dewpoint remains constant at 9 °C, suggesting a continuation of the monsoon break (not shown). Much farther to the south, the hurricane moves north-northwest to 20.3N and 105.6W at 0000 UTC, slightly west of Puerto Vallarta, Mexico (not shown). In addition to the convection due to the hurricane, satellite imagery shows widespread afternoon convection developing along the western slope of the Sierra Madre Occidental (figure 7b). Pibal data from

Puerto Peñasco in the northern gulf indicate southerly flow, but to the southeast at Puerto Libertad the pibal winds are from the southwest (figure 8b). The Guaymas rawinsonde in the central gulf also has weak low-level winds from the southeast, but the temperature and moisture profiles are not indicative of a surge. Furthermore, surface winds from nearby stations indicate a variable wind flow contrary to that seen during most surges. The only hint of a surge at this time is in the pibal data from Culiacan, in the southeast gulf, with a southeast wind speed of nearly 4 ms-1. Unfortunately only wind data are available at this site, and there is no knowledge of whether or not any cooling or moistening occurred as would be expected during a surge. Other surge characteristics such as sustained southeasterly flow over several hours also cannot be ascertained at Culiacan due to the infrequency of the observations. Surface observations throughout the Gulf of California at 0000 UTC 8 July indicate variable winds associated with the widespread convection evident from satellite imagery.

Satellite imagery continues to show an expanding area of deep convection along the gulf until 0300 UTC 8 July (not shown). Although the available data are not sufficiently refined to confirm the association between this expanding convection and surge development, the first indication of a surge is seen in the surface data at this time from stations located close to the region of convection. Surface observations show an organizing surge at 0200 UTC in the central gulf (figure 9). The surface winds at El Carrizo turn southeasterly at a speed of 1.3 ms-1 at 0200 UTC. Over the following 2 hours, the winds at El Carrizo remain southeasterly and increase to a speed of 7.9 ms-1 while the temperature cools 0.7 K and the relative humidity increases. This is the first indication of the surge in the observations.

A lack of consistent surface observations make tracking the movement of the surge along the coast difficult. While observations from El Carrizo indicate strong southeast winds until 1200 UTC, with a peak wind speed at 1100 UTC of 9.2 ms-1, the next station that indicates the surge is Empalme, located over 220 km to the northwest. Observations from Empalme are not recorded between 0300 UTC and 0600 UTC so the time of the passage of the leading edge of the surge over Empalme is not known, but at 0630 UTC the surface winds are southeasterly at 4.8 ms-1 and they remain southeasterly for at least 3 hours (figure 9). Although temperature data are not available from Empalme during this time period, the increase in humidity and the persistent southeast winds strongly suggest the passage of a surge.

The surface observations at 0630 UTC indicate the surge has also passed Puerto Libertad, in the northern gulf, with southeast winds at 6.5 ms-1 (figure 9) and surface temperatures subsequently cooling 1.1 K before slowly rising again at 0900 UTC. For the next 6 hours these winds remain southeasterly at speeds increasing to 14.4 ms-1. At La Sangre, to the east of Puerto Libertad, observational evidence suggests the surge passes at 0800 UTC (figure 9), when the winds turn southeasterly and remain so at speeds of up to 7.9 ms-1. Although the surface temperature does not decrease at La Sangre in association with the wind shift, downslope flow from mountains to the southeast may mask the cooling typically associated with the passage of a surge at this location.

Satellite imagery indicates a lingering area of residual cloudiness north and east of Empalme by 0900 UTC 8 July (not shown). Farther south, the NCEP surface charts show a weak low pressure center and light precipitation along the Mexican

coastline that appear to be all that remains of Hurricane Calvin (not shown). Although the convection has diminished, the surge continues to move up the gulf. The surface data from Sonoyta, on the Arizona border, indicate the surge may be moving into Arizona at 0900 UTC. Whereas the winds shift to southeasterly at speeds of 4 ms-1 to 8 ms-1 (figure 9), the surface temperature rises, leaving some doubt as to whether the surge actually passes Sonoyta.

By 1200 UTC 8 July the 850 mb winds over Tucson switch to southwesterly at a speed of 10 ms-1 (figure 6b). Additionally, the 850 mb dewpoint increases to 11°C while the temperature is 1°C cooler than 24 hours earlier suggesting the surge has passed Tucson. This observation confirms the passage of the surge over Sonoyta despite the questionable surface temperature data. Surface winds at Tucson are southeasterly as is typical owing to the terrain, and the surface dewpoint has increased to 60°C by 1500 UTC. Pibal data from 1200 UTC 8 July confirms the presence of strong southeasterly low-level winds all along the gulf with the strongest 950 mb winds at a speed of 15 ms-1 at the northernmost pibal location of Puerto Peñasco (figure 8c). The only gulf rawinsonde available is from Guaymas with a southeasterly flow at a speed of 18 ms-1 at 925 mb and cooling and moistening over the lowest 50 mb further substantiating the presence of a surge. Surface data at this time indicate strong southeasterly flow throughout the northern gulf with winds of 4-8 ms-1 while more varied winds are present in the southern gulf (figure 8c). Follwing the passage of the surge, convection increases in southeast Arizona on 8 July and central Arizona on 9 July.

An isochrone analysis of the progression of the surge (figure 10) suggests that it rapidly progresses northward over the waters of the eastern Gulf of California

at an average speed of 30 ms-1 between 0200 UTC and 0900 UTC. It is unfortunate that there is insufficient meteorological data of high enough resolution to determine the exact nature of the surge. The progression of the afternoon convection as observed on satellite imagery in conjunction with the observations suggests that convection may have initiated the surge, but the data are inconclusive.

2.2 13 August 1993

An unseasonably deep trough in the middle and upper-levels approaches the western United States at 1200 UTC 11 August (figure 11a). The 300 mb flow over Arizona is from the west at a speed of 17 ms-1 over Winslow, and northwest at a speed of 10 ms-1 over Tucson (figure 11a). The 850 mb temperature and dewpoint from Tucson are 27 °C and 7 °C, respectively, and weak northerly flow is observed (figure 12a), suggestive of dry conditions. In the lower levels, however; western Arizona is under southerly flow ahead of the trough. Surface dewpoints throughout southern Arizona are quite moist, with a 17 °F dewpoint at Tucson (not shown). Satellite imagery at this time indicates no cloudiness over the Gulf of California, with the nearest convection located about 175 km to the southeast of the gulf (figure 13a). Pibals and rawinsonde data from the gulf show a quiescent pattern with typical diurnal low-level flow, in agreement with surface observations (figure 14a).

Infrared satellite imagery at 1800 UTC 11 August (not shown) indicates the development of several convective cells over the eastern Pacific, from a point west of Manzanillo to just south of Mazatlan. Surface data from NCEP is mostly void over the gulf with little information about activity associated with the convection displayed on satellite, and no special data are available.

By 0000 UTC 12 August the trough approaching the western United States has moved inland. Satellite imagery indicates the initiation of convection over the western slopes of the Sierra Madre Occidental at 2100 UTC 11 August that intensifies by 2300 UTC (figure 13b). Over Winslow the 300 mb winds are westerly at 17 ms-1, while winds over Tucson are from the northwest at 5 ms-1 (not shown). The 850 mb winds over Arizona are weak, and the Tucson 850 mb dewpoint has increased to 9 °C (not shown). Along the gulf, the pibals and the Guaymas rawinsonde are indicative of strong onshore and upslope flow typical of the afternoon (figure 14b). Numerous outflows from convection affect many of the mountain observing sites, leading to surface observations that are quite varied. No indication of a prolonged southeasterly surge is evident.

The convection over the Sierra Madre Occidental peaks at 0300 UTC 12 August, followed by a reduction of cloud cover as observed from satellite imagery (not shown). Only limited surface observations are available throughout the early morning, but again no significant southeast flow is observed (not shown).

On 1200 UTC 12 August the trough in the middle and upper-troposphere continues to be the dominant feature over the western United States. The 300 mb winds over Arizona remain westerly with a speed of 20 ms-1 now evident at Winslow (not shown). Throughout the mid-troposphere very dry stable air is present over central Arizona. The 850 mb rawinsonde from Tucson sampled a much drier air mass with a dewpoint temperature of 5 °C (not shown). The surface dewpoint at Tucson also has dried and is now 14 °C (not shown). Farther to the south a large mesoscale

convective system that propagated north along the coast of Mexico during the early morning of 12 August is approaching the southeastern Gulf of California.

Although observations from the northern gulf do not indicate a surge, pibal and tethersonde observations from the central and southern gulf indicate the presence of a surge. Pibals from the southeastern gulf, at Culiacan and Los Mochis, show 950 mb southeasterly winds 6 ms-1 (figure 14c). Tethersonde observations from Tesopaco, in the central gulf, indicate a cooling of 6 K at 900 mb between 1200 and 1700 UTC, when the boundary layer is typically undergoing warming (not shown). The surface data indicate that the winds at Empalme and Puerto Libertad also switched to southeasterly by 1200 UTC, but it is unknown whether any cooling occurred at these locations. While the rawinsonde observation from Guaymas is not available for this time, the next sounding at 0000 UTC 13 August does show 4 K of cooling at 925 mb over the prior 24 hours. Considering the available data, it is not clear that a surge has progressed up the gulf on this date. Although the Tesopaco tethersonde and Guaymas sounding indicate cooling, there is little other observational data to support the presence of a surge.

Twelve hours later, at 0000 UTC 13 August, the upper-level trough has deepened over the northwest United States and southern California. A 300 mb jet streak of 36 ms-1 is shown off the west coast of California and the winds over Winslow are from the southwest at a speed of 23 ms-1 (not shown). The 300 mb winds over Tucson are from the west at 8 ms-1 and drying continues throughout the lower levels. The 850 mb dewpoint at Tucson dropped to 1°C and winds were from the northwest at a speed of 5 ms-1 (not shown). Surface observations throughout Arizona indicate continued drying and southwesterly flow, suggesting the gulf

moisture remains cut off. Satellite imagery again indicates afternoon convection along the western Sierra Madre Occidental, but this convection does not appear as strong as on the afternoon of 11 August (figure 13d). Afternoon surface observations indicate predominately southwest flow along the gulf and there is no indication of the surge observed earlier in the day (figure 14d) that has evidently dissipated.

The surface data show evidence of a surge in the central Gulf of California at Empalme beginning at 0100 UTC 13 August. The wind shifts to the southeast and increases to 4 ms-1 as the surge passes (figure 15) while the temperature cools 2.2 K by 0300 UTC. Meanwhile, farther up the gulf at La Colorada, the wind turns southeasterly at 0200 UTC with a speed of over 3.9 ms-1, which increases to 7.9 ms-1 by 0430 UTC (figure 15). A cooling of 1.7 K also is evident despite the apparent downslope flow. The wind at La Colorada strengthens and remains from the southeast until at least 1200 UTC. Surface data from Puerto Libertad show the passage of the surge at 0830 UTC with southeasterly winds that increase to over 14 ms-1 (figure 15) and a cooling of 0.3 K. Other stations farther to the north, La Sangre and Sonoyta, also indicate a wind shift at 0600 UTC and 1000 UTC, respectively (figure 15).

At 1200 UTC 13 August Arizona remains under strong southwesterly flow ahead of the upper-level trough. Although the winds at Winslow are missing, the 300 mb winds over Grand Junction, Colorado are from the southwest at 31 ms-1 (figure 11b). The 300 mb winds over Tucson are from the west at 15 ms-1. The 850 mb winds over Tucson were southerly at 3 ms-1 ahead of the 850 mb trough which is over the Colorado river valley and the 850 mb dewpoint at Tucson is 3 °C (figure 12b).

Central Arizona is dry as seen in the soundings from Luke Air Force Base at 1200 UTC 13 August and at 1200 UTC 14 August (not shown).

Satellite imagery at this time indicates several bands of cloudiness extending up the gulf as remnants from earlier convection (figure 13e). The tethersonde observation from Puerto Peñasco indicates a cooling of 8 K between 0000 UTC 13 August and 0000 UTC 14 August, suggesting the passage of a surge sometime during this 24 hours period (not shown). Furthermore, pibals from Hermosillo and Los Mochis show low-level southeasterly winds of 6.4 ms-1 and 4.8 ms-1, respectively, which support the presence of a surge (figure 14e). Increased convection is observed in eastern and southeastern Arizona following the passage of the surge.

For this case the observational data are a little more useful in determining the type of boundary that traversed the gulf. Vertical temperature and wind data are available from several sites along the gulf in addition to surface observations. Although the data are still insufficient to isolate the nature of the surge, they do more clearly indicate the progression of cooling and moistening that are observed throughout the gulf. An isochrone analysis for the 13 August case shows the mean speed of the surge throughout its 9 hour lifespan is 14.5 ms-1 (figure 16). As in the July case, the observations are insufficient to accurately determine the nature of the surge. To determine whether or not large-scale patterns can be used to predict surges, we examine the conceptual model of Stensrud et al. (1996).

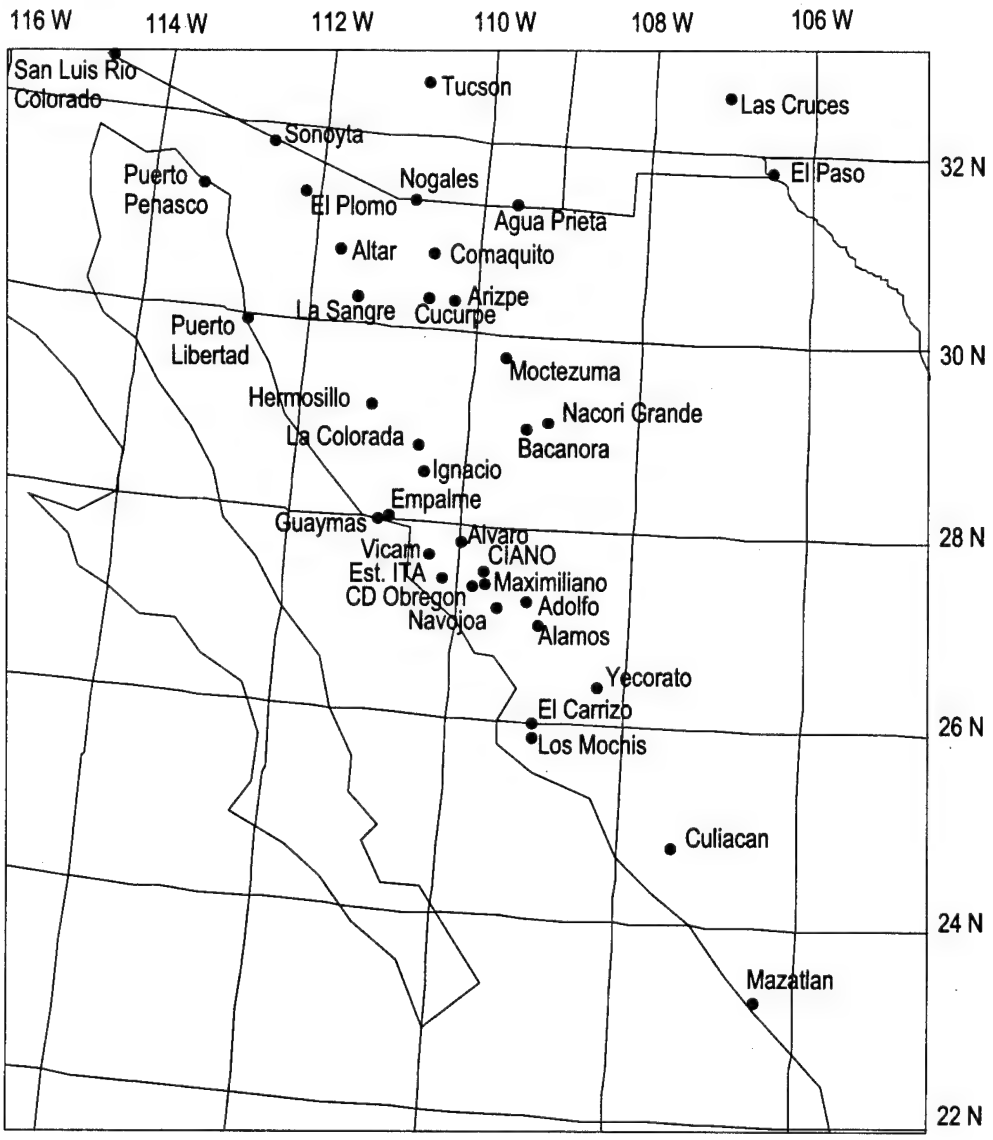

Figure 4) Diagram of selected observing sites used during EMVER-93 and SWAMP-93.

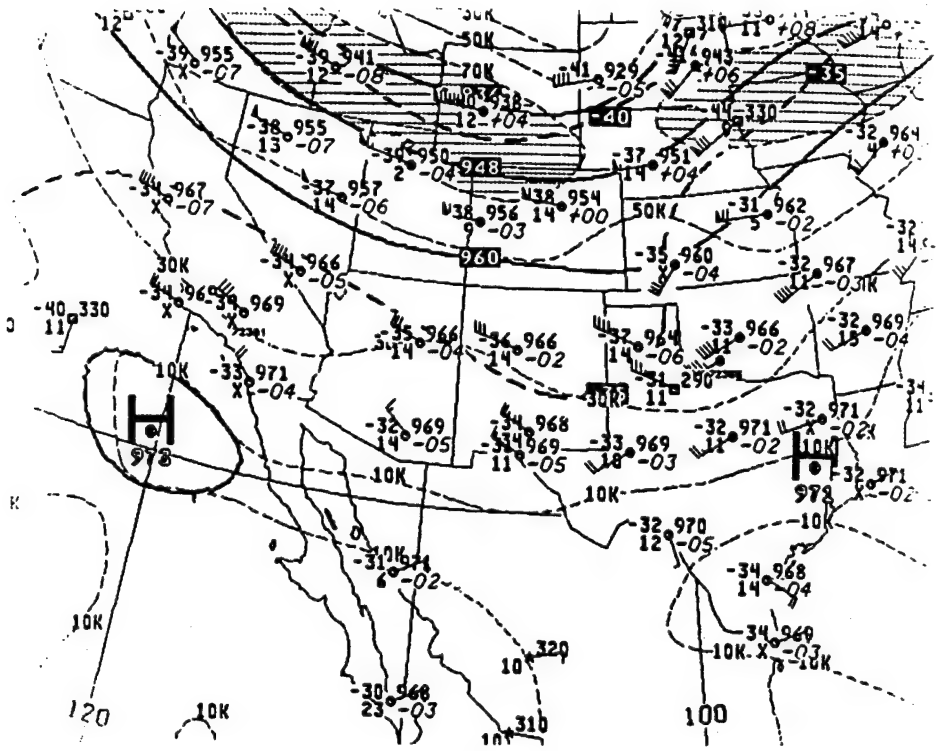

Figure 5a) NCEP 300 mb analysis charts at 1200 UTC 7 July.

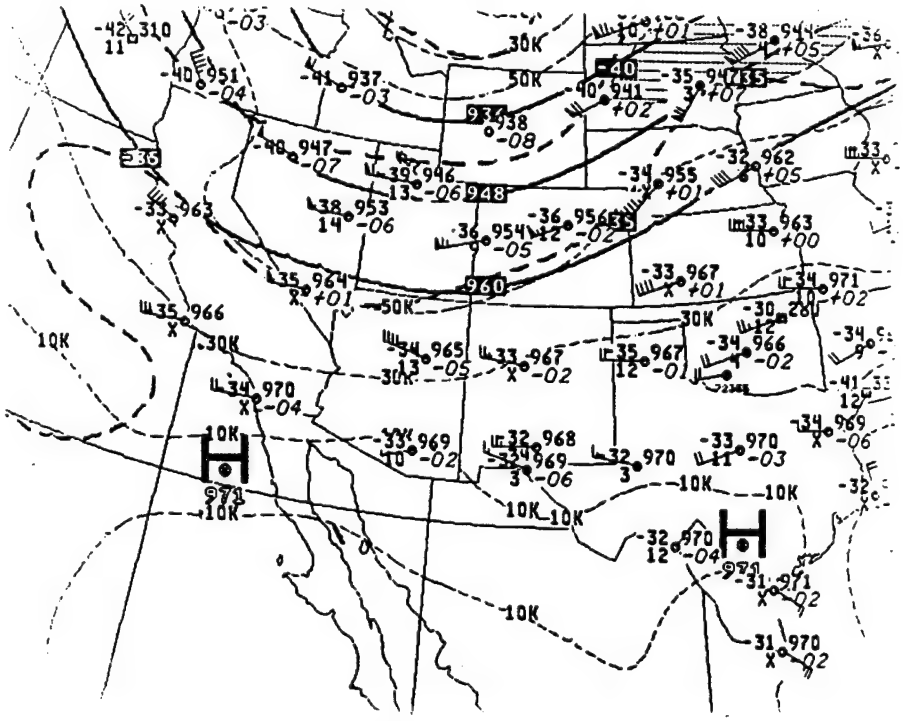

Figure 5b) Same as figure 2a, except at 1200 UTC 8 July.

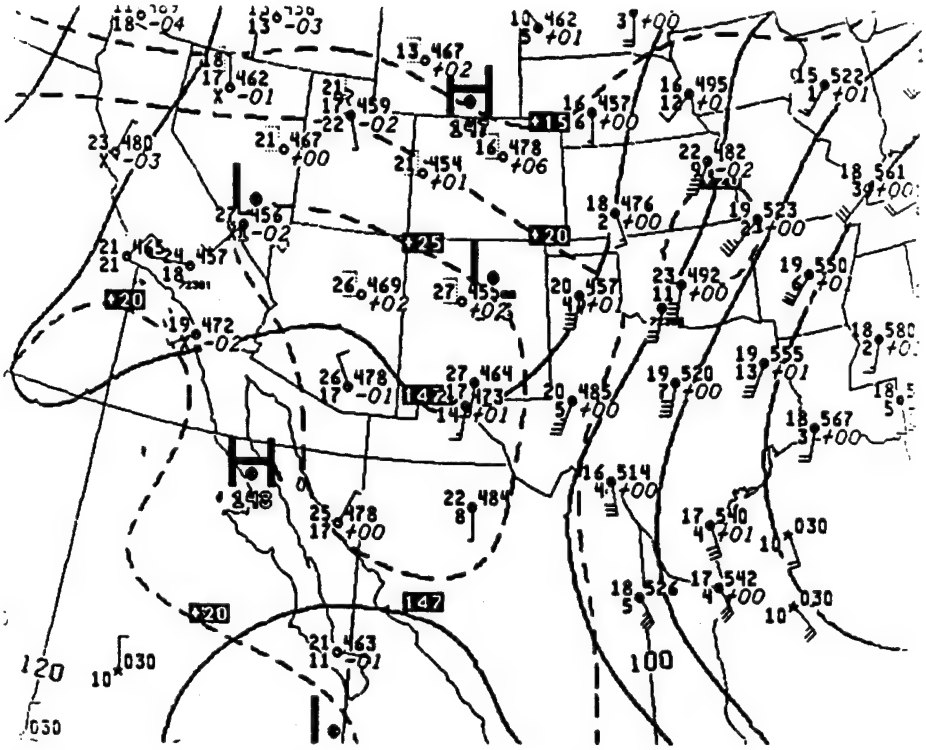

Figure 6a) NCEP 850 mb analysis charts at 1200 UTC 7 July.

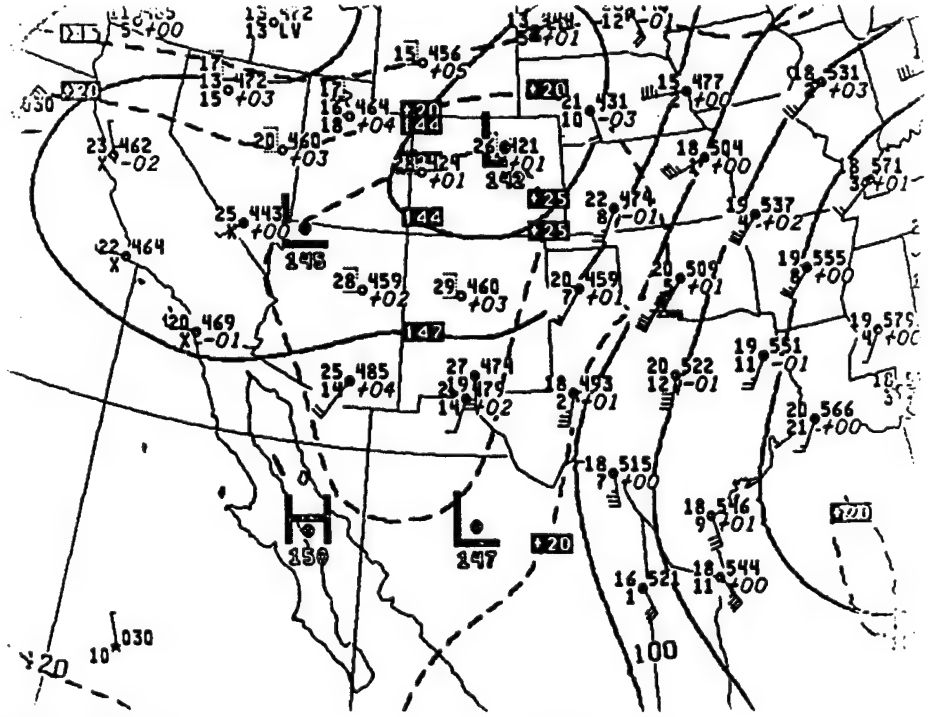

Figure 6b) Same as figure 6a, except at 1200 UTC 8 July.

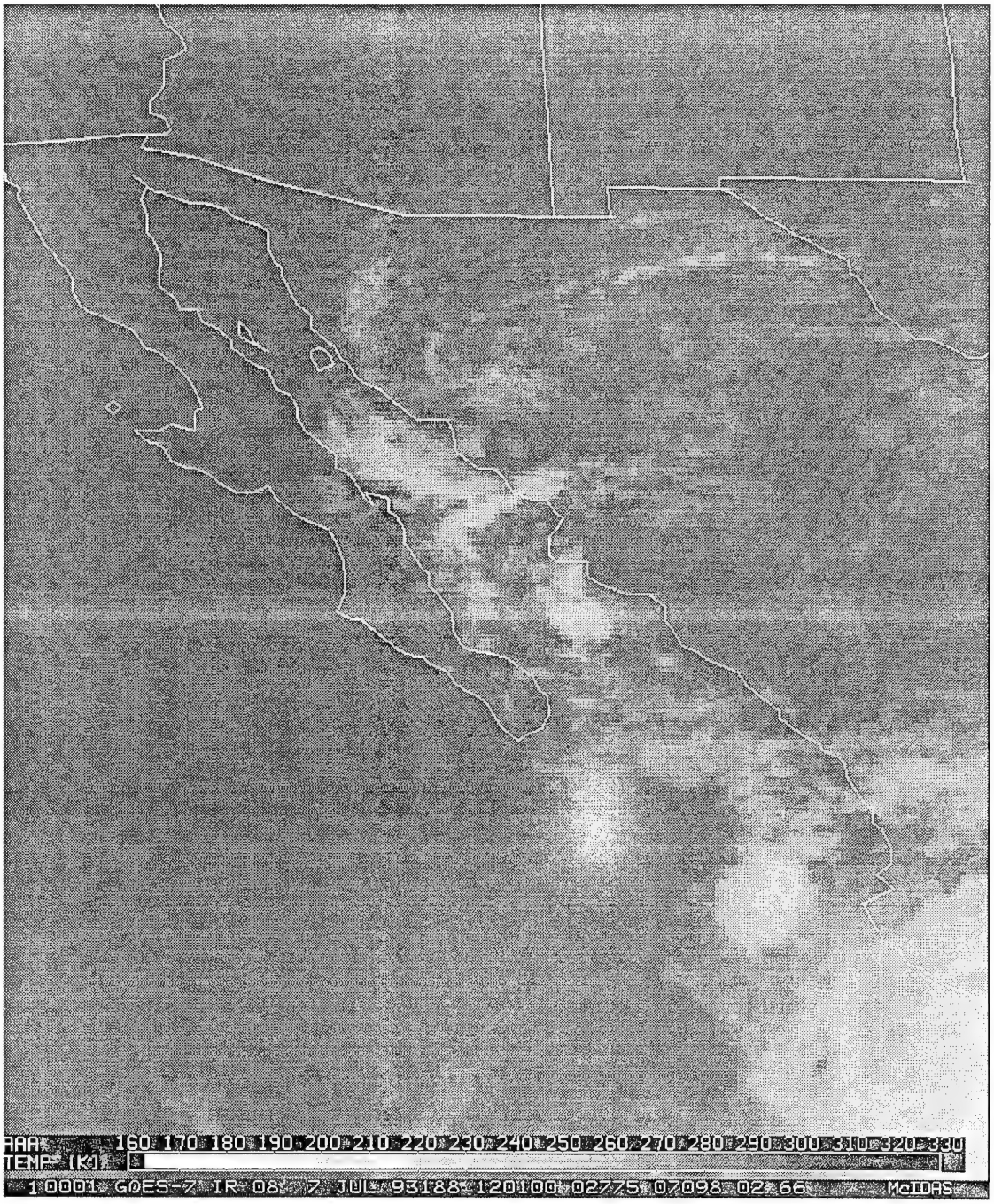

Figure 7a) Infrared satellite imagery at 1200 UTC 7 July.

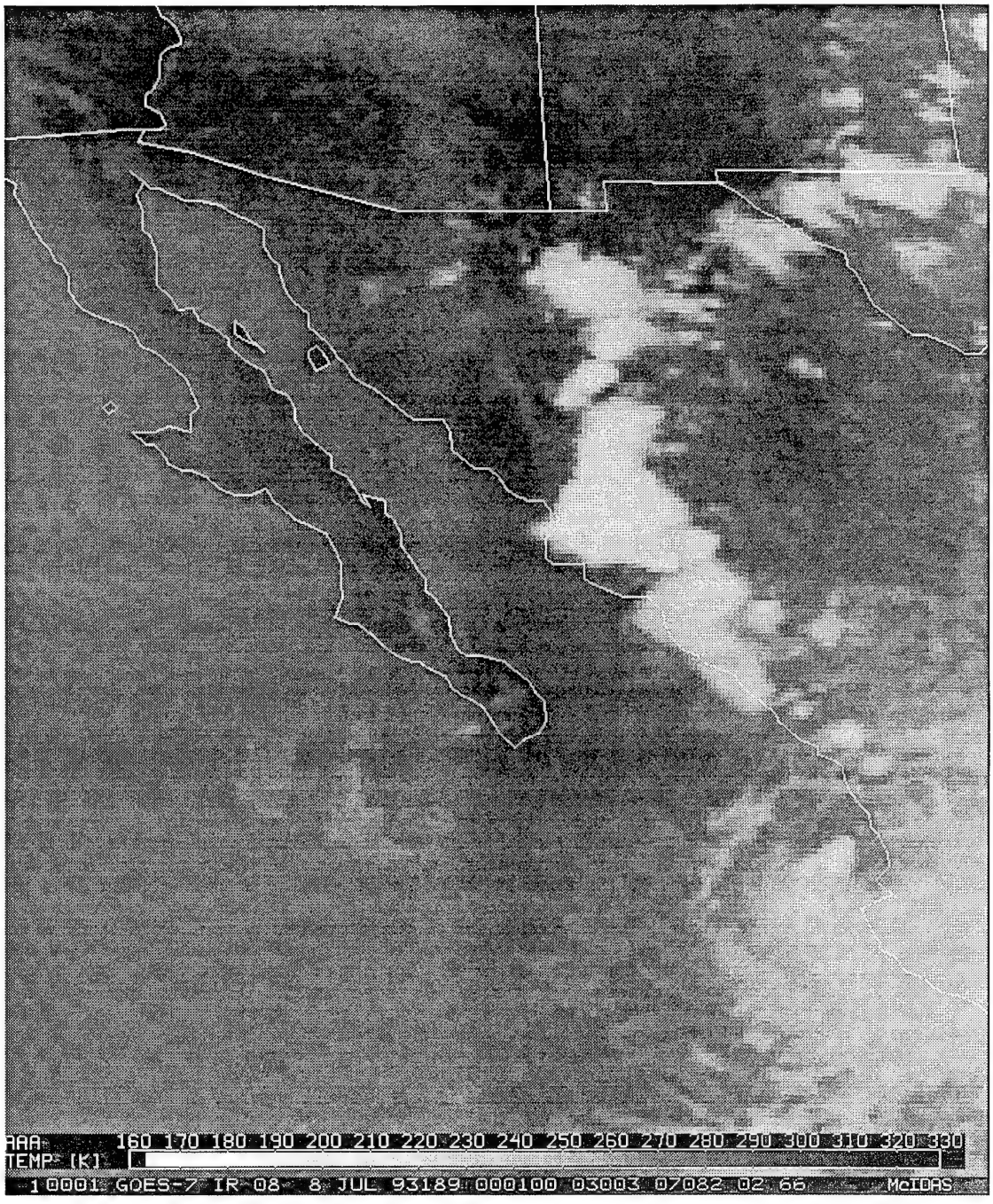

Figure 7b) Same as figure 7a, except at 0000 UTC 8 July.

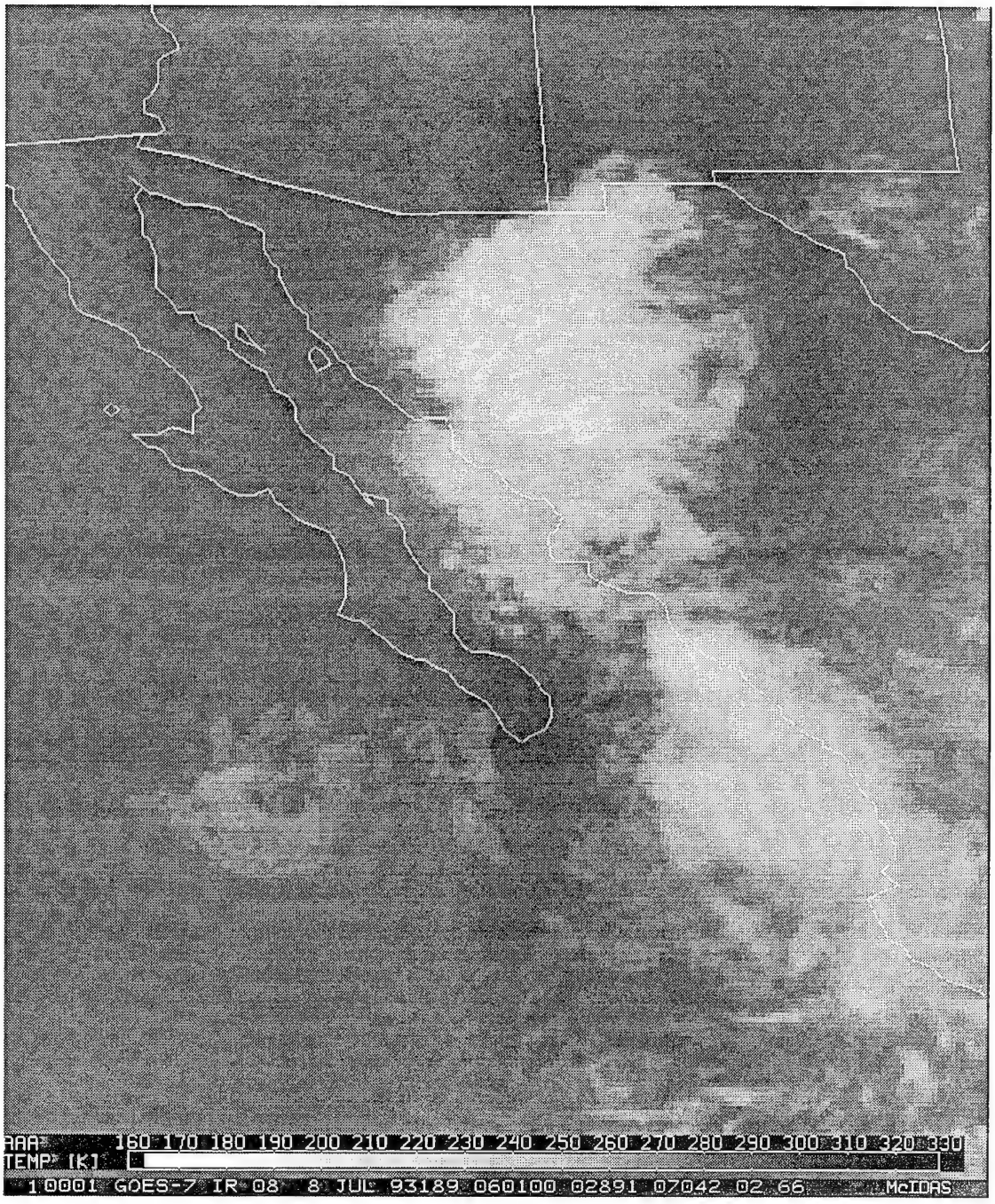

Figure 7c) Same as figure 7a, except at 0600 UTC 8 July.

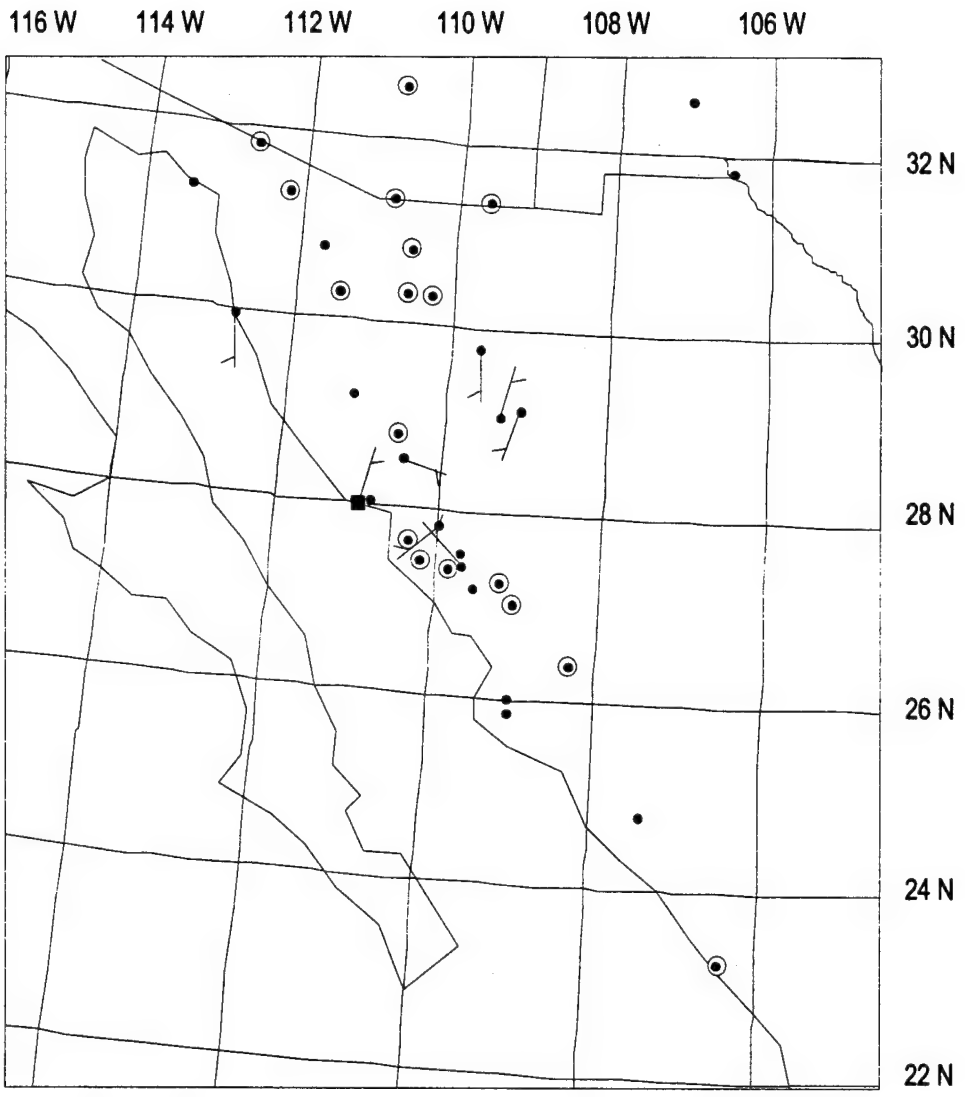

Figure 8a) Plot of surface (circles) and 950 mb pibal (squares) winds along the Gulf of California at 1200 UTC 7 July. Full barb is 10 ms-1.

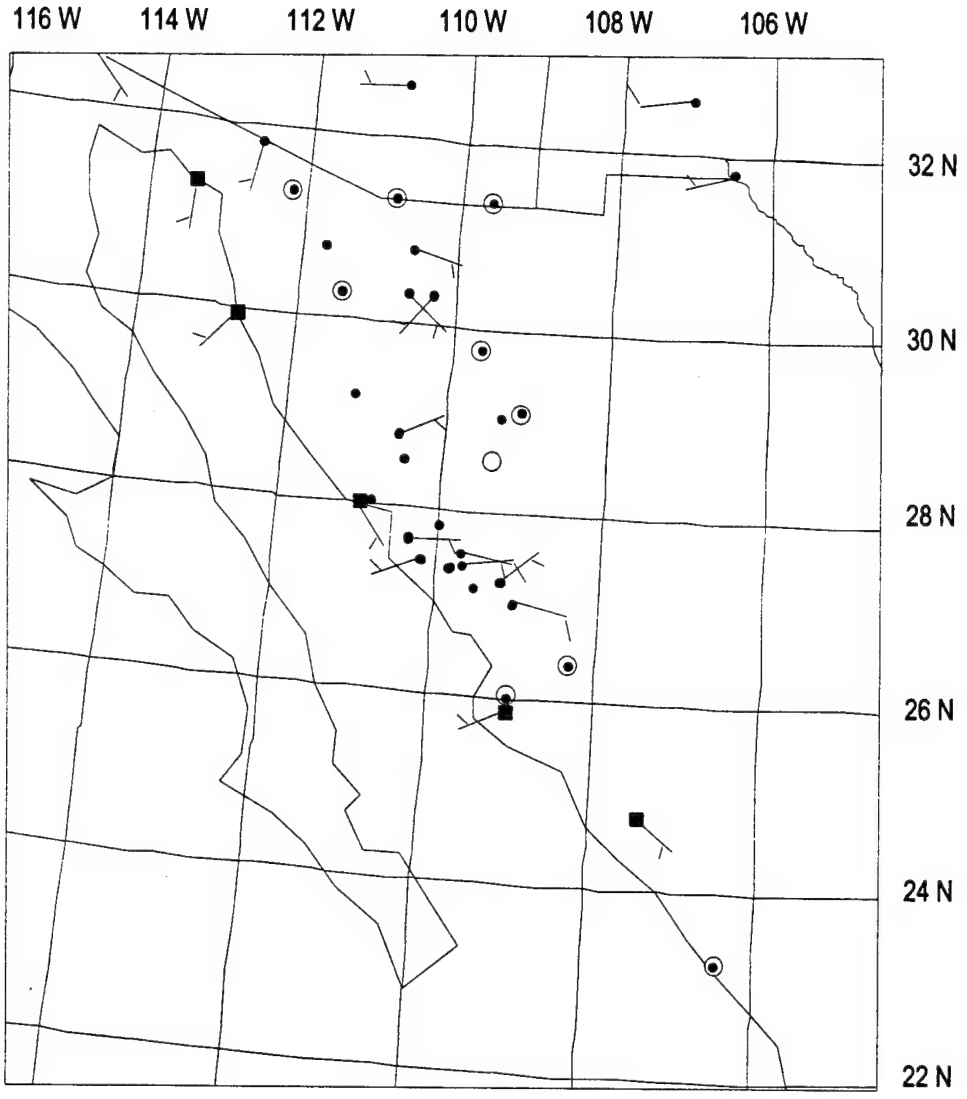

Figure 8b) Same as figure 8a, except at 0000 UTC 8 July.

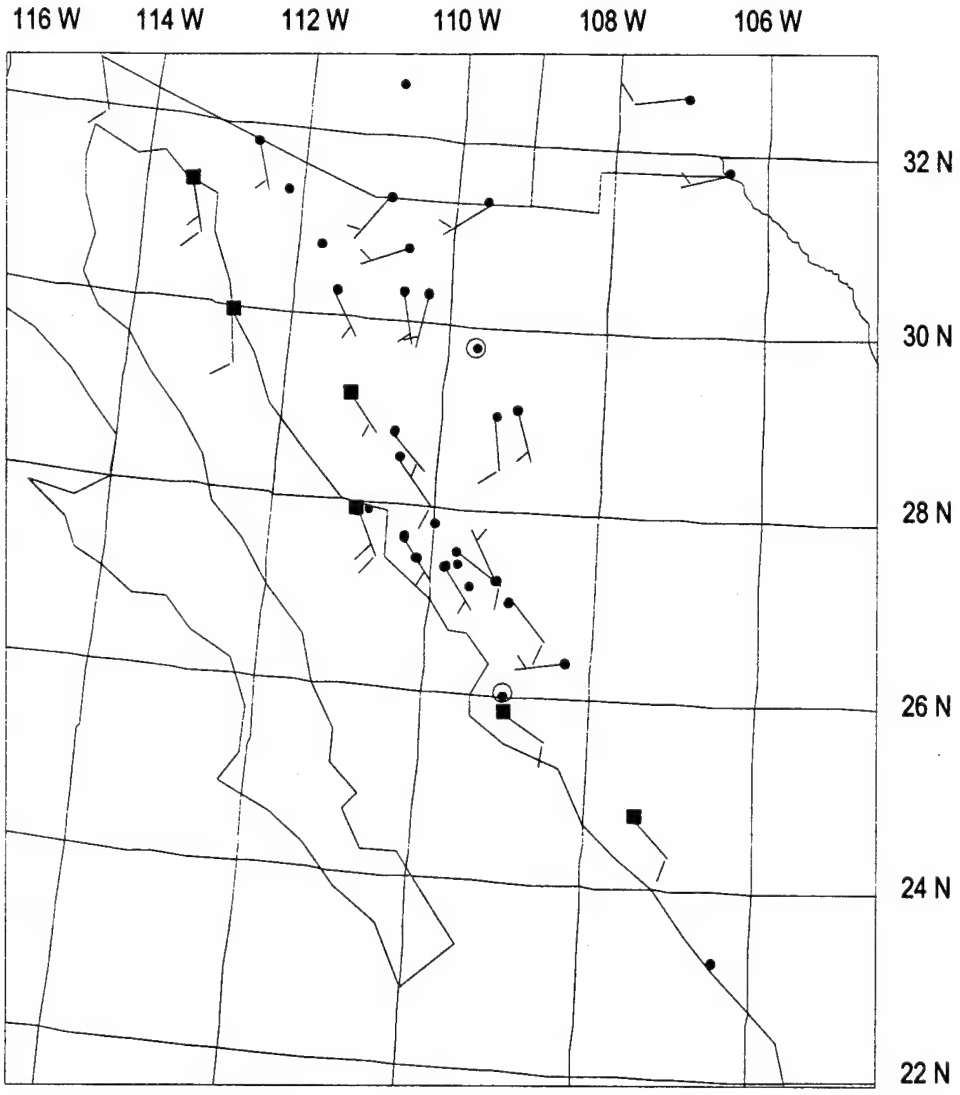

Figure 8c) Same as figure 8a, except at 1200 UTC 8 July.

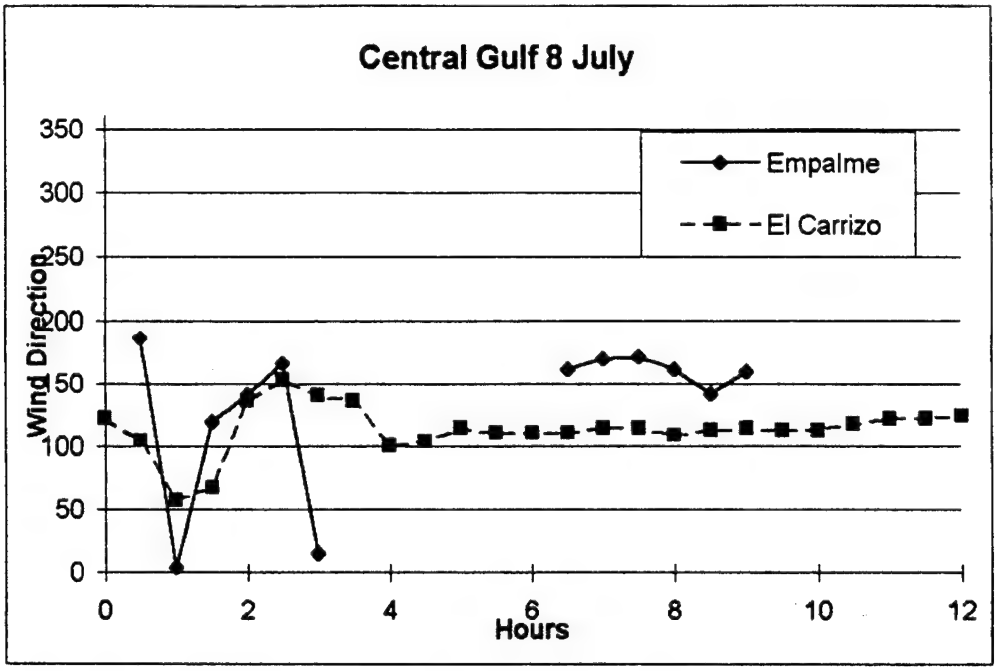

Figure 9a) Time-series plots of wind direction of selected surface observations along the central Gulf of California of California from 0000-1200 UTC 8 July.

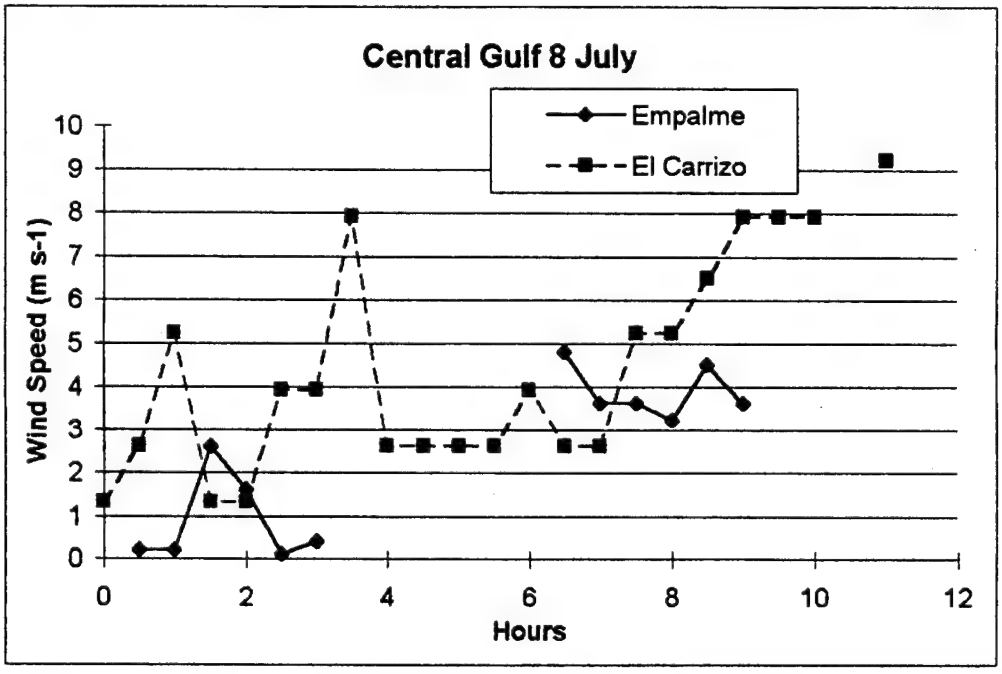

Figure 9b) Same as figure 9a, except time-series of wind speeds, ms-1.

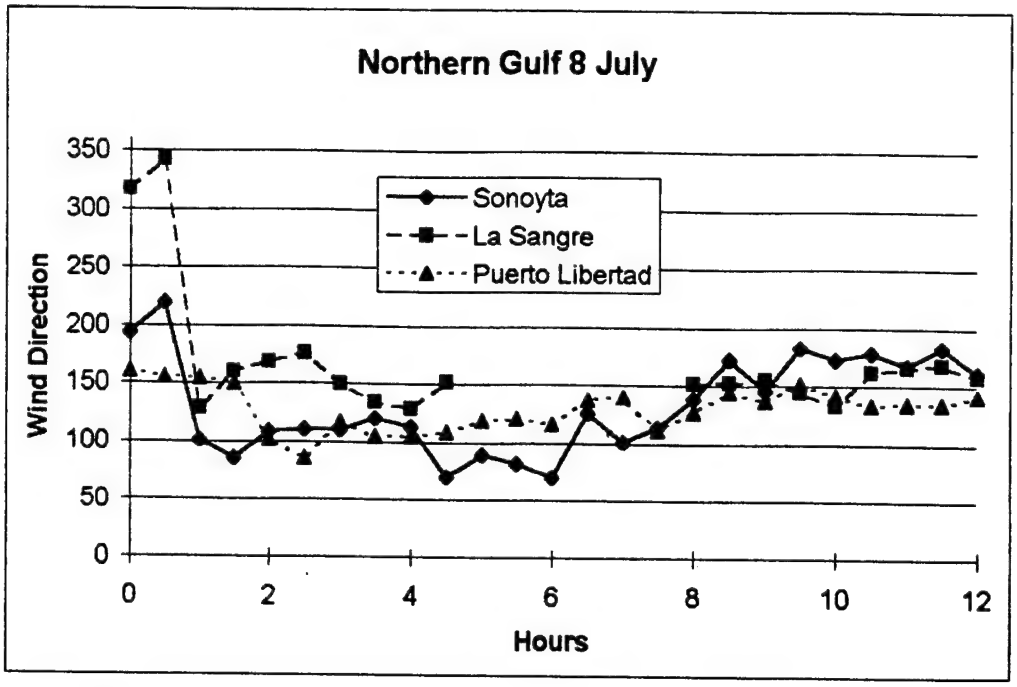

Figure 9c) Same as figure 9a, except northern Gulf of California.

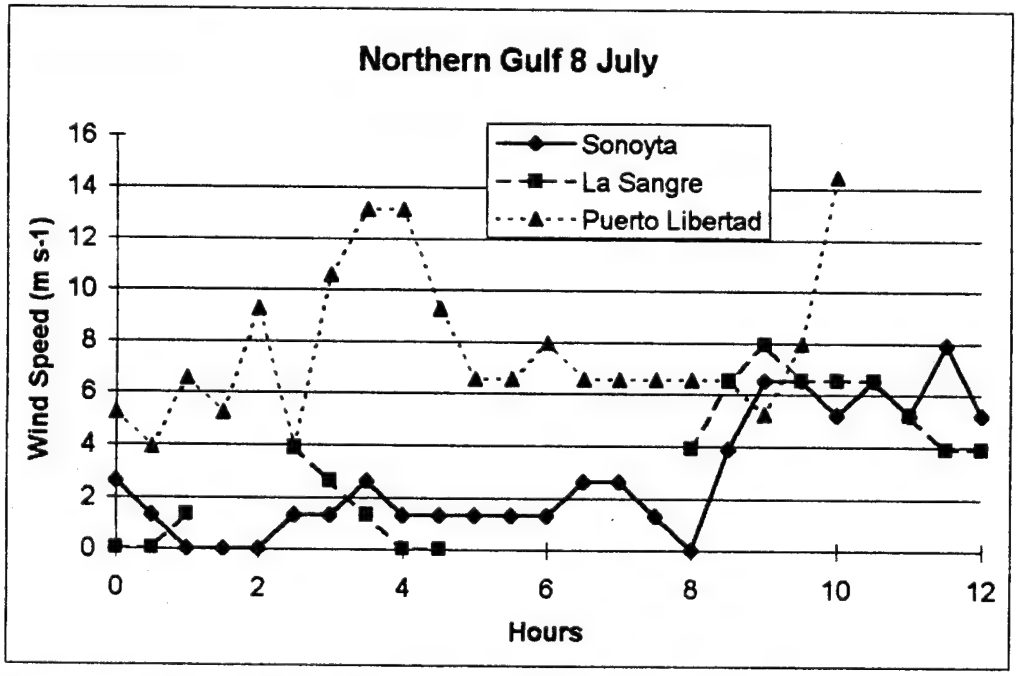

Figure 9d) Same as figure 9b, except northern Gulf of California.

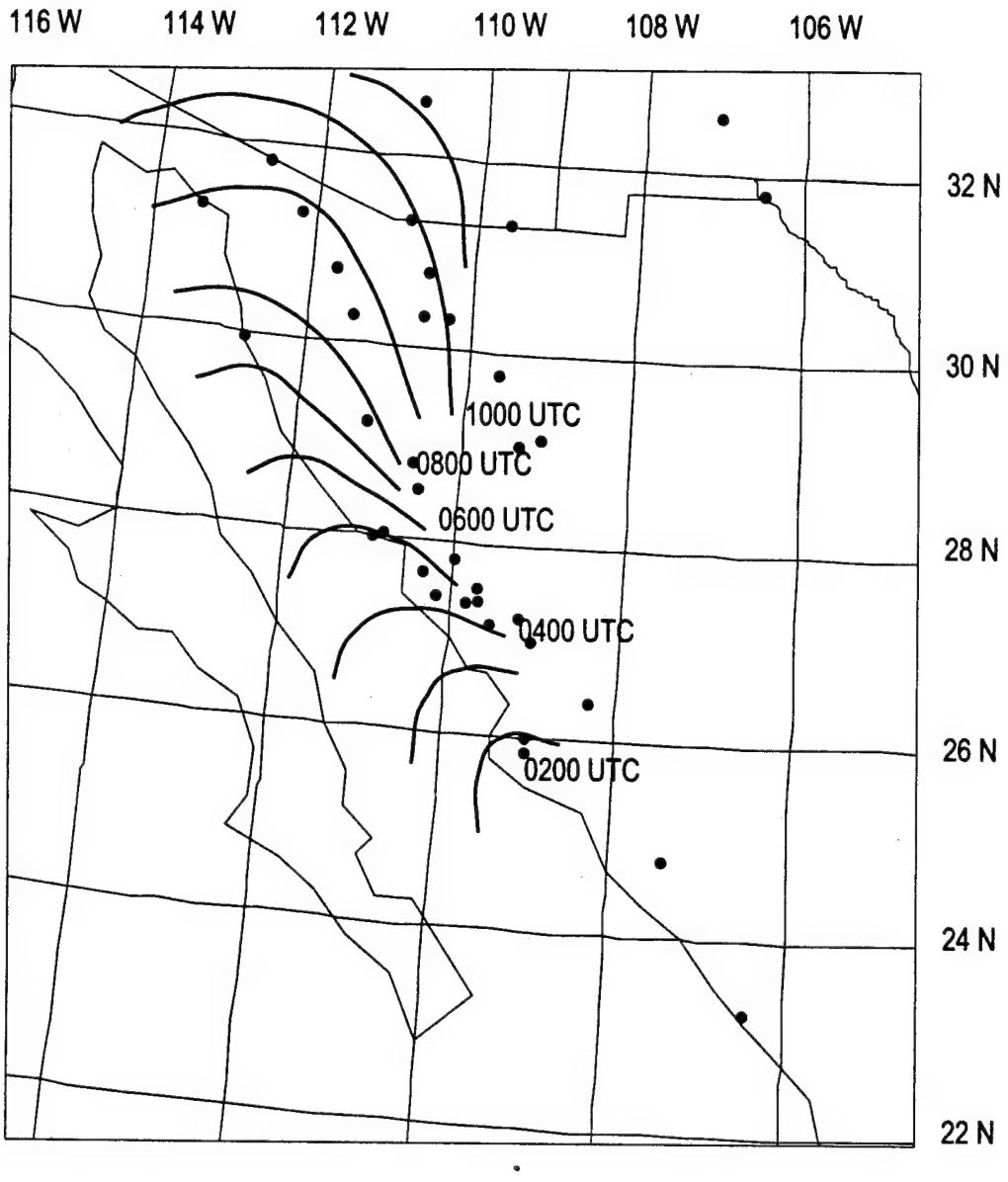

Figure 10) Isochrone analysis of leading edge of surge observed on 8 July.

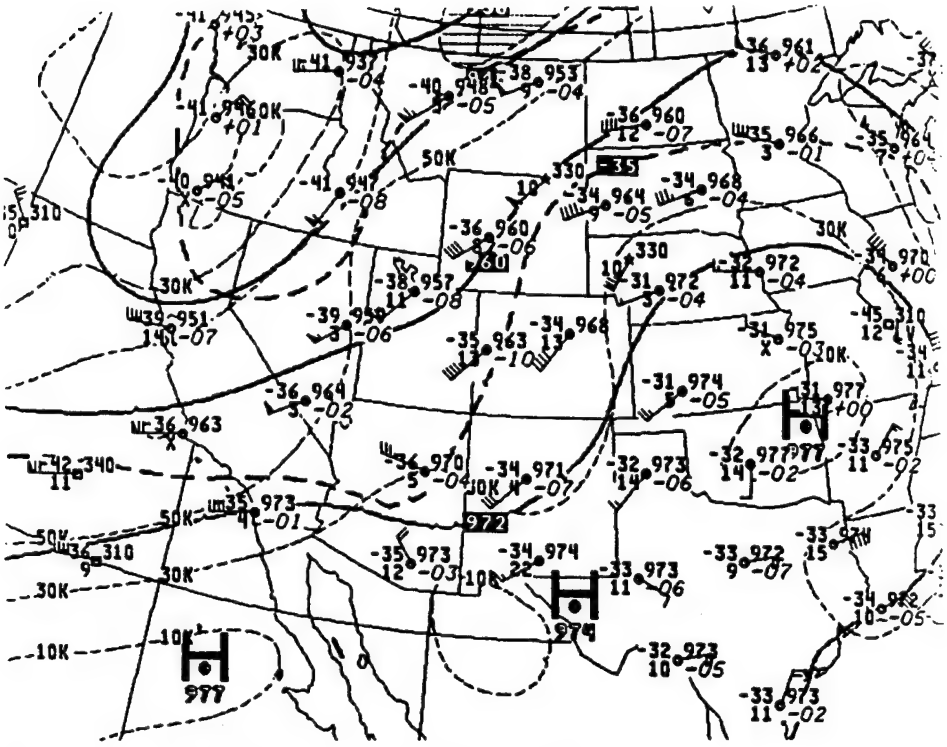

Figure 11a) NCEP 300 mb charts at 1200 UTC 11 August.

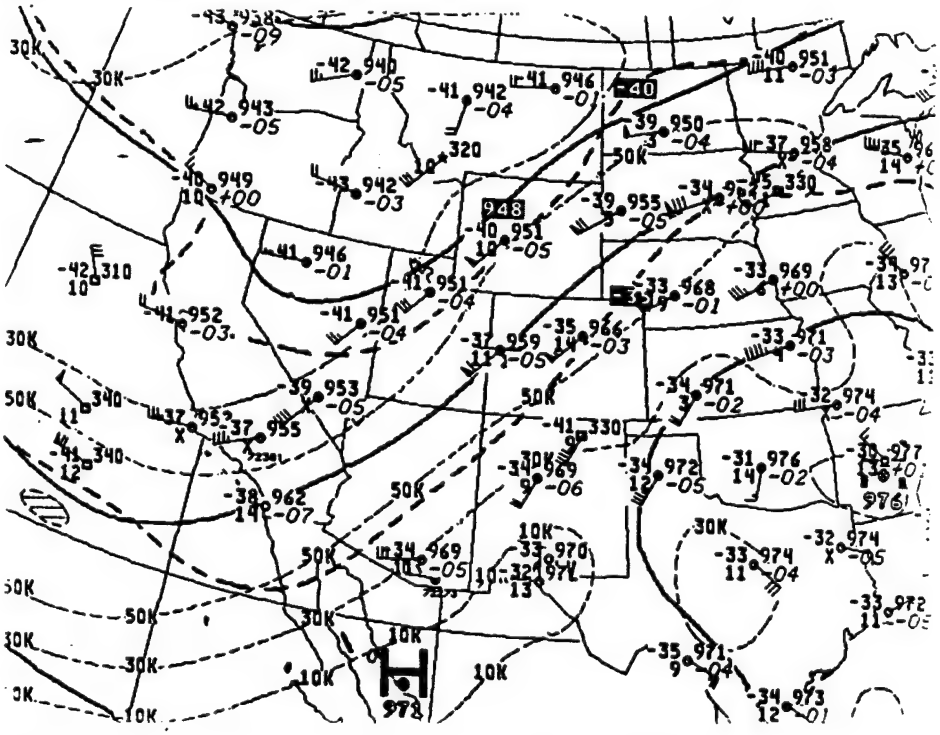

Figure 11b) Same as figure 11a, except at 1200 UTC 13 August.

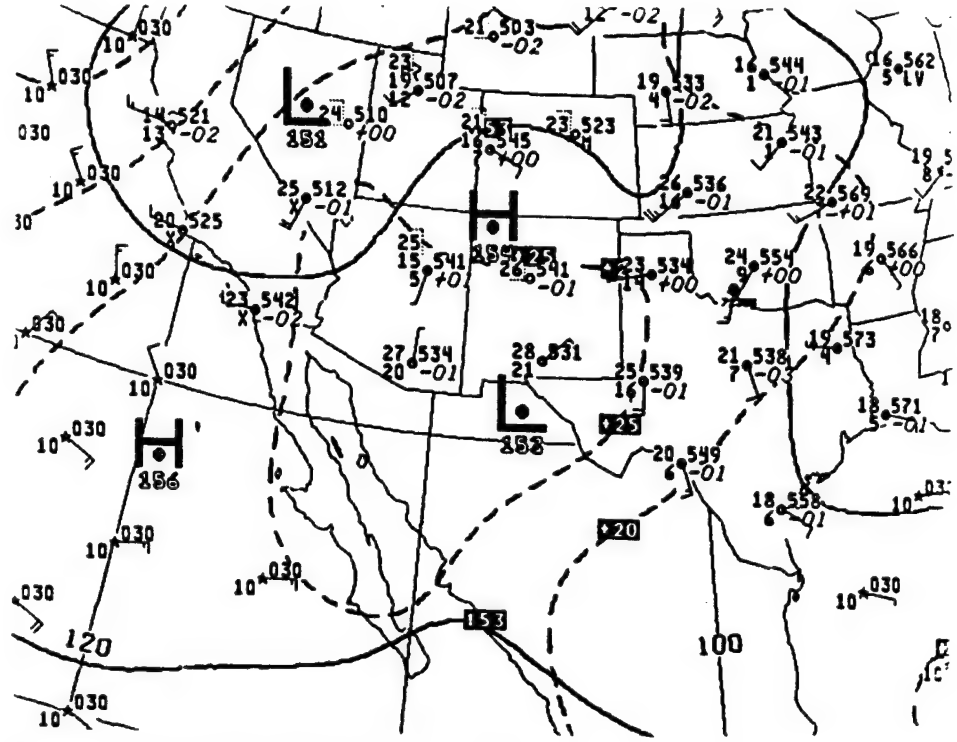

Figure 12a) NCEP 850 mb charts at 1200 UTC 11 August.

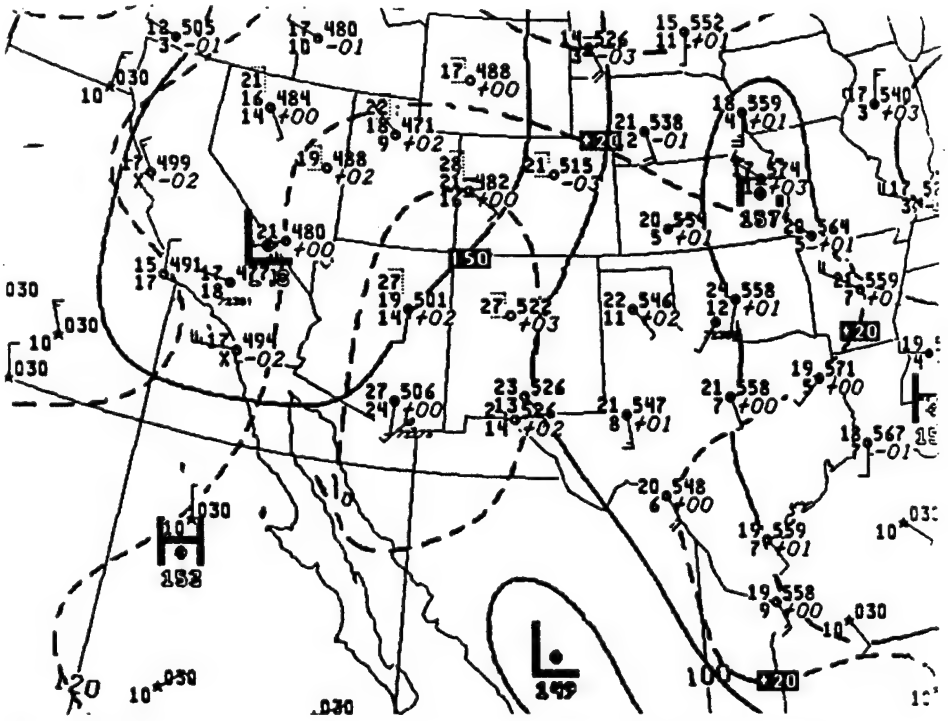

Figure 12b) Same as figure 12a, except at 1200 UTC 13 August.

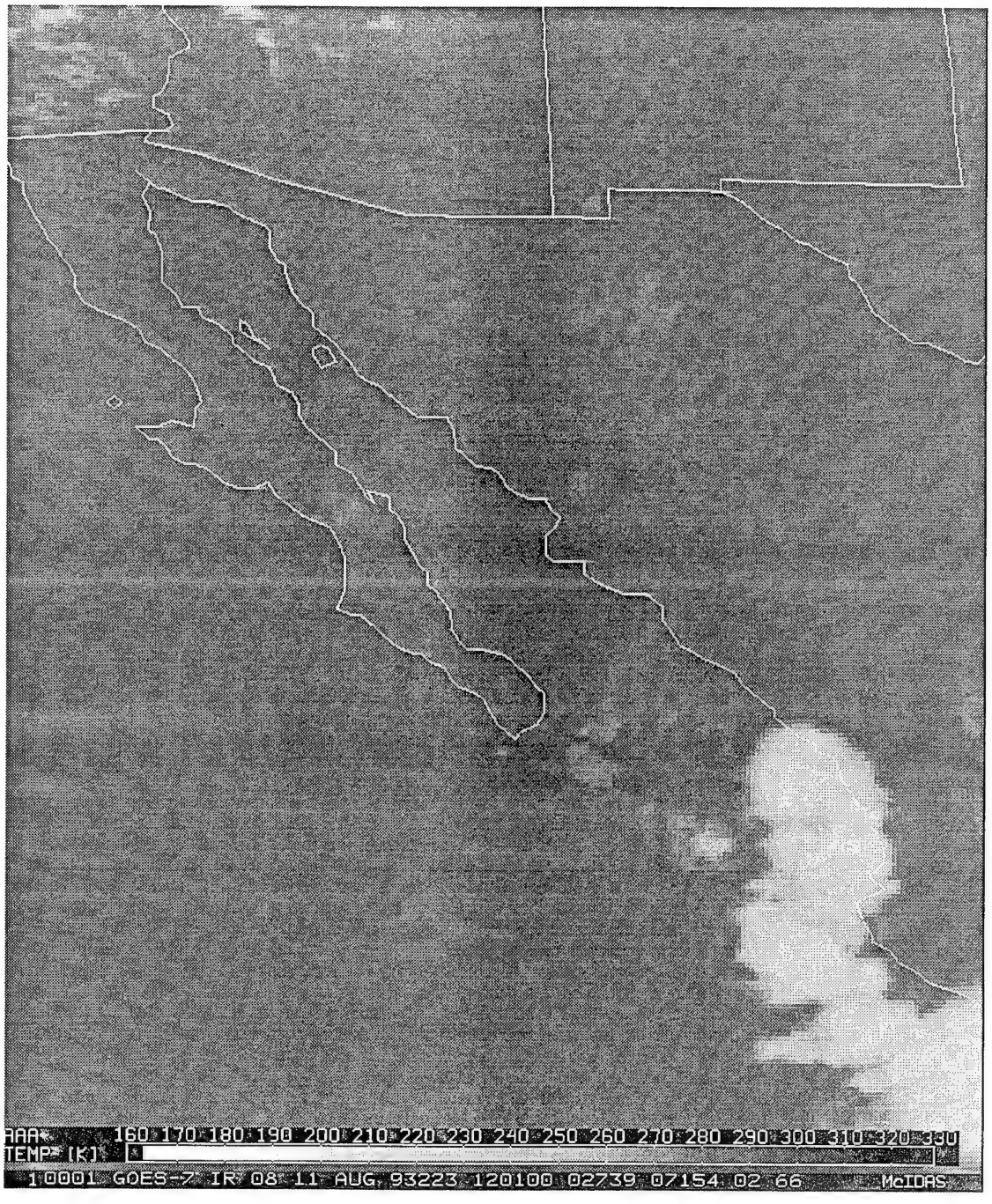

Figure 13a) Infrared satellite imagery at 1200 UTC 11 August.

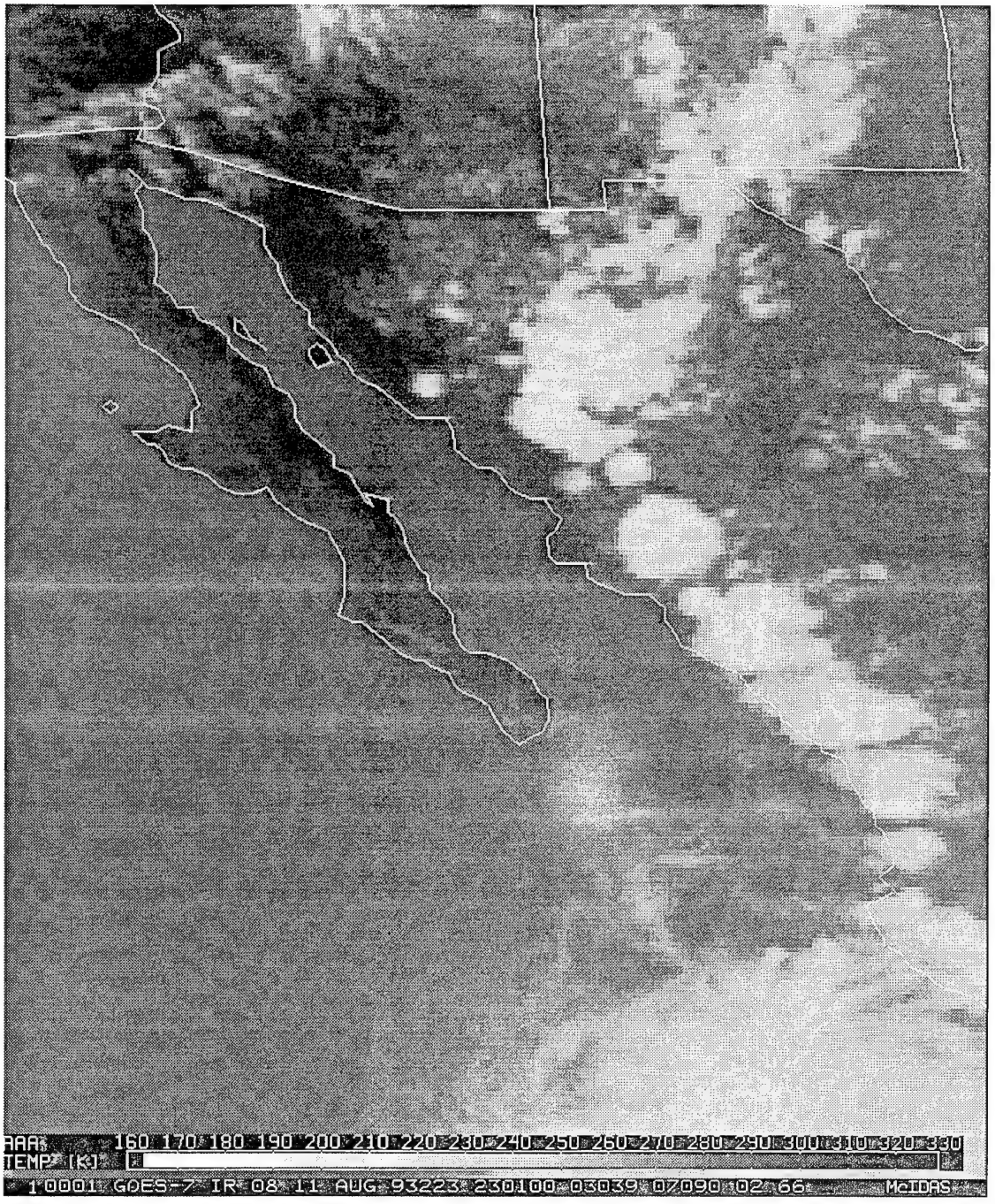

Figure 13b) Same as figure 13a, except at 2300 UTC 11 August.

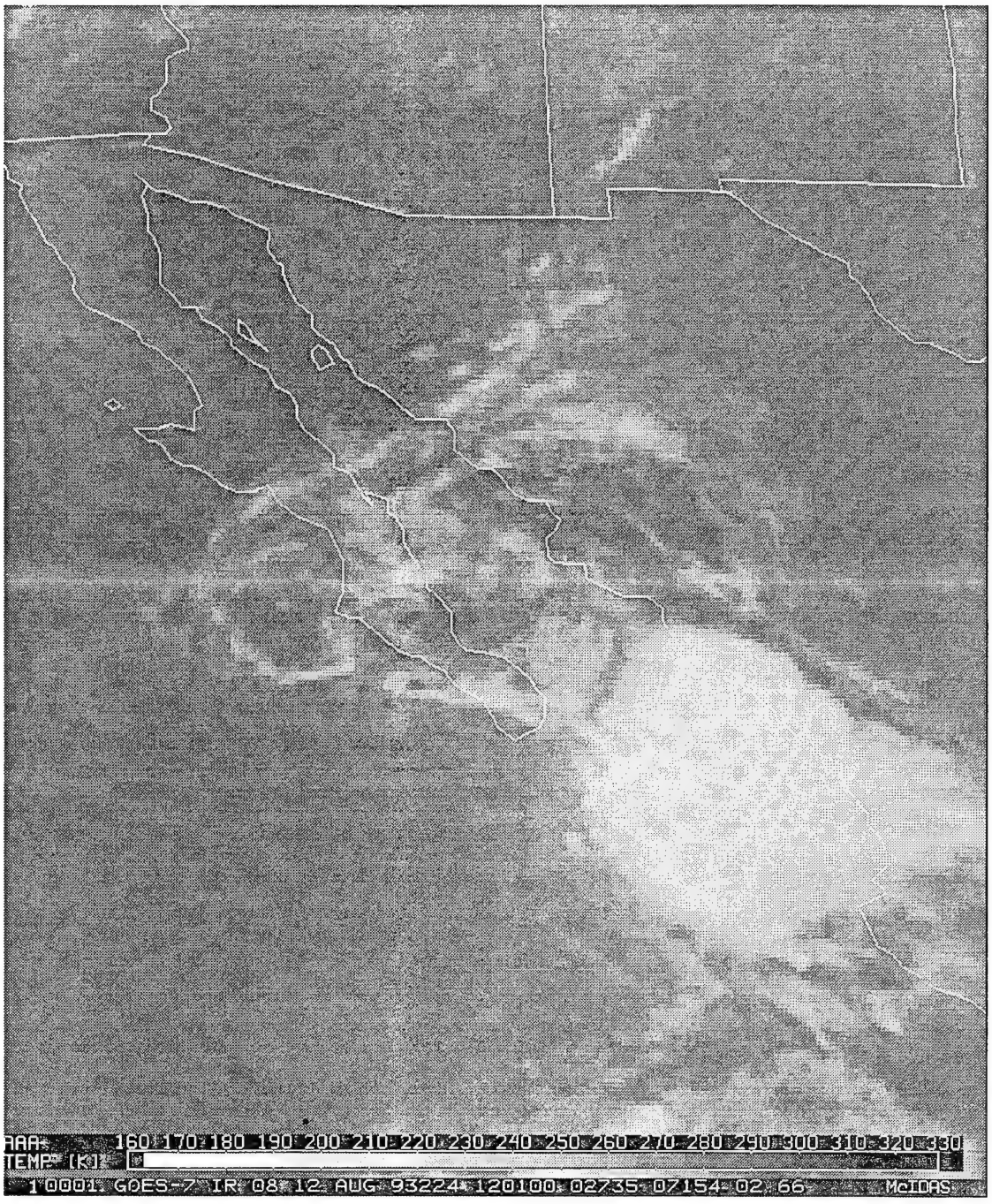

Figure 13c) Same as figure 13a, except at 1200 UTC 12 August.

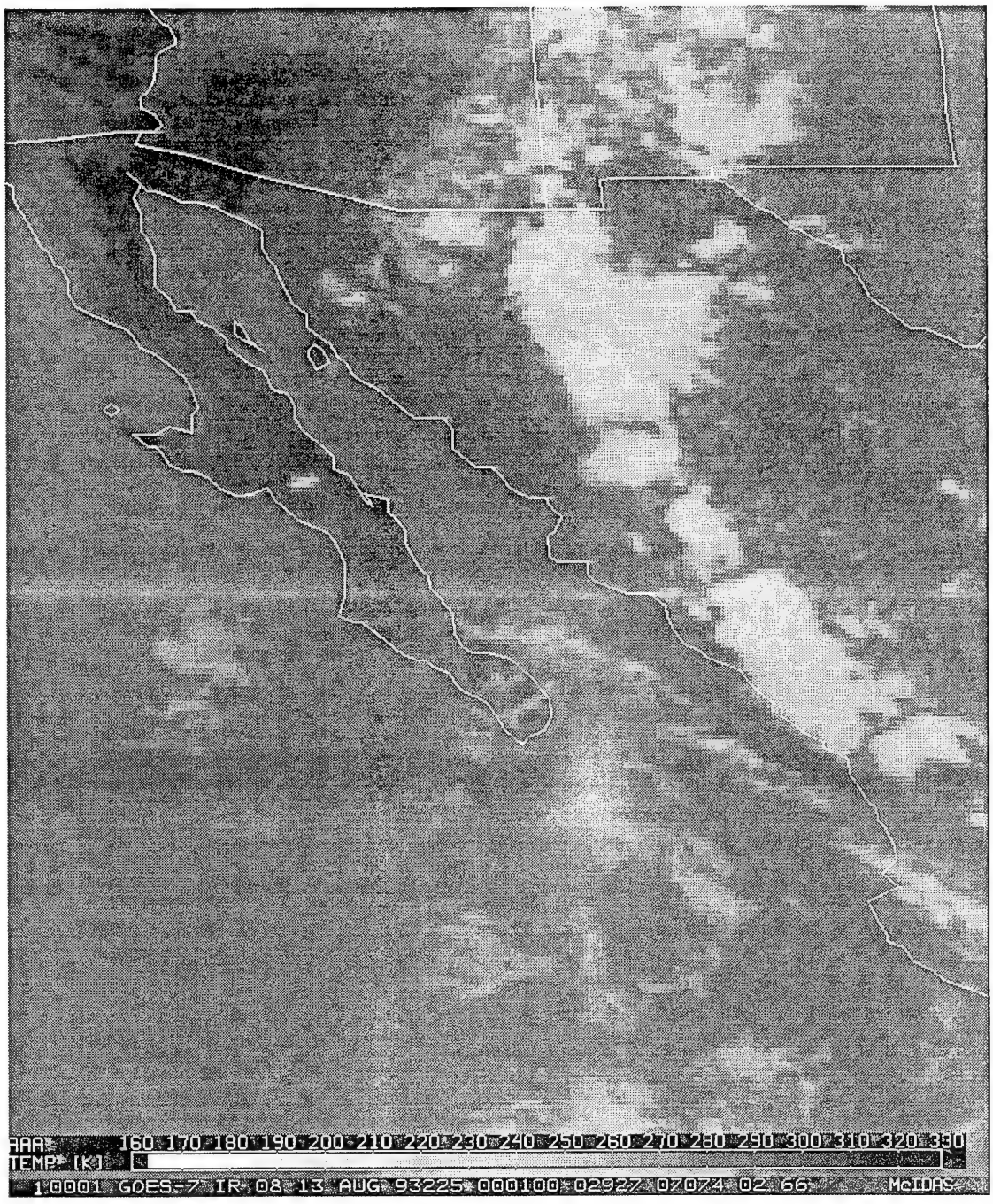

Figure 13d) Same as figure 13a, except at 0000 UTC 13 August.

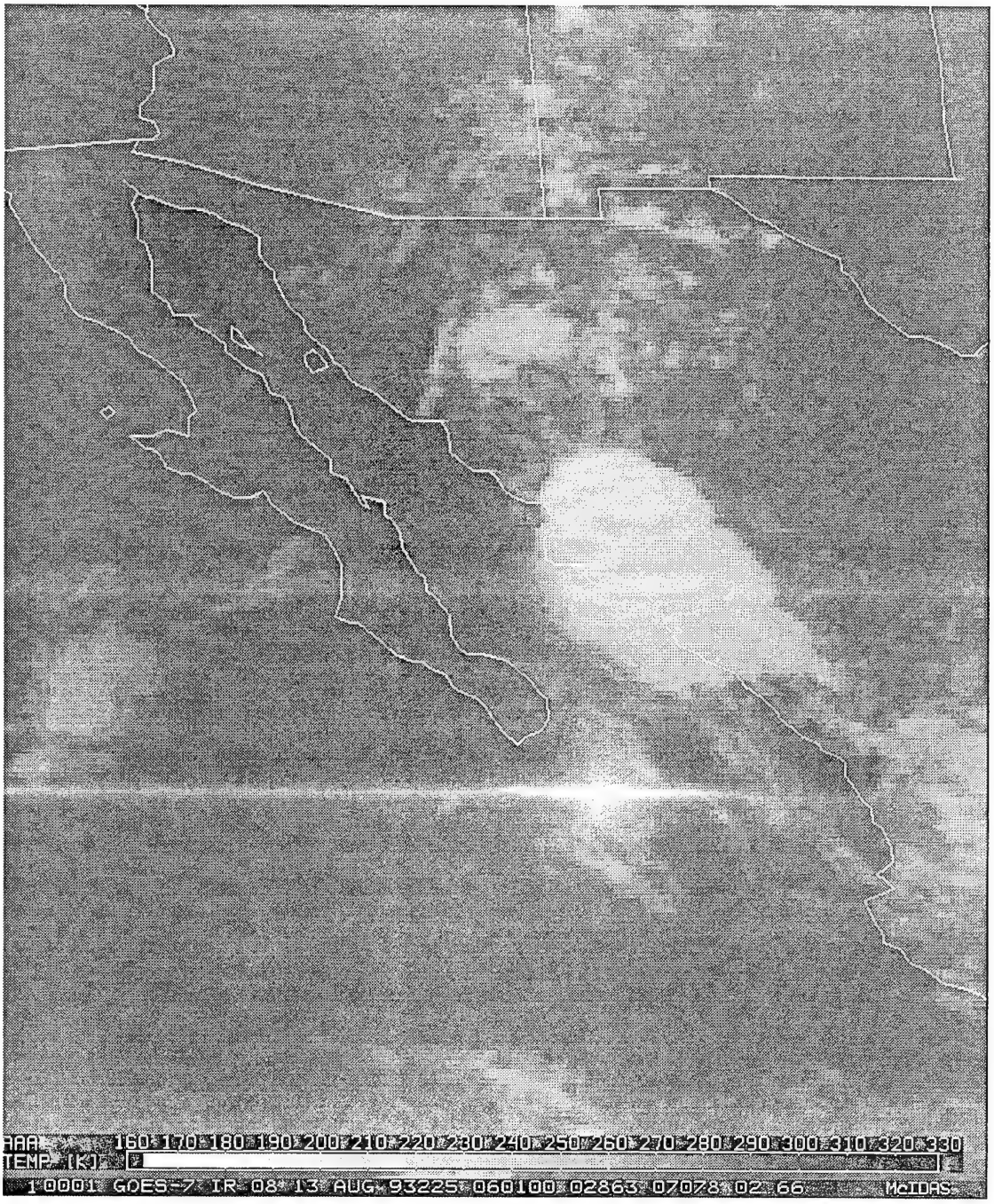

Figure 13e) Same as figure 13a, except at 0600 UTC 13 August.

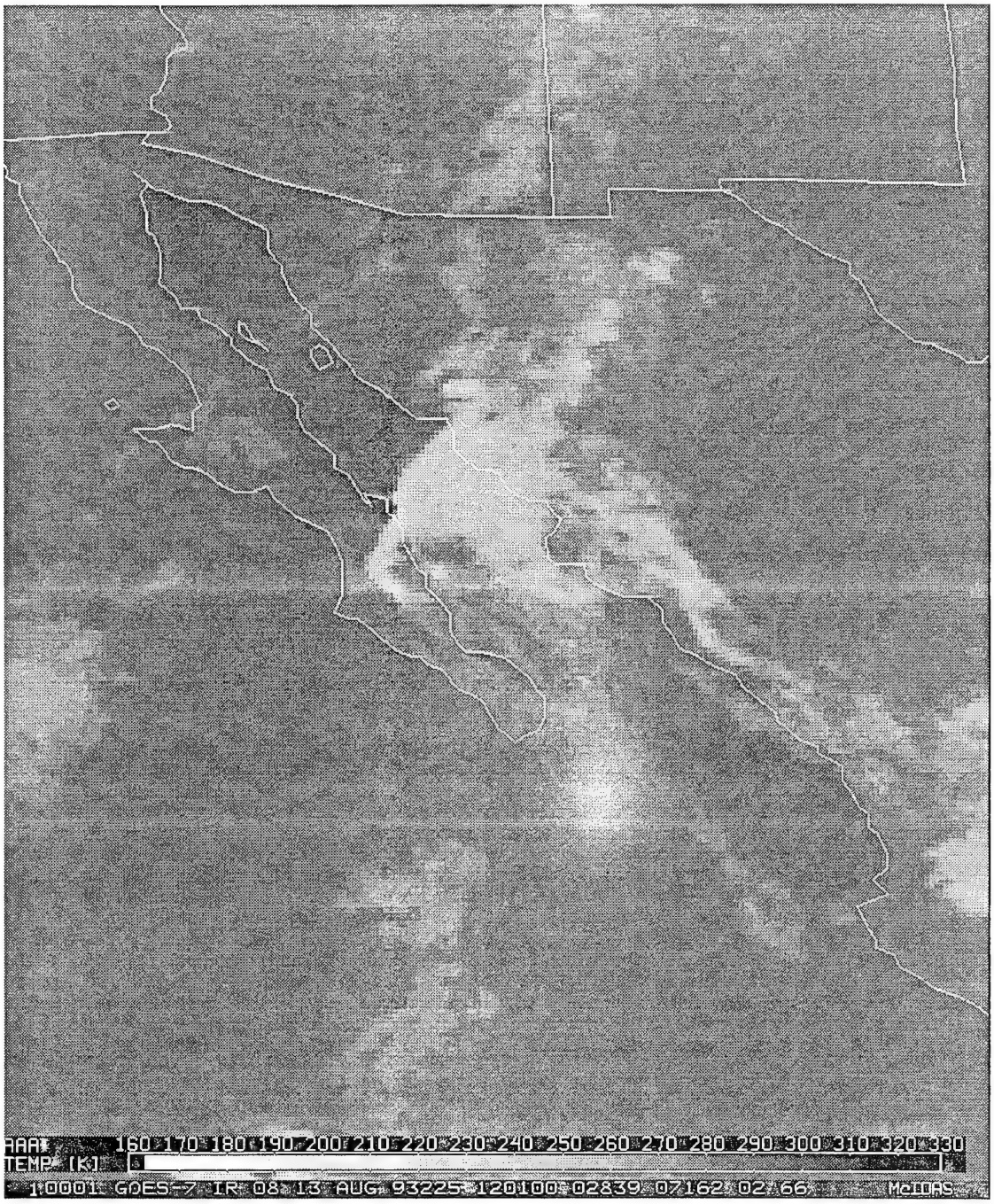

Figure 13f) Same as figure 13a, except at 1200 UTC 13 August.

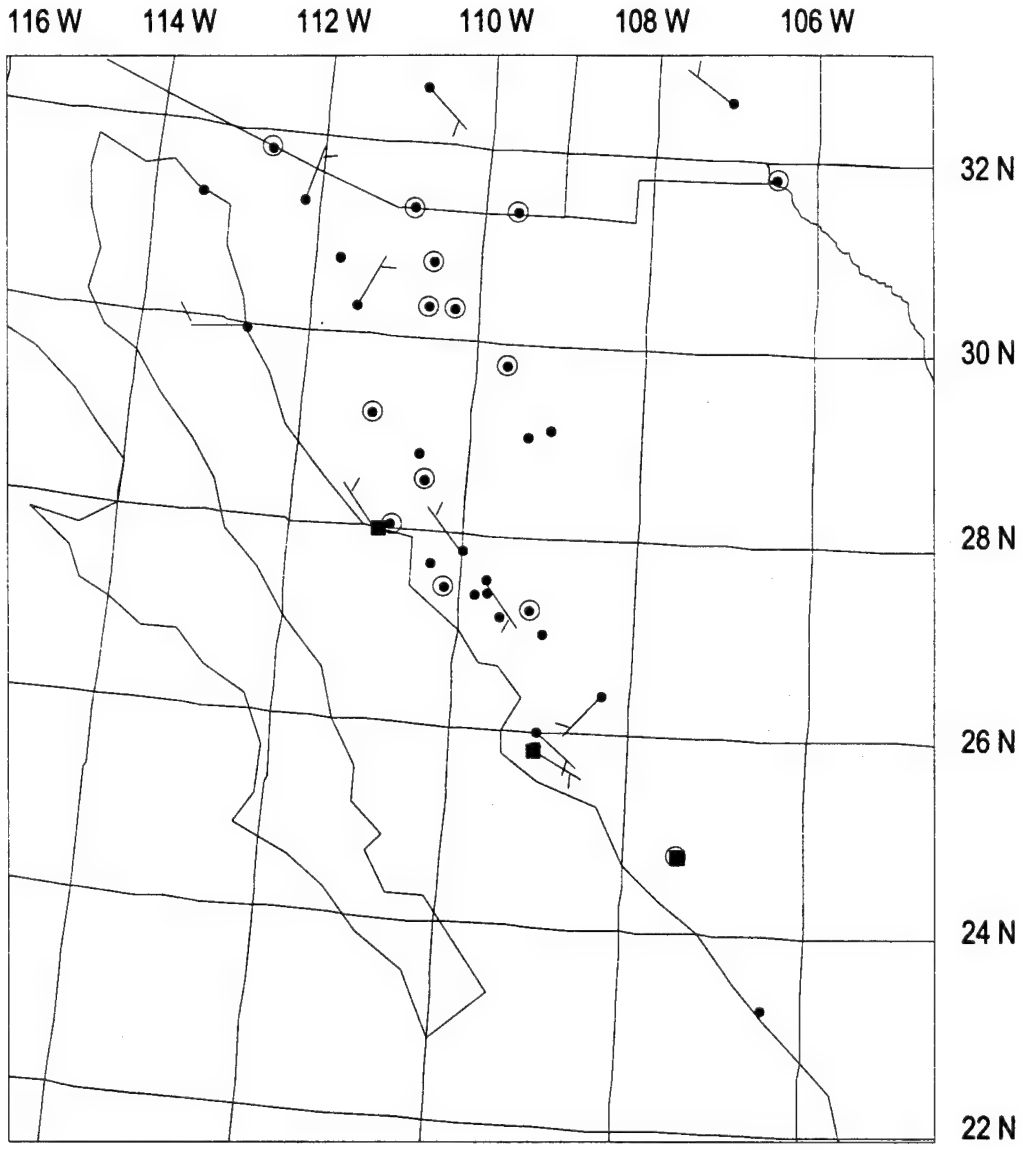

Figure 14a) Plot of surface (circles) and 950 mb pibal (squares) winds along the Gulf of California at 1200 UTC 11 August. Full barb is 10 ms-1.

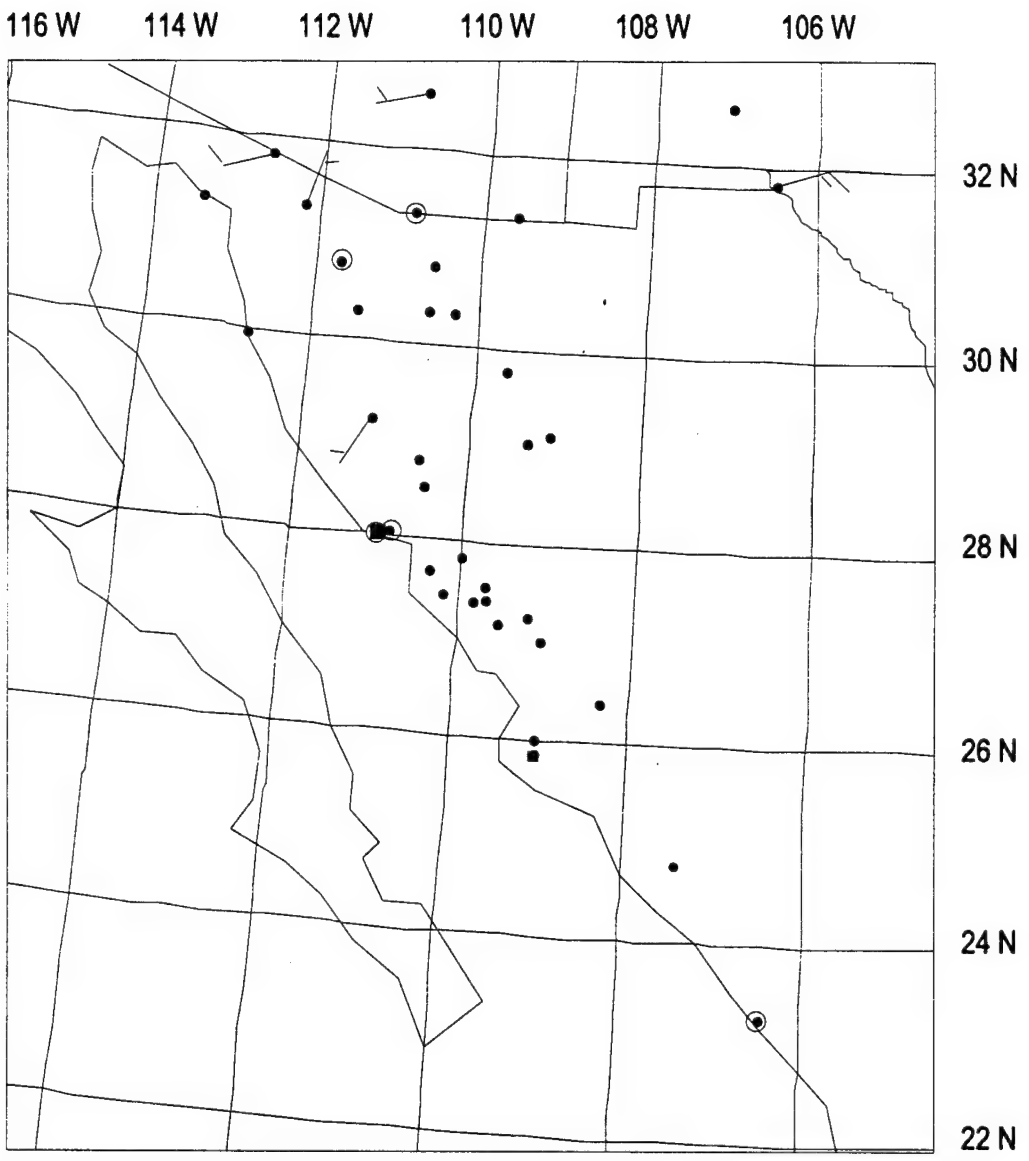

Figure 14b) Same as figure 14a, except at 0000 UTC 12 August.

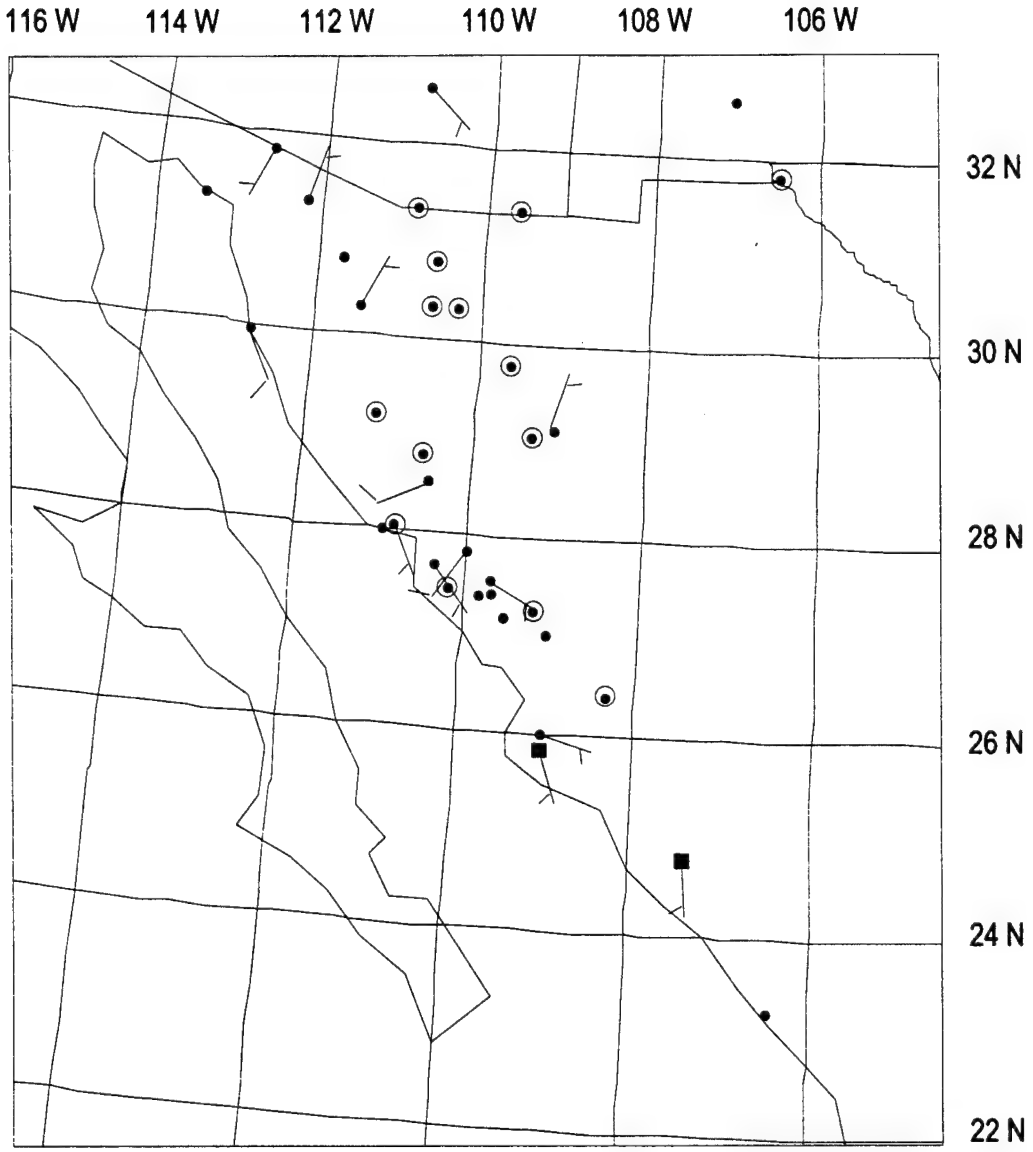

Figure 14c) Same as figure 14a, except at 1200 UTC 12 August.

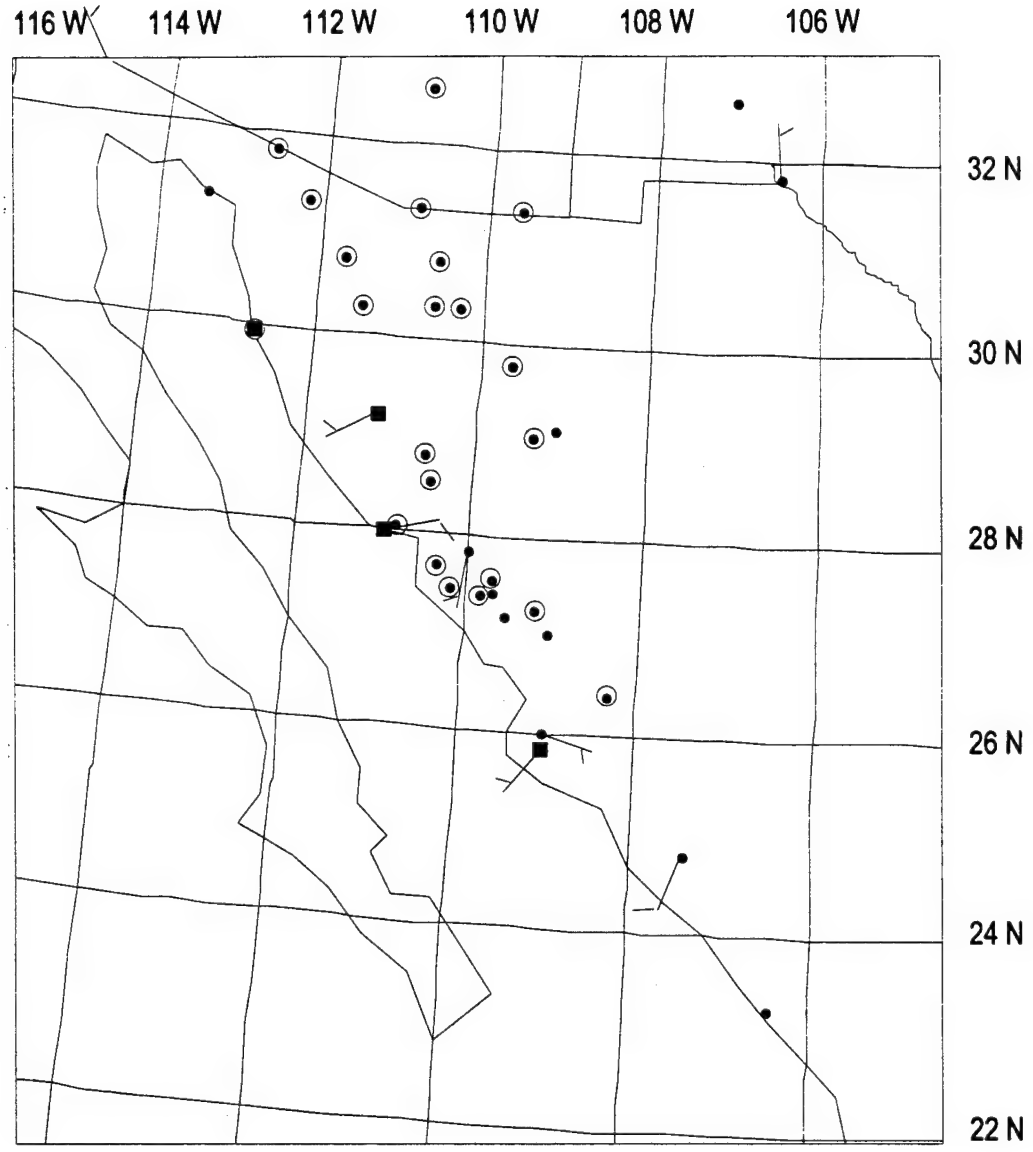

Figure 14d) Same as figure 14a, except at 0000 UTC 13 August.

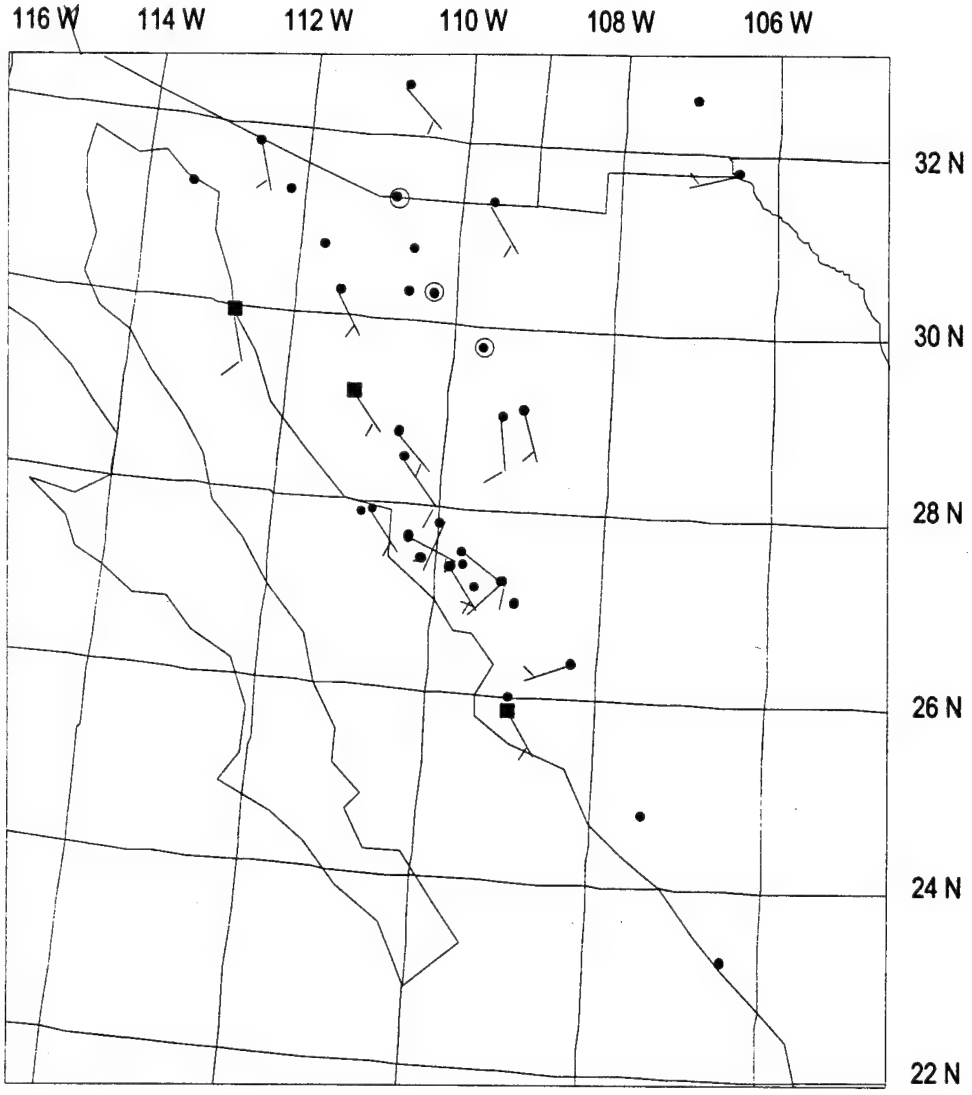

Figure 14e) Same as figure 14a, except at 1200 UTC 13 August.

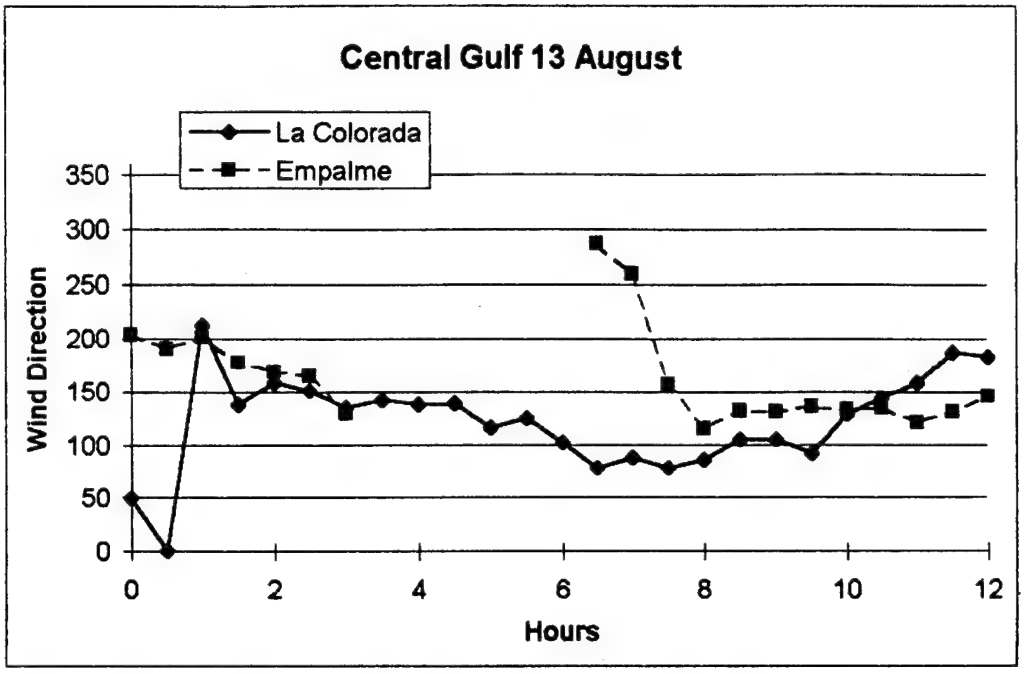

Figure 15a) Time-series plots of wind direction of selected surface wind observations along the central Gulf of California of California from 0000-1200 UTC 13 August.

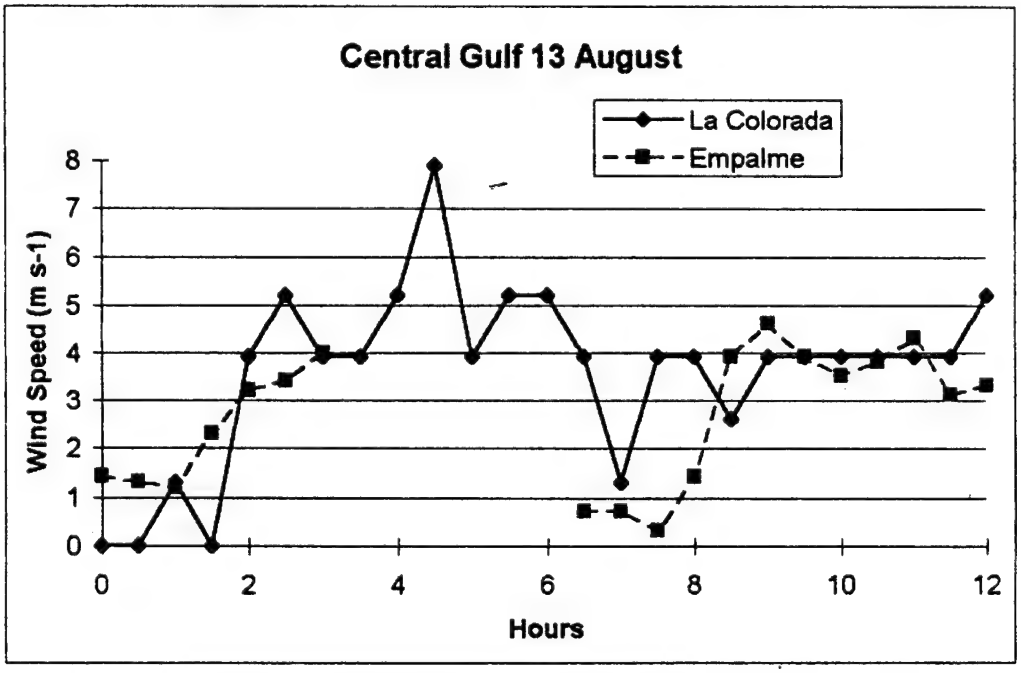

Figure 15b) Same as figure 15a, except time-series of wind speeds, ms-1.

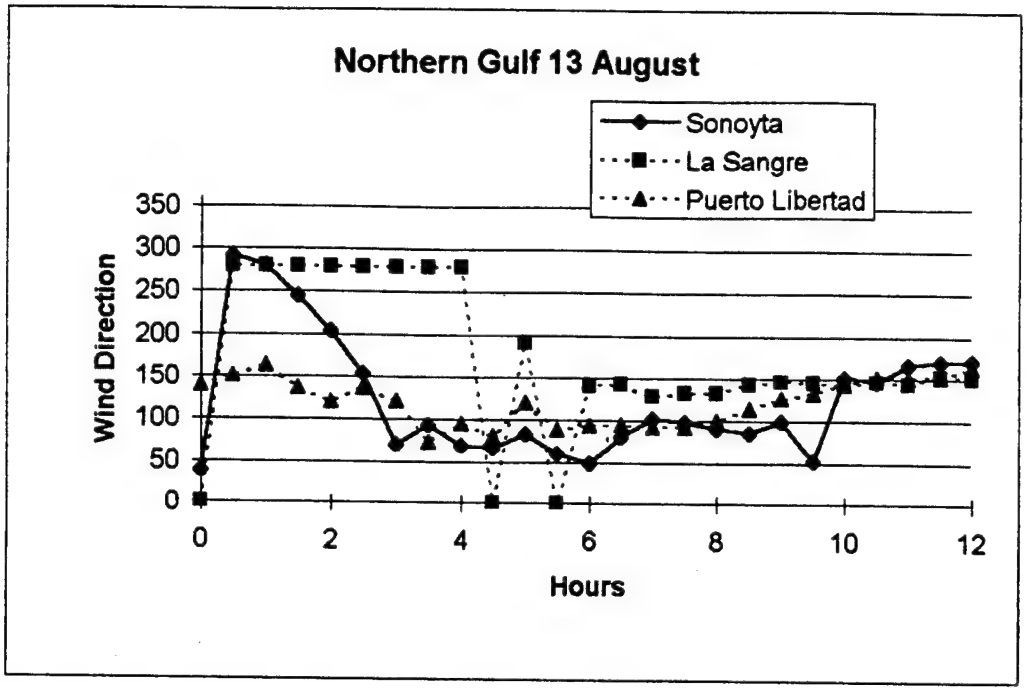

Figure 15c) Same as figure 15a, except northern Gulf of California.

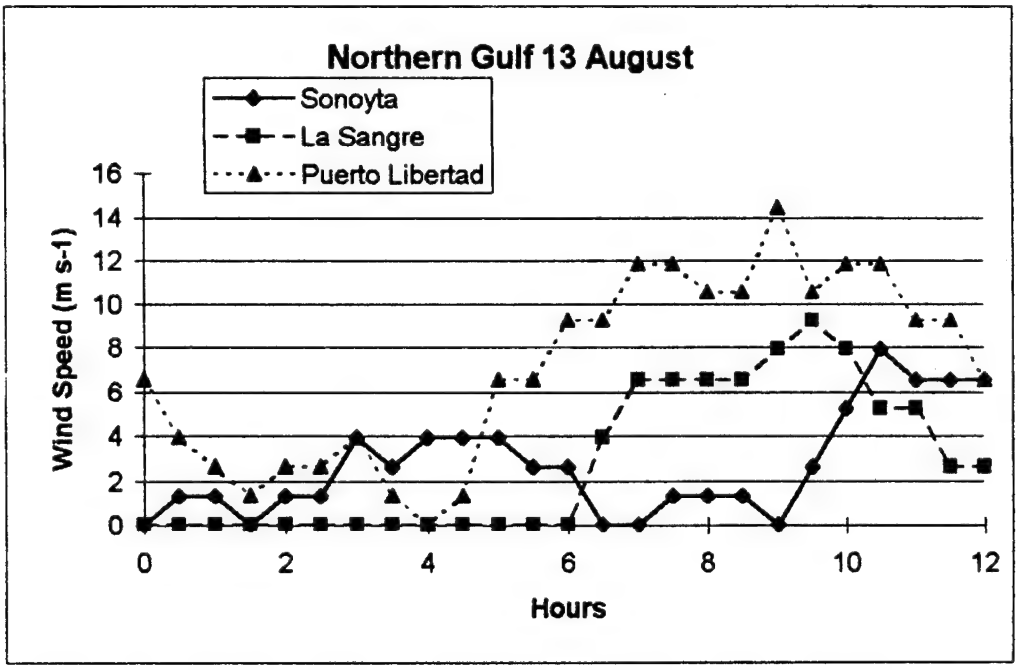

Figure 15d) Same as figure 15b, except for northern Gulf of California.

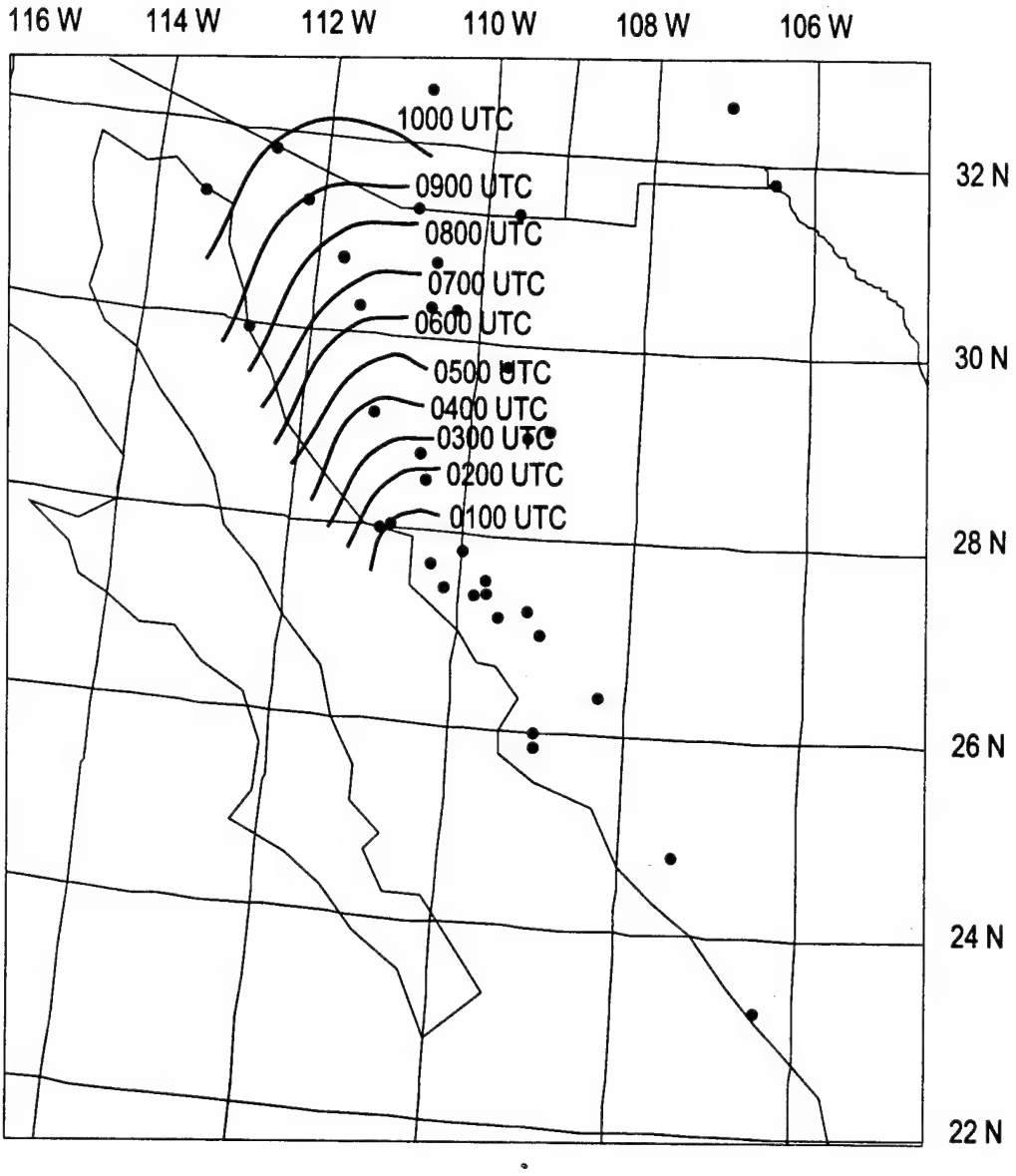

Figure 16) Isochrone analysis of leading edge of surge observed on 13 August.

CHAPTER 3

Evaluation of Conceptual Model

The conceptual model proposed by Stensrud et al. (1996) describes a possible mechanism for the development of strong gulf surges. They performed 32 consecutive 24 hour simulations using a hydrostatic version of the Pennsylvania State University / National Center for Atmospheric Research (PSU / NCAR) mesoscale model version 4 (MM4) (Anthes and Warner 1978; Anthes et al. 1987) and data from SWAMP-90 to study the Mexican monsoon. Results indicate a phase relationship between the 300 mb mid-latitude flow well north of the gulf and easterly waves in the tropics. Strong surges develop when a mid-latitude trough passes north of the Gulf of California 1-2 days prior to the passage of an easterly wave south of the gulf. They propose that gulf surges originate from these easterly waves that assist in the generation of Kelvin waves that propagate up the gulf. Further, they theorize that weak gulf surges can occur owing to the passage of an easterly wave alone, but these surges are unlikely to reach the United States.

Following the procedure of Stensrud et al. (1996), two Hovmöller diagrams are made for the EMVER-93 season (figures 17 and 18) using the NCEP global analyses. For the 8 July 1993 gulf surge, the 300 mb Hovmöller diagram from 40 N (figure 17) indicates that a persistent weak trough remains northwest of the gulf (110 W) for several days before the surge, suggesting that any surge that develops will be weak. The 850 mb Hovmöller diagram from 19 N (figure 17) indicates the passage of an easterly wave over 110 W after the surge. Actually, this easterly wave is Hurricane Calvin that significantly affected the flow in the southern gulf. For this case, the

conceptual model does not necessarily indicate the proper conditions for a strong surge. The northern Hovmöller diagram suggests that a short-wave trough passed to the north of the gulf two days before the observed surge, but does not indicate the passage of the large scale trough. Based upon the observed Hovmöller diagrams, the conceptual mode of Stensrud et al. does not indicate the potential for a strong gulf surge. Since the observations confirm the existence of a surge, the conceptual model of Stensrud et al. fails for this case.

For the 13 August 1993 gulf surge, the 300 mb Hovmöller diagram for 40N (figure 17) again indicates the presence of a persistent trough at 110W which remains throughout the surge. The 850 mb Hovmöller diagram for 19N (figure 18) indicates the passage of an easterly wave 3 days prior to the surge. In this case, the conceptual model again fails to indicates the potential for a strong gulf surge.

This analysis highlights the difficulty of predicting based upon rules of thumb or simple conceptual models. Certainly, the monsoon season during the summer of 1993 was anomalous in that few surges were observed making this a challenge for any forecasting tool. But the best hope in the forecasting of surges comes from numerical prediction models. Therefore, we turn our attention to the ability of the operational ETA model to forecast these two surges during 1993.

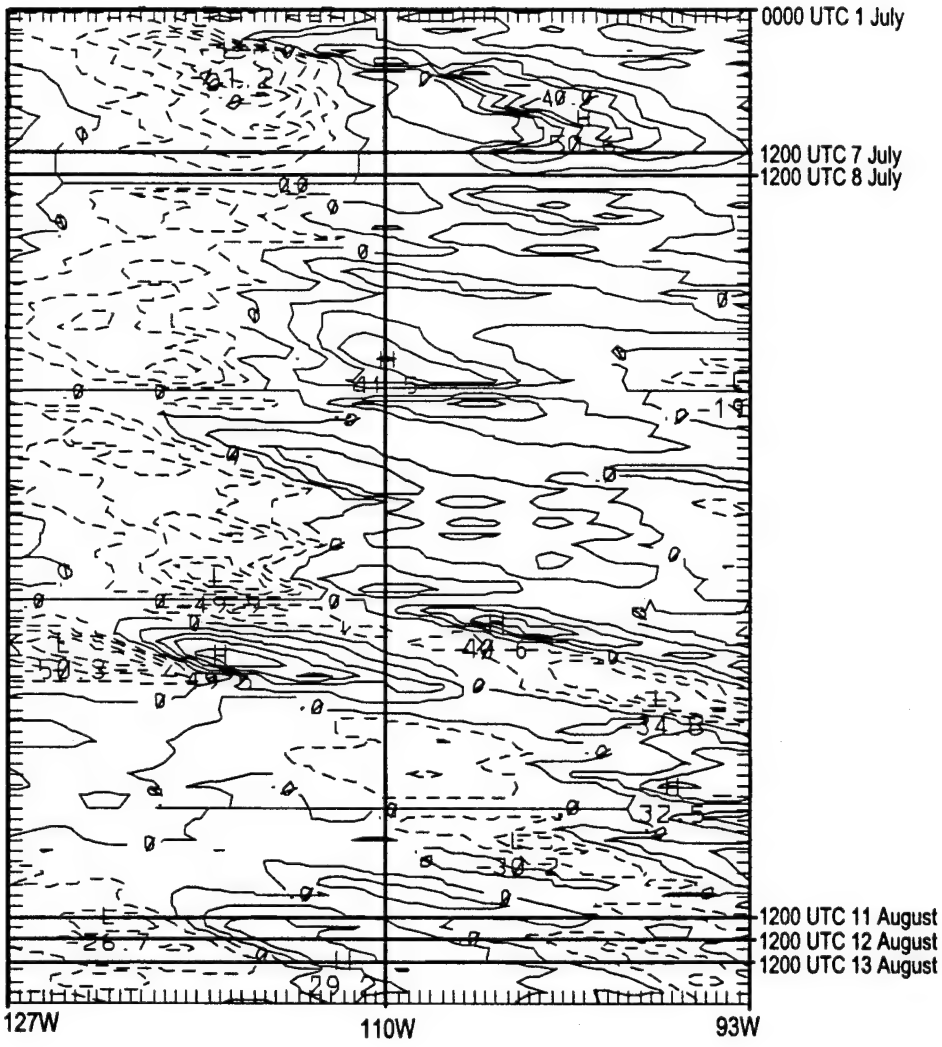

Figure 17) Hovmöller diagram of 300 mb meridional wind component at 40N. From 127W to 93W. Southerly winds are depicted as solid contours. Contour interval is 10 ms-1.

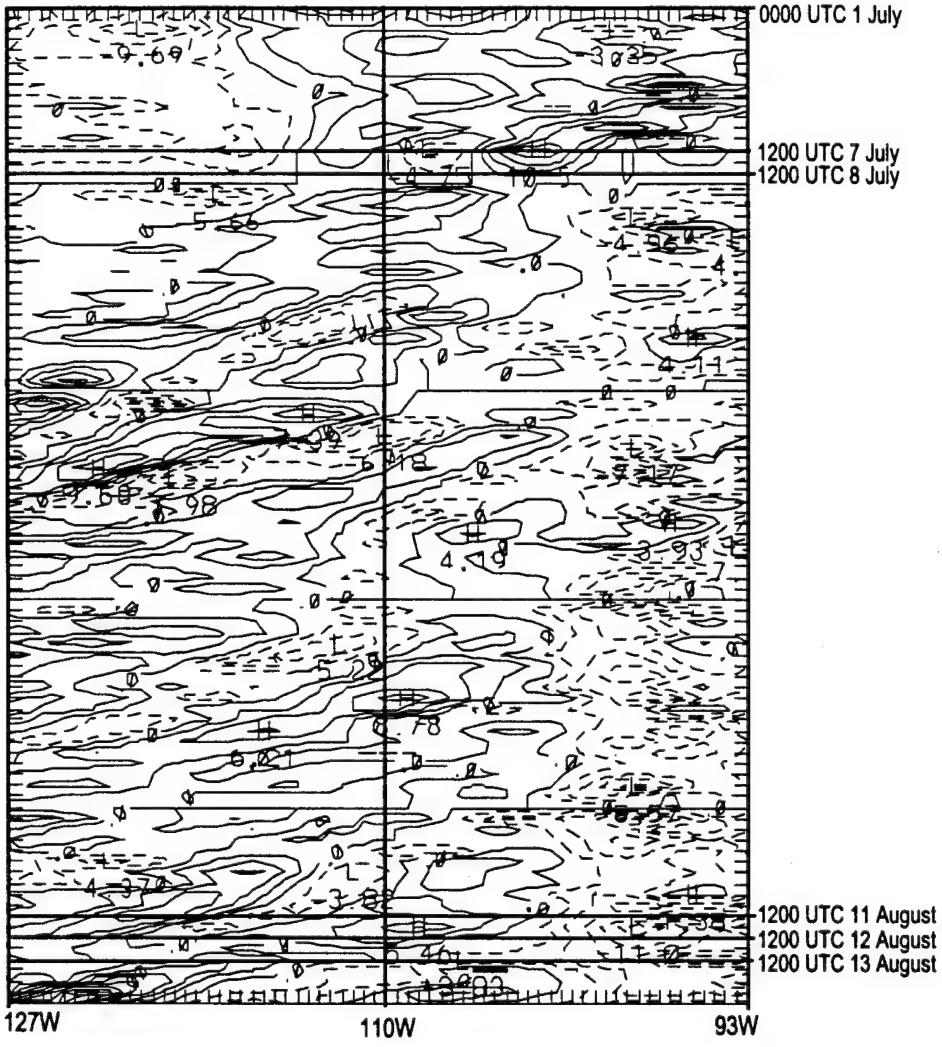

Figure 18) Hovmöller diagram of 850 mb meridional wind component at 19N. From 127W to 93W. Southerly winds are depicted as solid contours. Contour interval is 2 ms-1.

CHAPTER 4

ETA Model Results

The NCEP operational ETA (Messinger et al. 1988; Janjic 1990) model forecasts from this period are compared to observations since the ETA model represents the latest development of operational models available during the 1993 monsoon season. Knowledge of how well the ETA model generates gulf surges will benefit forecasters trying to predict their occurrence. Although the ETA model was run with a 81 km grid, results from Dunn and Horel (1994a,b) suggest that the 48 km version of the model behaves in a similar fashion.

The ETA model forecast beginning at 1200 UTC 8 July (figures 19 and 20) indicates that the low-level flow initially is weak throughout the Gulf of California with most of the moisture confined to the mountains of the Sierra Madre Occidental and the southeast gulf. Over the next 24 hours the ETA model is able to generate weak southwest flow and slightly increases moisture in the northern gulf. Precipitation develops in the southern Gulf of California and along the western slopes of the Sierra Madre Occidental, east of the southern gulf with amounts of less than 5 mm. For this case, the ETA model gives a slight indication of a surge event, although not up to Arizona as seen in the observations.

Since there was a small indication of a surge on 12 August in the central gulf prior to the more clearly observed surge on 13 August we look at the ETA model forecasts beginning 48 hours prior to 1200 UTC 13 August. For the 1200 UTC 13 August surge event, a 48 hour forecast is not available. Because of this, two 24 hour

ETA model simulations are examined. The first 24 hour simulation is valid at 1200 UTC 12 August (figures 21 and 22) and the second at 1200 UTC 13 August (figures 23 and 24). The first ETA model simulation generates convection and increases moisture in the southern Gulf of California by 0000 UTC 12 August. By the end of the simulation, the air mass over the northern gulf drier due to northwesterly flow, while the southern gulf is moist with southerly flow (figure 21). Obviously the model was able to pick up on the increased cloudiness and convection in the southern gulf throughout the afternoon and evening, but it appears to have over forecast the convection and northward extent of the moisture at this time.

For the second model run, the ETA model starts out considerably drier than indicated in the prior forecast with northerly low-level flow throughout the northern gulf (figure 23a). By the end of the simulation the model again increases the moisture in the southern and central gulf with weak southerly flow. The northern gulf remains dry and under southwesterly winds, while upslope southwest winds are evident in the central gulf. Cyclonic trajectories of air parcels entering into Arizona suggest the moisture in the gulf is still shut off. There is no indication of the observed surge up to Arizona in this simulation.

From the perspective of a forecaster, none of these ETA simulations would have indicated the progression of a gulf surge into southern Arizona. Although the ETA model was able for forecast flow up into Mexico with precipitation over the Sierra Madre Occidental, this is a common occurrence and does not indicate an impending surge. Instead, the ETA model forecasts for all three days show southwesterly cyclonic flow over Arizona typical of a dry pattern.

It is important to mention that since only these three ETA model simulations are examined, they are not a valid sampling and cannot indicate the accuracy of the operational 1993 ETA model during most conditions. They do, however, show that for two relatively well observed surge events the ETA model was unable to develop a surge. Therefore, the ETA model was unable to tap into the gulf moisture for these cases, and would not be able to accurately forecast any resulting precipitation in Arizona. This result substantiates the conclusions of Dunn and Horel (1994a,b) regarding the inability of the ETA model to accurately forecast Arizona precipitation during the monsoon. It should be noted that the ETA model has been revised within the last 3 years and that changes to the model will hopefully result in better predictions of surge events and increased convection over the desert southwest. After reviewing the inability of the 1993 ETA model to simulate surges, a mesoscale model is used to determine the ability of a higher resolution model with different parameterizations to simulate gulf surge events.

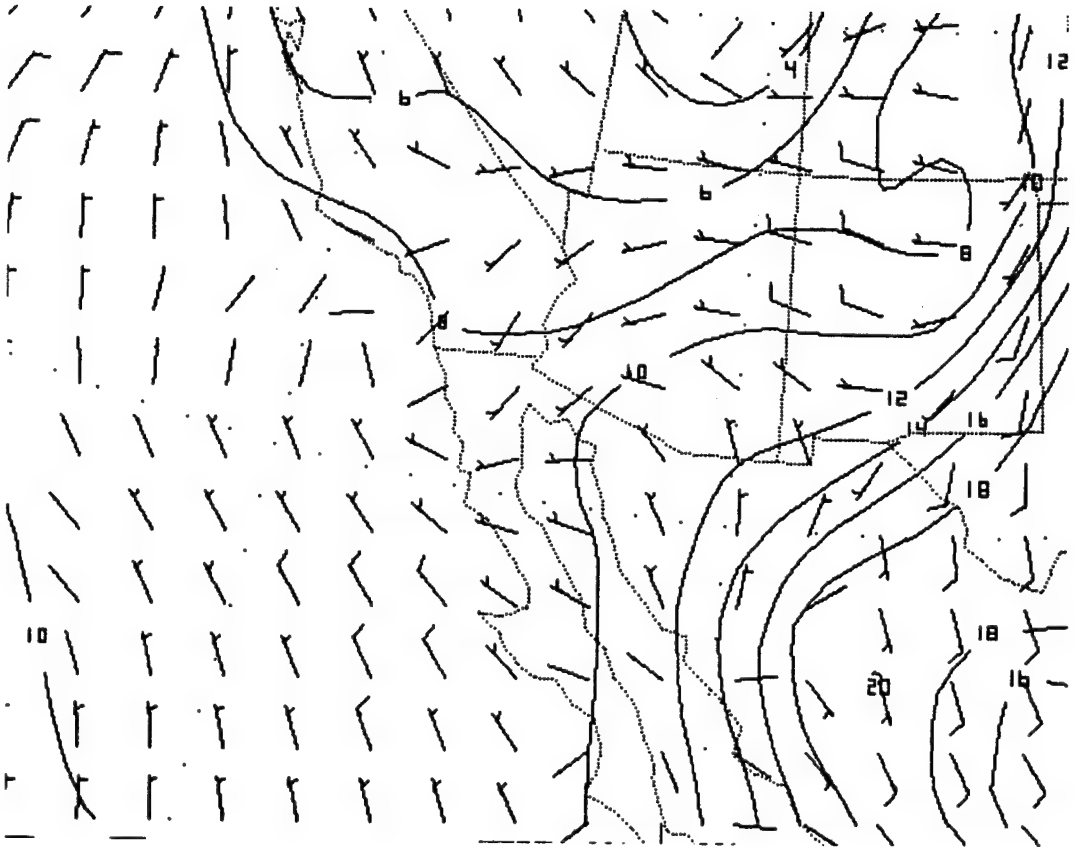

Figure 19a) 1200 UTC 7 July ETA model 1000 mb winds and mixing ratios (g kg-1), valid 1200 UTC 7 July. Full barb is 10 ms-1.

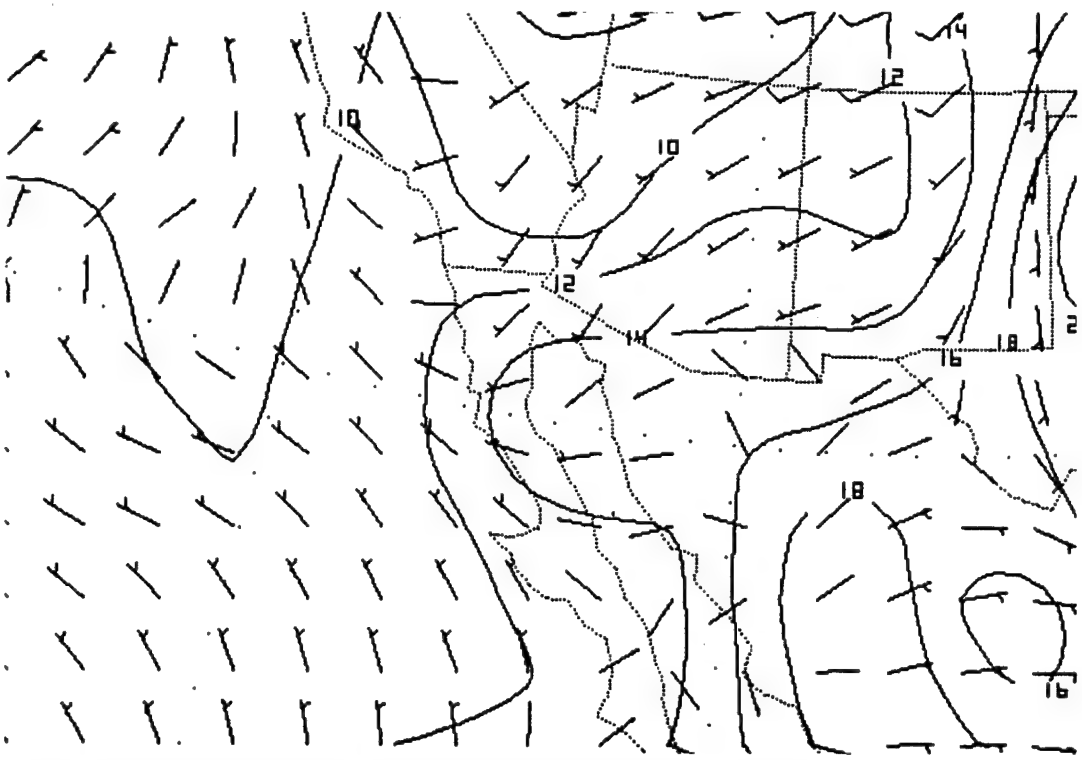

Figure 19b) Same as figure 19a, except valid at 0000 UTC 8 July.

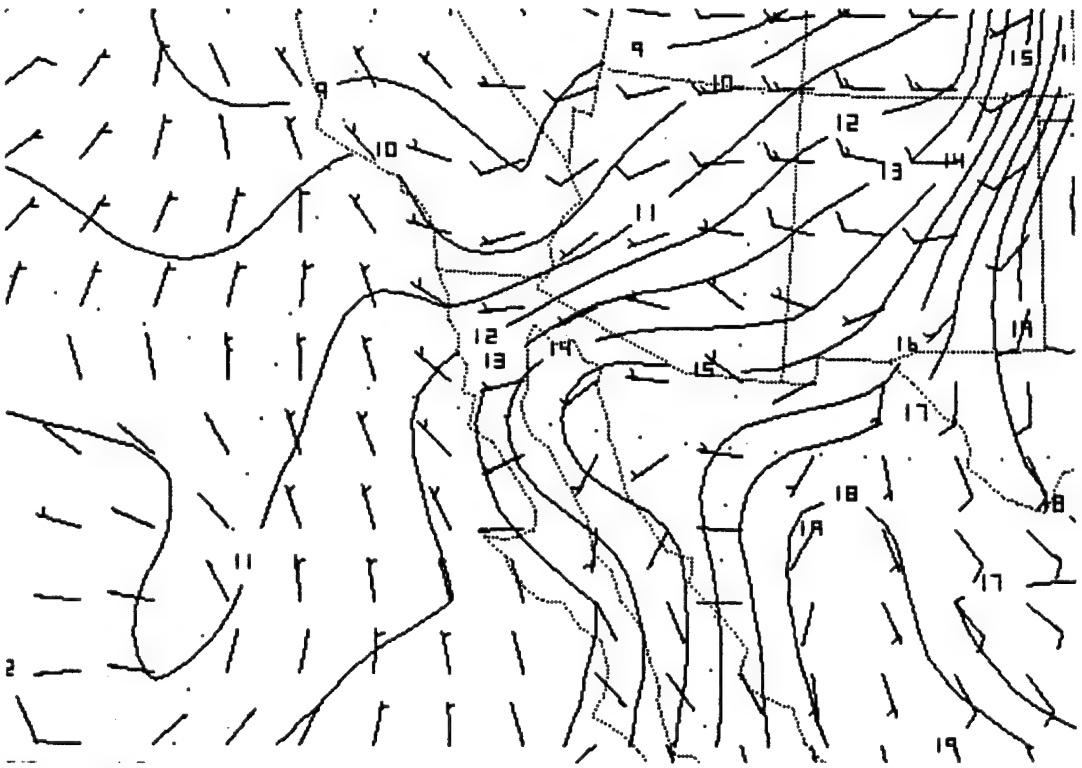

Figure 19c) Same as figure 19a, except valid at 1200 UTC 8 July.

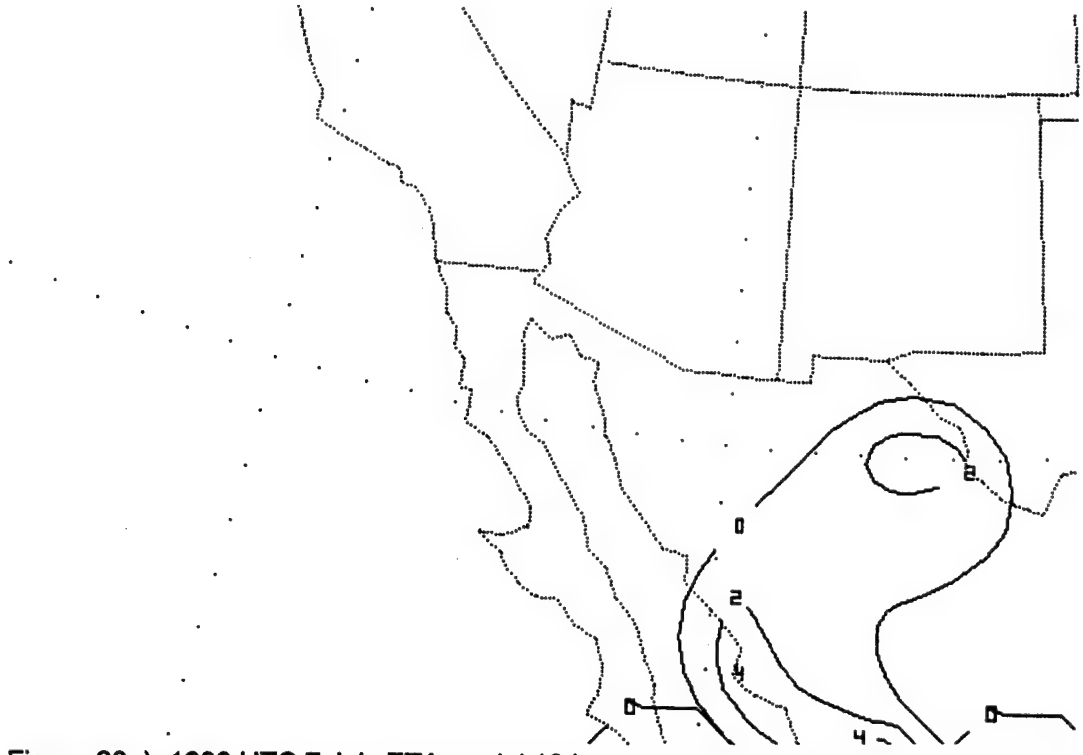

Figure 20a) 1200 UTC 7 July ETA model 12 hour convective and explicit precipitation (mm) valid 0000 UTC 8 July.

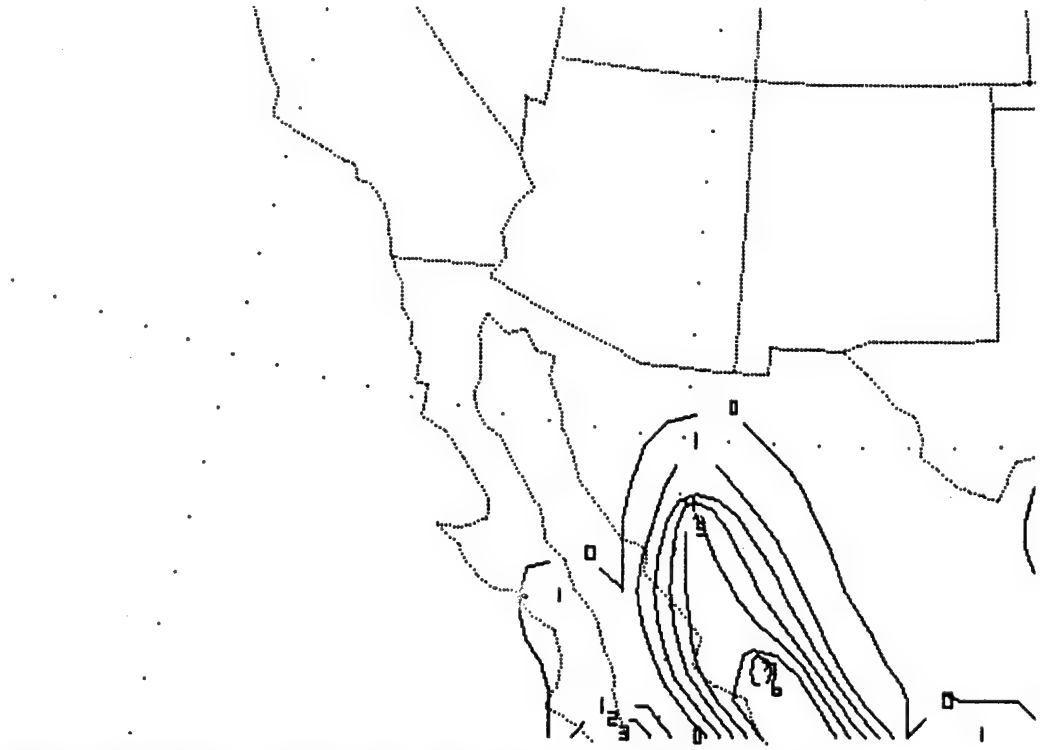

Figure 20b) Same as figure 20a, except valid at 1200 UTC 8 July.

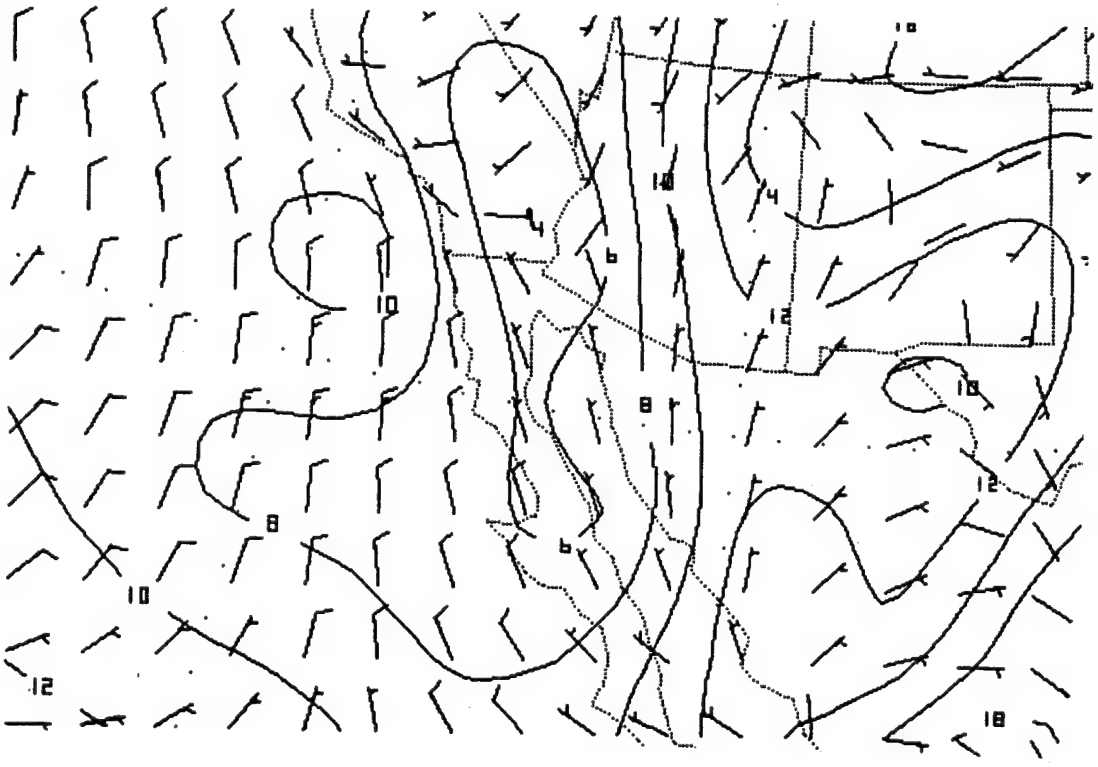

Figure 21a) 1200 UTC 11 August ETA model 1000 mb winds and mixing ratios (g kg-1) valid 1200 UTC 11 August. Full barb is 10 ms-1.

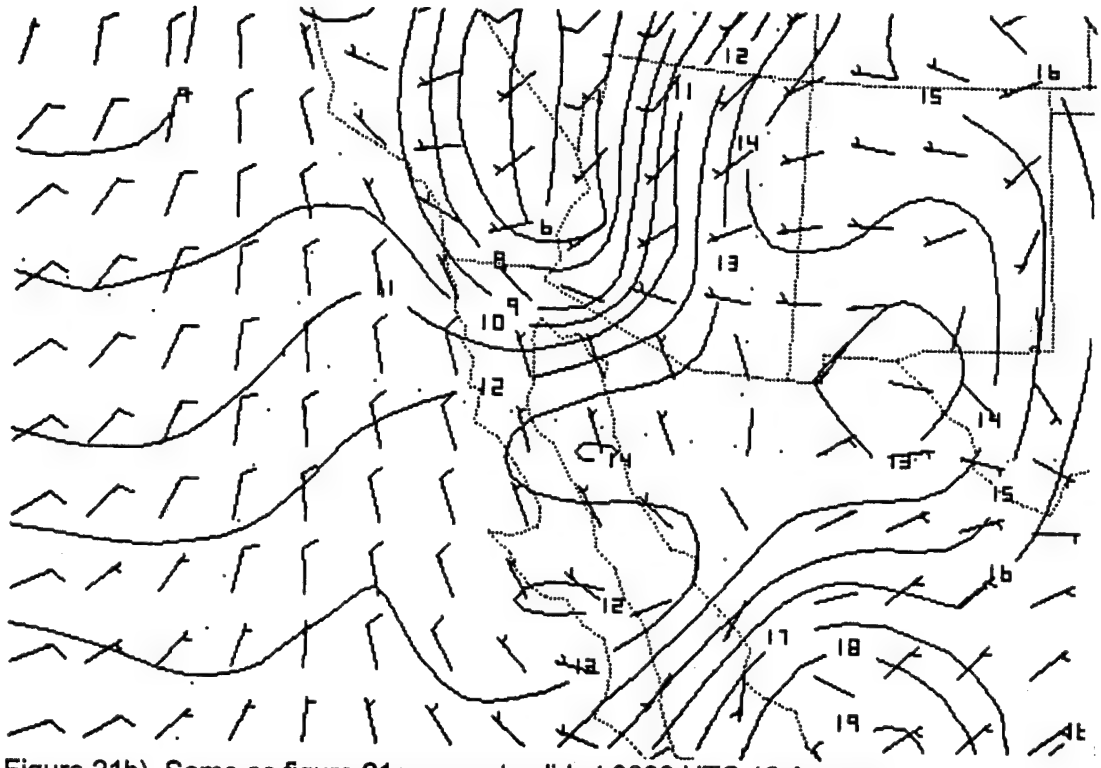

Figure 21b) Same as figure 21a, except valid at 0000 UTC 12 August.

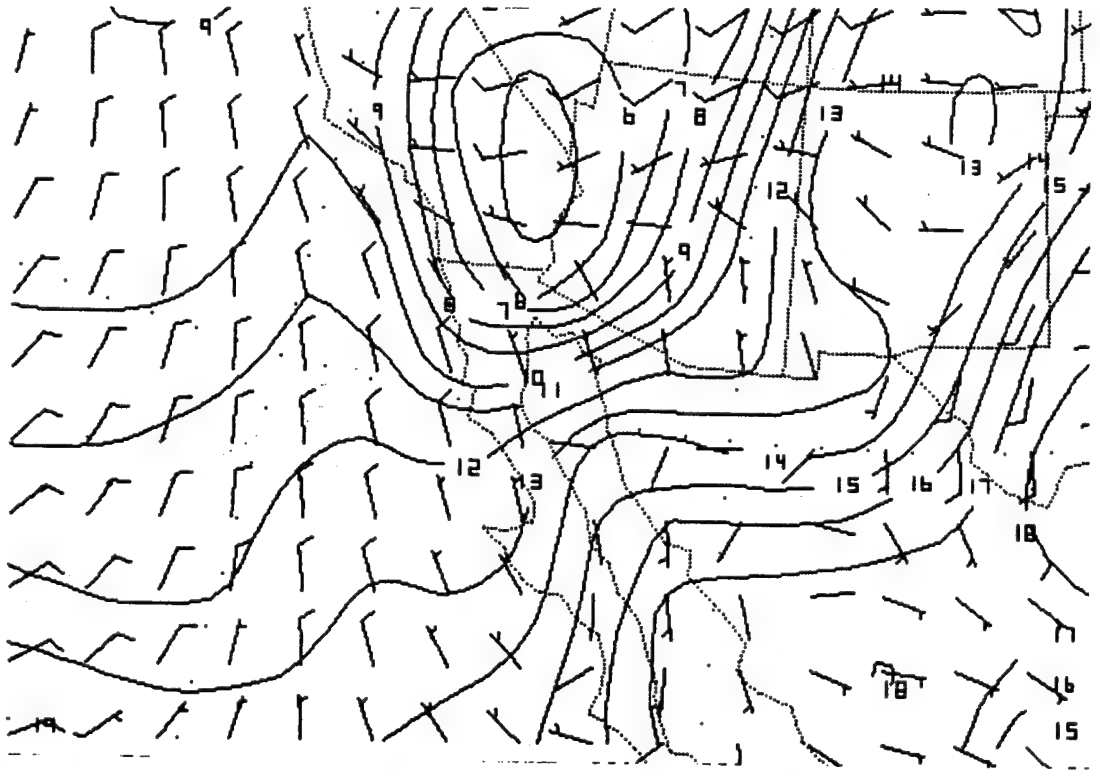

Figure 21c) Same as figure 21b, except valid at and 1200 UTC 12 August.

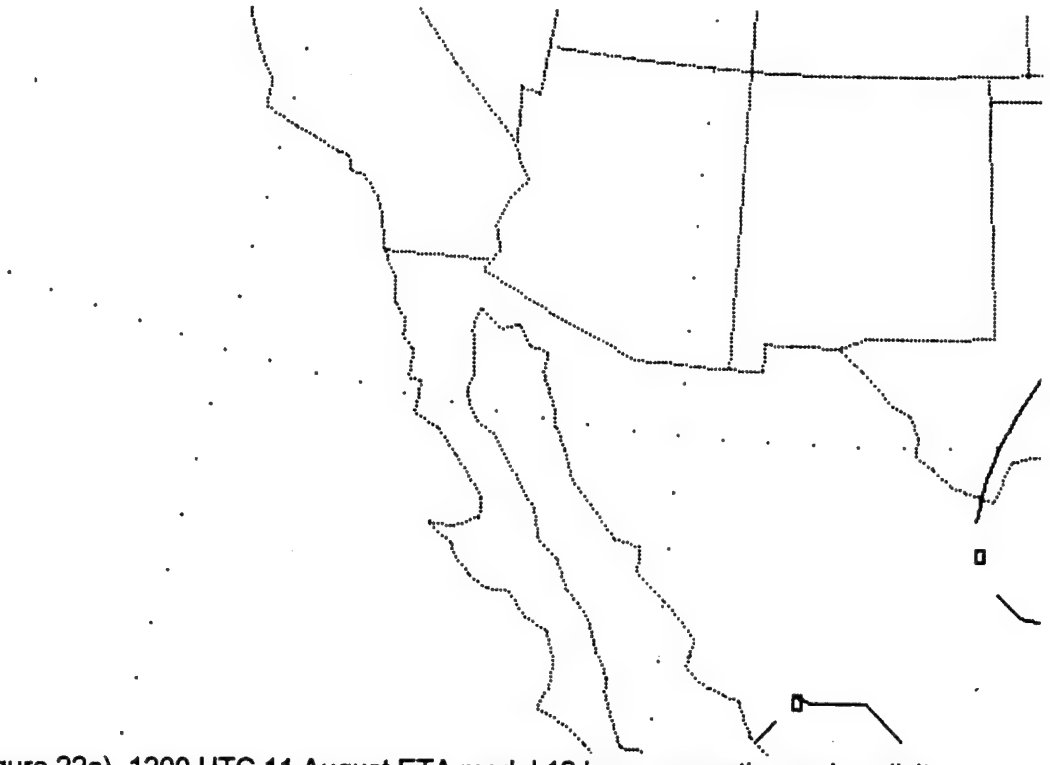

Figure 22a) 1200 UTC 11 August ETA model 12 hour convective and explicit precipitation (mm) valid 0000 UTC 12 August.

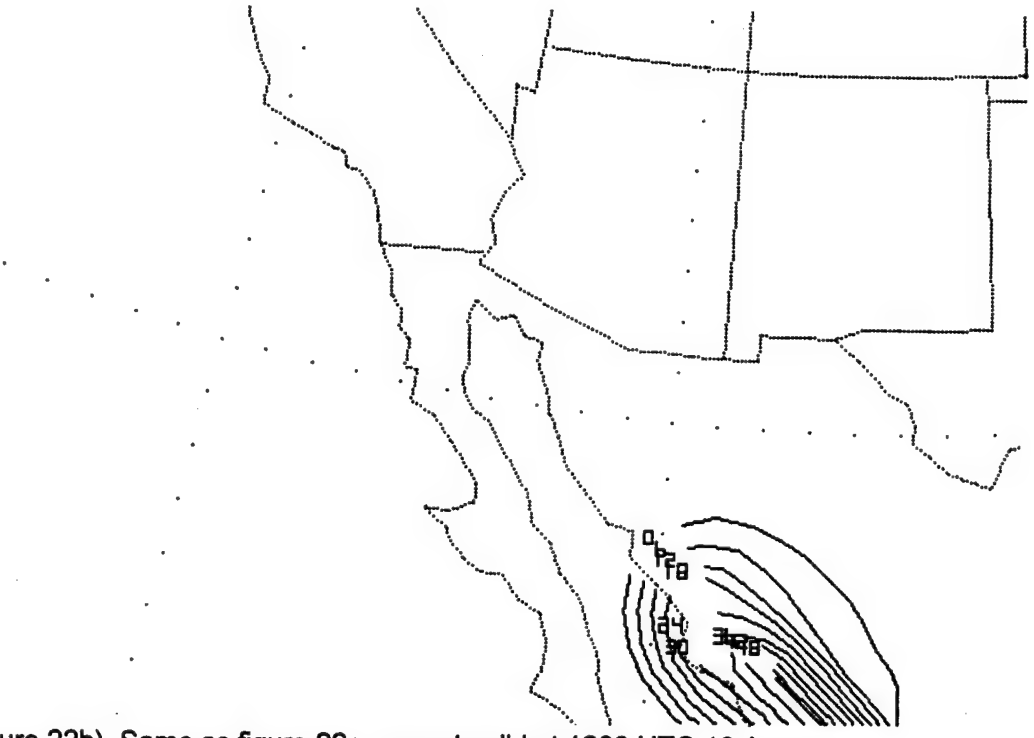

Figure 22b) Same as figure 22a, except valid at 1200 UTC 12 August.

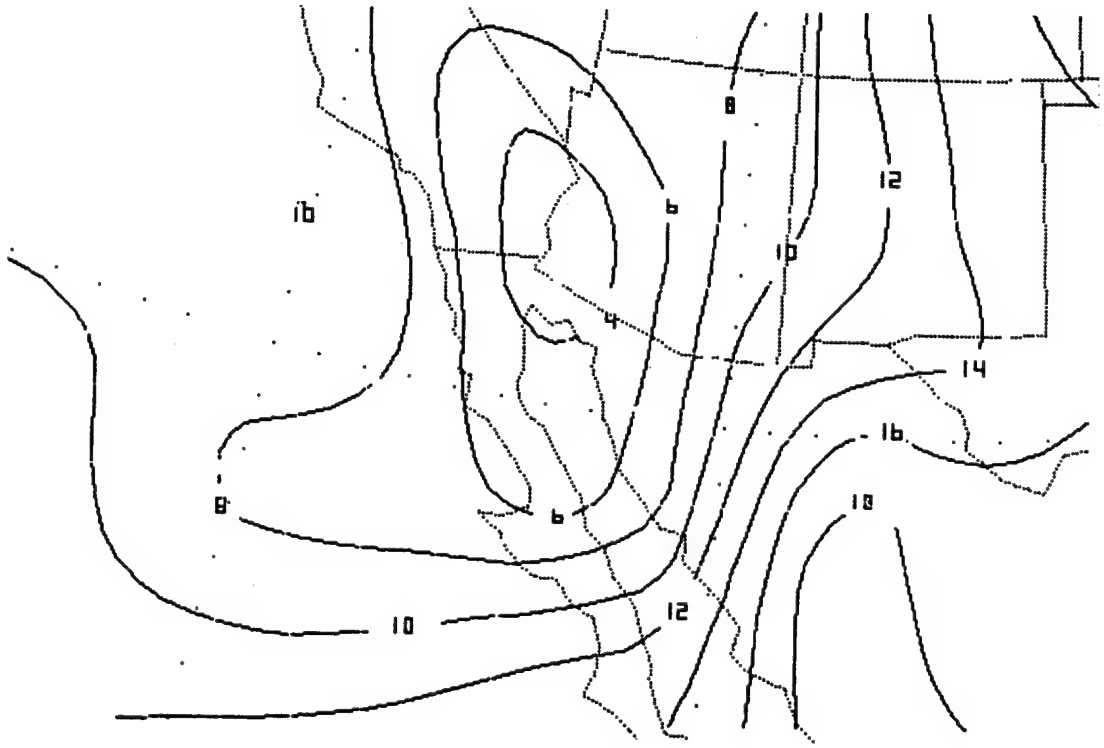

Figure 23a) 1200 UTC 12 August ETA model 1000 mb winds and mixing ratios (g kg-1) valid 1200 UTC 12 August. Full barb is 10 ms-1. (Winds are missing from figure 23a).

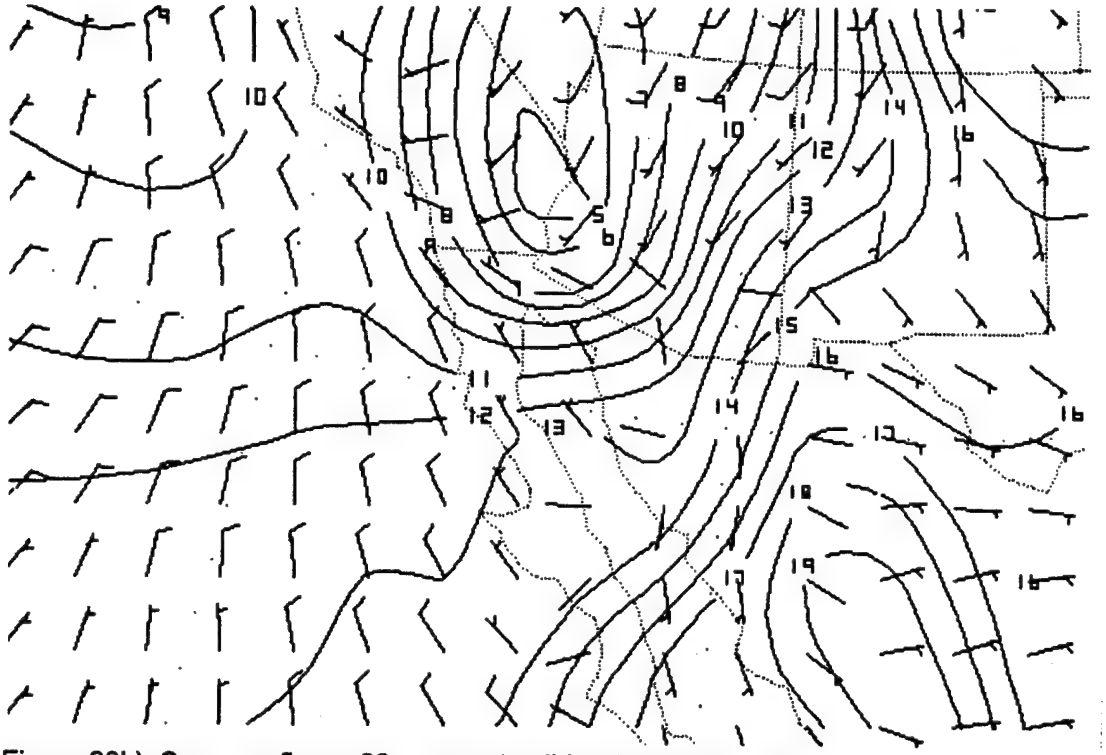

Figure 23b) Same as figure 23a, except valid at 0000 UTC 13 August.

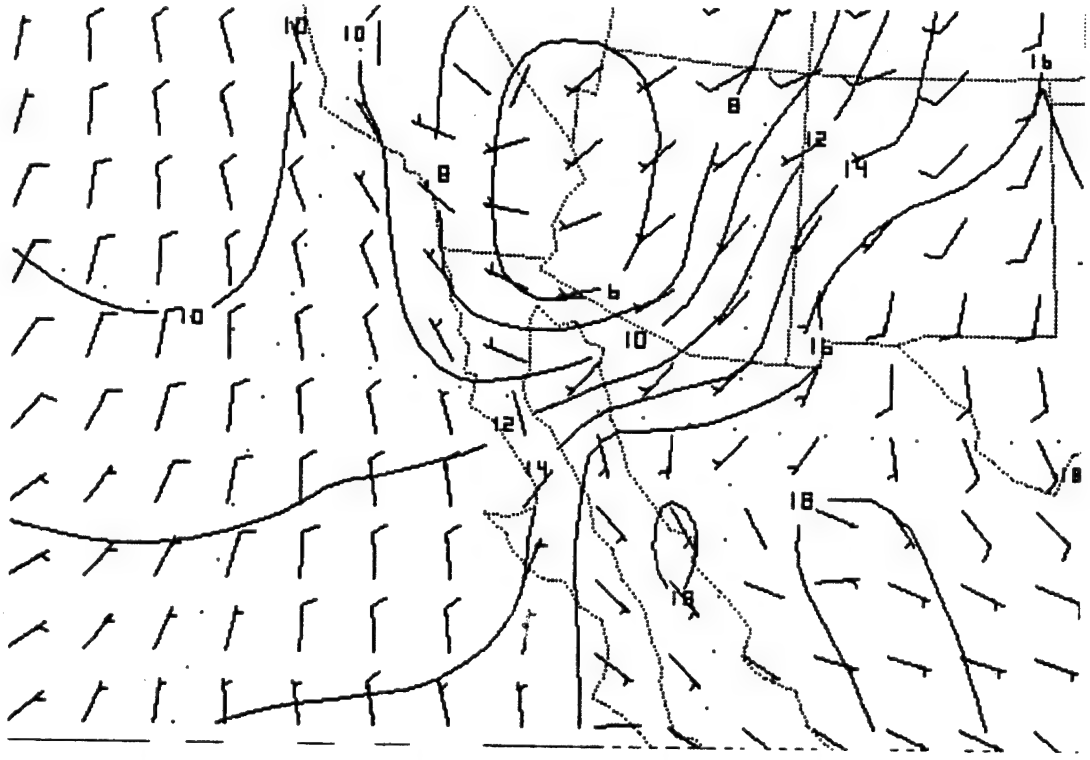

Figure 23c) Same as figure 23b, except valid at and 1200 UTC 13 August.

Figure 24a) 1200 UTC 12 August ETA model 12 hour convective and explicit precipitation (mm) valid 0000 UTC 13 August.

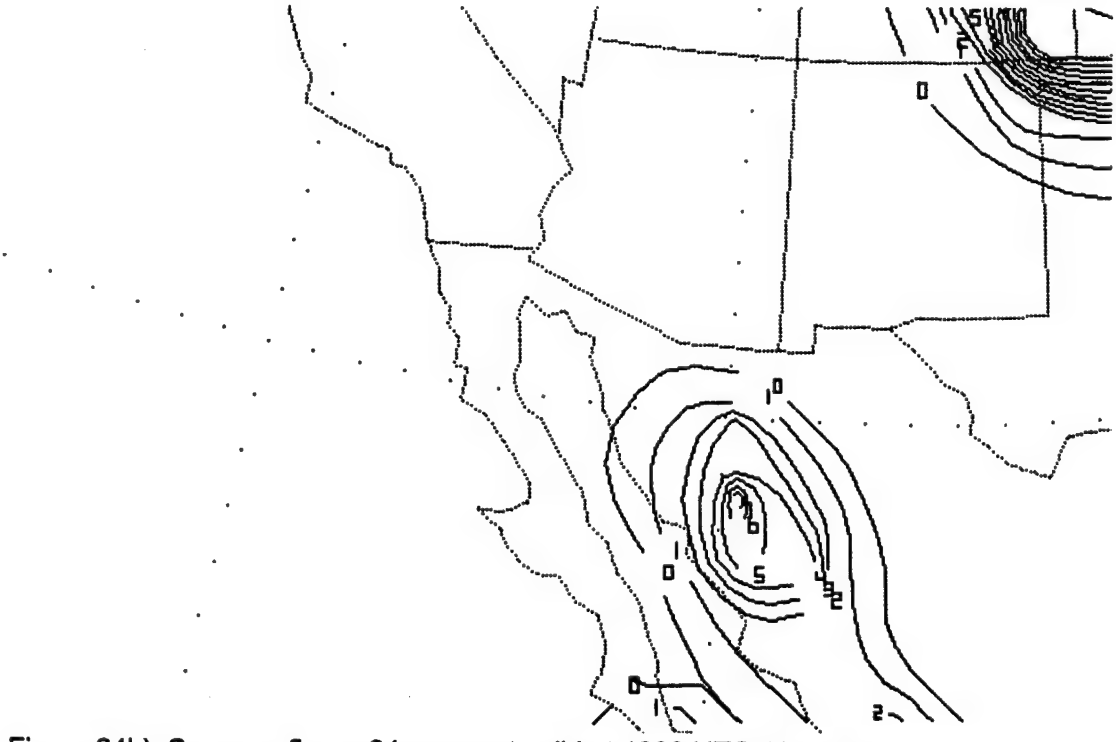

Figure 24b) Same as figure 24a, except valid at 1200 UTC 13 August.

CHAPTER 5

Mesoscale Model Description

A non-hydrostatic version of the Pennsylvania State University / National Center for Atmospheric Research (PSU/NCAR) mesoscale model version 5 (MM5) (Grell 1993; Haagenson 1994; Dudhia 1993) is used to simulate these surge events. The parameterization schemes and basic model structure are described briefly because it is necessary to know the assumptions of the model parameterization schemes in order to interpret the results of the simulations. These are:

Planetary boundary layer: Modifications are made to the standard version of this model to include a 1.5 order Gayno-Seaman turbulence closure scheme (Gayno 1994) within the planetary boundary layer.

Grids and terrain: A 18 km by 18 km coarse grid is used with two-way interactive 6 km by 6 km nested grid (figure 25). A terrain following vertical σ coordinate is used and is defined as $\sigma = (p - p_t) / (p_s - p_t)$, where p_t is the pressure at the top of the domain set at 50 mb, and p_s is the surface pressure. The sigma coordinate is defined with 30 layers that are approximately 20 mb thick near the surface and deepen well above the surface. The terrain field is interpolated from global terrain data with 30 second resolution. Additionally, the terrain database considers 13 land use categories (Guo 1994). A two-way interactive nested grid is used only with the July case and is positioned over the region where the coarse model domain developed a surge. An outline of the nested grid domain is depicted on coarse grid terrain map (figure 25).

Convective parameterization: A Kain-Fritsch (Kain and Fritsch 1980) convective parameterization scheme for deep convection is used for both grids. This scheme sequentially lifts 60 mb deep layers within the lowest 300 mb, beginning with the lowest layer, and evaluates whether or not deep convection can occur based upon the trigger function specified in Fritsch and Chappell (1980).

Explicit convective parameterization: An explicit bulk convective scheme is used to predict cloud water, rain water, snow and ice based on microphysical processes (Dudhia 1989; Grell et al. 1994). Supercooled water is not accounted for and falling snow immediately turns to water at the melting level.

Static Initialization: A static initialization is used in which the model initial conditions are specified using NCEP global analyses. The NCEP analyses at the model start time and at each succeeding twelve hour point are interpolated onto the model grid. This provides the initial conditions for the model, and boundary conditions for the coarse grid throughout the model simulation. NCEP analyses then are modified using a successive-correction objective analysis technique (Benjamin and Seaman 1985) to blend in rawinsonde data throughout the domain and enhance the quality of the analyses. Special pibal data from the SWAMP-93 and EMVER-93 data sets are included in the initialization. An additional correction is made to the model initial conditions for the water temperatures of the Gulf of California. These are modified to reflect the measurements of Ripa and Marinone (1989) and values of 29 °C and 31 °C are used for the months of July and August, respectively.

The simulation for the 8 July 1993 gulf surge is initialized at 1200 UTC 7 July and run for 24 hours. For this case, the NCEP global data are missing at 0000 UTC 8 July and the boundary conditions are interpolated between 1200 UTC 7 July and 1200 UTC 8 July. The simulation for the 13 August 1993 gulf surge is initialized at 1200 UTC 11 August and run for 48 hours in order to attempt to model the cooling in the central gulf on 12 August and the gulf surge on 13 August.

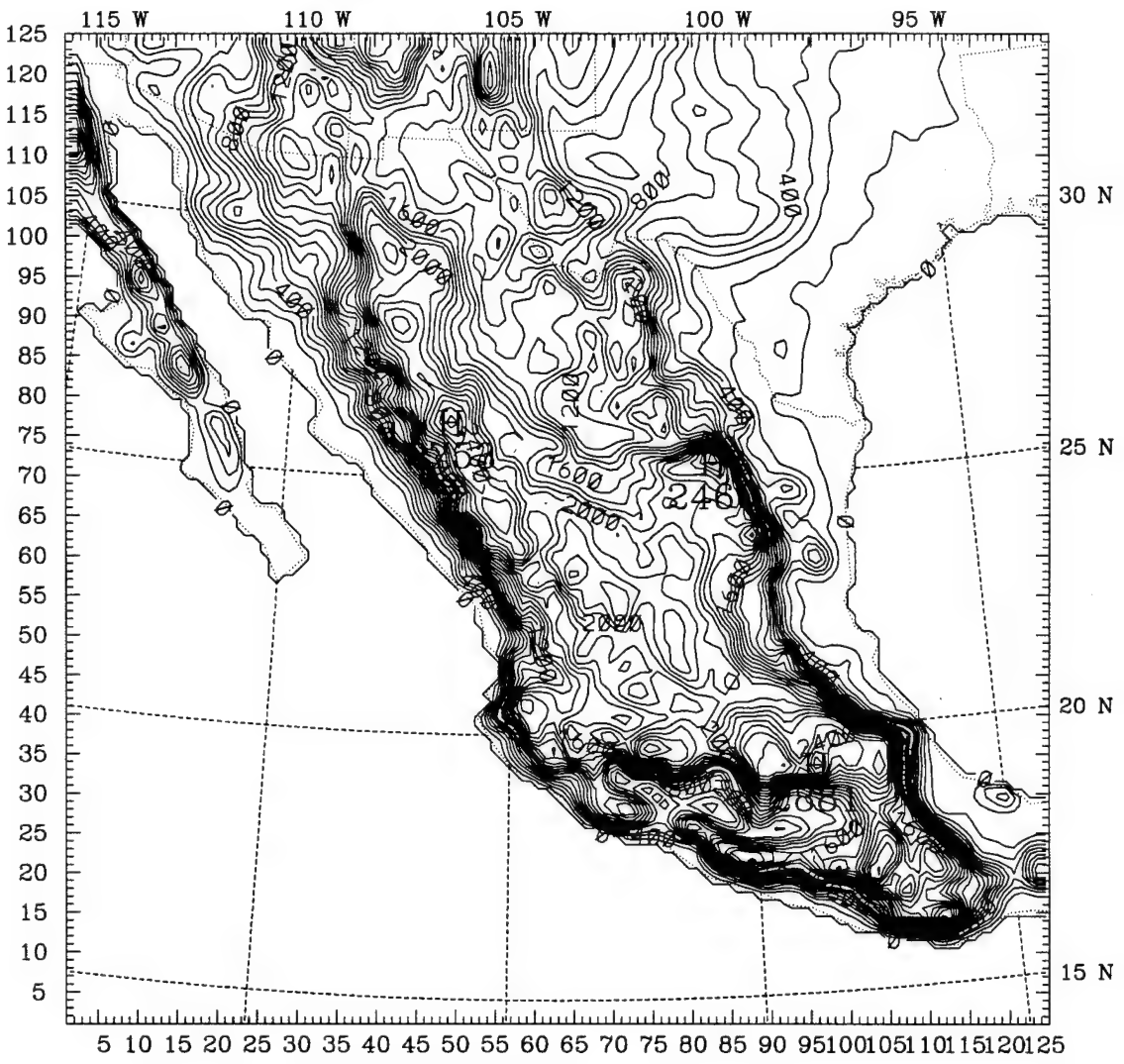

Figure 25) MM5 coarse grid domain and terrain field contoured every 100m. Outline indicates the nested domain used in the July simulation.

CHAPTER 6

Mesoscale Model Results

6.1 8 July 1993

The mesoscale model initializes at 1200 UTC 7 July with weak and variable low-level winds throughout the Gulf of California and no indication of a surge (figure 26a). A tropical depression centered at 17.0N, 105.0W also is initialized in the mesoscale model (not shown). By 1500 UTC the model moves the tropical depression due west to 17.0N, 106.0W while generating 2 cm of rainfall to the east of the cyclone during the previous 3 hours (not shown). The model also begins to develop weak convection over the western slopes of the Sierra Madre Occidental, even though the low-level flow remains relatively weak. Satellite imagery confirms the presence of a developing tropical cyclone, but to the northeast of the MM5 circulation (not shown). The imagery also does not show any convection over the Sierra Madre Occidental. Surface observations indicate primarily weak flow during this time that corresponds well with the model results (not shown).

Over the next 3 hours the mesoscale model begins to develop significant convection over the western slopes of the Sierra Madre Occidental with 3 hour precipitation totals of 1.77 cm to the northeast of Los Mochis and nearly 1 cm to the east of Mazatlan (not shown). The model tropical cyclone moves northwestward to 17.5N, 106.9W and intensifies slightly. During this same time, the observed tropical cyclone is upgraded to Hurricane Calvin and is located 280 km northeast of the model prediction (not shown). The model generates more than 8 cm of precipitation due to

the cyclone. Surface observations and model output continue to indicate light winds along the coastal zone, but MM5 continues to produce precipitation over the mountains over the Sierra Madre Occidental (figure 26b) while none is indicated on satellite imagery (not shown). Evidently the convective parameterization scheme is being triggered too early, possibly owing to inaccuracies in either the trigger function, the model initial condition, or both.

By 2100 UTC observations indicate the development of convection over the western slopes of the Sierra Madre Occidental (not shown) where the mesoscale model has been generating precipitation over the previous 5 hours. Although satellite imagery depicts a considerable increase in cloudiness, the model is still creating a larger area of precipitation than can be accounted for in the satellite imagery. MM5 moves the hurricane to the north at 18.7N, 107.1W and continues to generate a large amount of precipitation associated with it. The observed hurricane also moved to the northwest during this time and is now at 20.0N, 105.2W, approximately 220 km northeast of the MM5 location. The low-level wind field along the entire eastern Gulf of California increases to 5-7 ms-1 of upslope flow (not shown). Observations along the coast agree with the relatively weak onshore flow seen in the model output.

During the late afternoon convection increases and by 0000 UTC 8 July satellite imagery indicates a large area of convection over all of the western Sierra Madre Occidental (figure 7b). The mesoscale model continues to produce convection over the Sierra Madre Occidental but the coverage has lessened over the past three hours. The strongest model convection is now along the southern portion of the Sierra Madre Occidental (figure 27c). MM5 moves the hurricane to the northeast to 19.6N, 106.5W with heaviest convection remaining to the east of the hurricane center, while

observations place Hurricane Calvin at 20.3N, 105.6W, only about 125 km away from the mesoscale model. The model wind field along the Gulf of California shows upslope of 5-10 ms-1 along the northern gulf, and 5-7 ms-1 along the southern gulf, in agreement with the limited observations (figure 8b).

Infrared satellite imagery at 0300 UTC 8 July (not shown) continues to show a large area of cloudiness, but the evolution of the infrared temperatures suggest the clouds are comprised of thick cirrus from the earlier thunderstorms rather than newly developed convection. MM5 in general shows diminishing convective activity with the strongest areas associated with Calvin and north of Mazatlan. Whereas during the previous 15 hours the model data indicated no distinct, cohesive surge-like feature, low-level winds along the eastern coastal zone of the southern Gulf of California are beginning to have an organized structure. Between the southern Gulf of California and the higher slopes of the Sierra Madre Occidental, a zone of southeasterly winds 145 km wide and 425 km long develops (figure 27a). Associated with this wind zone are higher surface pressures and lower temperatures. This feature is a gulf surge that has formed close to the location of strong convection in the southern gulf and is hereafter referred to as the southern model surge. The location of this southern model surge agrees remarkably well with observations from El Carrizo that shows the passage of a surge at 0200 UTC (figure 9).

Over the next hour the southern model surge moves northwest at speed of 9.3 ms-1 (figure 29), about one-third the observed surge speed of 30 ms-1 (figure 10). This southern model surge has widened to 180 km and lengthened to 470 km. The model also develops a cohesive band of southerly flow along the eastern coastal zone of the northern gulf that is 510 km ahead of the southern model surge with a

width of 130 km and length of 360 km (figure 28a). This second surge is hereafter referred to as the northern model surge. The character of each MM5 gulf surge is different in each of these cases, with stronger cooling and stronger southeasterly winds occurring with the southern surge.

Satellite imagery and mesoscale model output both indicate decreasing convection by 0600 UTC 8 July (figures 7c and 26b), although MM5 is still producing precipitation along the southern Sierra Madre Occidental and associated with the tropical cyclone. The upslope flow along the northern gulf weakens with model wind speeds typically between 5-7 ms-1 (figure 28c). The leading edge of the northern model surge has moved north-northwestward along the northeastern gulf coastal zone at 10.3 ms-1. The leading edge of the southern model surge has also moved northwest along the gulf coastal zone at 10.3 ms-1 (figure 27c). Model winds behind the northern surge are predominantly southerly with speeds of 5-15 ms-1 (figure 28c). Model winds behind the southern surge are southeasterly with speeds of 10-20 ms-1 (figure 27c). While the model indicates two surges, the limited observations only show one surge.

By 0700 UTC the southern model surge loses some of its cohesiveness owing to increased convection to the north and northeast of the surge that produces low-level cold pools. While the southern surge clearly extends over a distance of 670 km, the leading edge is not easily resolved due to the convective outflows. The southern model surge regains its structure again over the next hour and by 0800 UTC it is 270 km wide and 740 km long with sustained low-level winds of 10-20 ms-1 throughout (figure 29). During these 2 hours the northern model surge continues moving, but in a more northward direction than before (figure 29). The speed of the leading edge of

the northern model surge has increased to 15.1 ms-1 while the winds behind it remain at 5-10 ms-1. Recall that the leading edge of the observed July surge moves at 30 ms-1.

A large area of cold cloud tops continues to be seen in the 0900 UTC 8 July satellite imagery (not shown), but they do not appear to be associated with new convective development. MM5 continues to convect along the southern Sierra Madre Occidental and produces strong southeasterly flow along the southeast coast of the Gulf of California (figure 26d). The observed surge moves into southern Arizona by this time while the northern model surge moves to just south of the Arizona border (figures 27c and 28c). The observed surge continues to move at 30 ms-1, while the northern model surge has accelerated to only 13.6 ms-1. Clearly the model is not discerning the true nature of the surge, but it does develop one.

The model simulation ends at 1200 UTC 8 July with continued convection over the southern Sierra Madre Occidental extending weakly over the southern Gulf of California (figure 26e). Satellite imagery shows clouds over the entire region in which MM5 is convecting but does not clearly indicate any deep convection (figure 7d). By this time southeasterly flow is observed virtually all of the way up the eastern gulf in the model owing to the merging of the southern and northern model surges (figures 26e, 27d and 28d). The flow is strongest in the middle of the gulf behind the leading edge of the southern model surge, which is in agreement with observations from several sites along the gulf indicating moderate southeasterly flow. Pibal observations from Puerto Peñasco show increasing low-level southerly flow at this time consistent with the evolution of the northern model surge that passed Puerto Peñasco at 1000 UTC (figure 8c). Whereas the speed of the northern model surge cannot be

determined at this time, because it extends beyond the model domain, the southern model surge has accelerated to 11.9 ms-1 (figure 29).

While the model does produce a surge on this day, actually two surges, the evolution of the modeled surge disagrees with the limited observations. However, the recognition of the limited nature of the observations leads to some interesting speculation. There is evidence in the observational data to suggest two separate surges, even though these data by themselves are not sufficient to warrant a two surge interpretation. This question may be academic to some extent, but has a significant influence on the evaluation of the physical mechanisms of gulf surges. But before we proceed to this evaluation, let's investigate whether or not the mesoscale model can reproduce the salient features of the August surge.

6.2 13 August 1993

The model initializes at 1200 UTC 11 August with a weak low-level flow throughout the Gulf of California (figure 30a). Satellite imagery shows anvil clouds in the southern gulf associated with weakening overnight convection (figure 13a), but it is unclear from the imagery whether or not deep convection still is occurring. Pibal and surface observations indicate weak diurnal flow (figure 14a).

The model begins to develop convection over the mountains of the Sierra Madre Occidental by 1800 UTC (figure 30b) as also indicated by satellite (not shown). The temperatures of the satellite observed cloud tops become colder at this time and MM5 develops precipitation over the same region. Both the satellite imagery and the mesoscale model develop an isolated cell over Baja California peninsula between 1500

UTC and 1800 UTC. By 2100 UTC healthy convection is evident over the Sierra Madre Occidental and the southern Rocky Mountains in both MM5 and observations (not shown). The model continues to develop more convection over Baja California although none is observed. Also, satellite imagery indicates cold cloud tops along the coast south of Los Mochis and over the southern gulf that is not indicated by the model. Upslope low-level flow in the model corresponds well with the available surface observations.

While satellite imagery at 2300 UTC 11 August indicates increasing convection along the coastline and eastern gulf waters, weaker convection is occurring over the mountains of the Sierra Madre Occidental (figure 13b). MM5 fails to develop convection over the gulf by 0000 UTC, although it continues to develop precipitation over the mountains (figure 30c). The model does indicate strong convection along the coast of Mexico, in agreement with the satellite observations. The low-level model winds show upslope of 5-10 ms-1 into the Sierra Madre Occidental. Surface wind observations agree with the model and there is no indication of a surge (figure 14b).

The model indicates the development of a surge in the south central Gulf of California at 0300 UTC (figure 31a). Over the following hour the model surge becomes better defined as a distinct shift to southerly flow along with a rise in surface pressure. The surge is 110 km wide and 360 km long with winds of 2-4 ms-1 behind it (figure 32). Due to lack of observations, there is no observational evidence to either support or refute the model evolution.

By 0600 UTC 12 August, MM5 moves the convection more into the eastern gulf with the heaviest precipitation in the central gulf and isolated convection over the

Sierra Madre Occidental (figure 30d). Satellite imagery is inconclusive as a large portion of the gulf is covered in cold cloud tops that do not appear to be mostly anvil cirrus from earlier convection (not shown). The model surge moves to the northwest at 19 ms-1 between 0400 UTC and 0600 UTC (figure 32). The model surge extends throughout the southern 2/3 of the gulf with low-level winds of only 5 ms-1 or less throughout the surge (figures 31b and 32). Surface observations indicate that coastal winds begin increasing from the southeast with winds speed of 5 ms-1, although due to a lack of dense observations, the surge is not evidenced by surface data.

MM5 moves all of its convection over the gulf by 1200 UTC with precipitation extending up to the central gulf, even though the strongest convection is in the southern gulf (figure 30e). The model surge has propagated into Arizona (figure 31). Satellite imagery indicates clouds over the southern gulf, but the amount of deep convection is unclear (figure 13c). Surface observations indicate a surge through the southern 2/3 of the gulf, as evidenced by the tethersonde cooling at Tesopaco between 1200 UTC and 1700 UTC (figure 14c). This area is well behind the model surge, although surface observations also indicate southerly flow in the northern gulf. The average speed of the model surge is 19 ms-1.

Satellite imagery continues to show clouds throughout the southern half of the gulf by 1800 UTC 12 August and MM5 continues to develop convection along the gulf (figure 30f). The model winds all along the western gulf coast of Mexico are southeasterly to southerly at 5-7 ms-1 within the surge. Surface observations indicate weak flow, but more typical diurnal upslope rather than along shore flow as seen in MM5 and there is no indication of the earlier observed surge (not shown).

MM5 convection continues throughout 0000 UTC 13 August and the southeast winds behind the surge increase along the western gulf coast of Mexico (figure 30g). Surface observations along the coast contradict this with southwest upslope surface flow observed at most locations (figure 14d). The pibals at Los Mochis also indicates southwesterly flow at 4 ms-1 at 950 mb. It is not clear how the increased development of model convection along the gulf relates to the continuation of strong southerly and southeasterly winds, but both of these are contrary to the observations.

The model continues to generate convection throughout the entire gulf at 1200 UTC (figure 30i). While the model shows a southeast flow all along the western gulf coast of Mexico at 7-10 ms-1, it also indicates convection all along the eastern gulf. MM5 even generates almost 1 cm of precipitation over Puerto Peñasco between 1100 UTC and 1200 UTC. Satellite imagery was missing during the morning hours of 13 August, but there is no indication in the observations of any convection in the northern gulf (figure 13e). The model does agree somewhat with the 1200 UTC pibal data from Los Mochis and Culiacan with winds the south at 6 ms-1, and it does have southerly winds over Puerto Peñasco at 5-7 ms-1, but associated with convection (figures 14e and 30i).

The model developed a surge on 12 August that moves up the entire length of the gulf initially at a speed of 16.7 ms-1 and then later at a speed of 20.0 ms-1. Observations indicate a surge throughout the southern 2/3 of the gulf that subsequently weakened until redeveloping again on the morning of 13 August when it moved at 14.5 ms-1. Behind the model surge the winds continue to be southerly to southeasterly and the model develops continued convection contrary to the

observations. By the end of the simulation the observed surge extended throughout the gulf with flow similar to the model, but for different reasons.

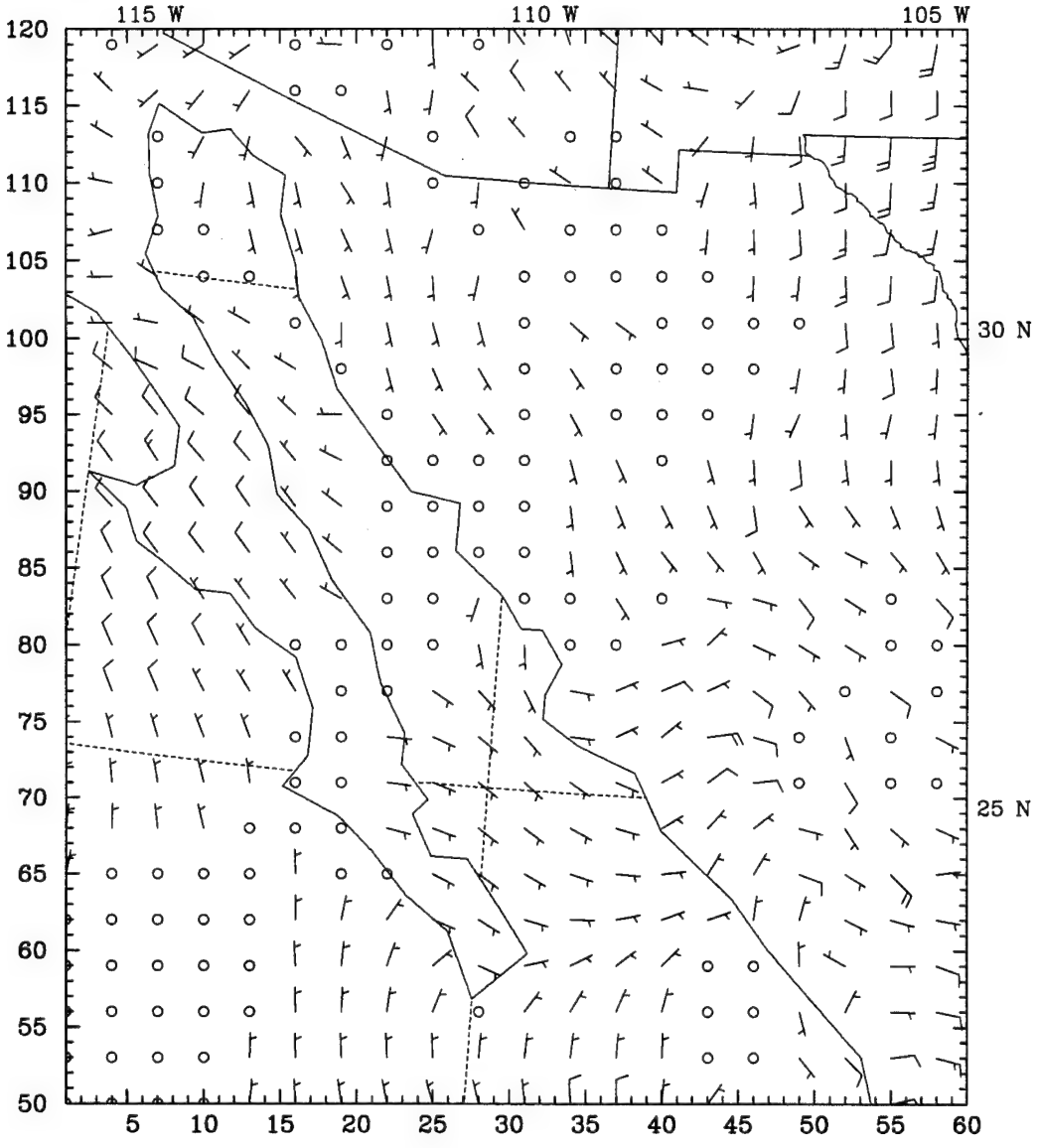

Figure 26a) MM5 coarse grid 6 hour convective and explicit precipitation amounts (mm 6h-1) and 970 mb at 1200 UTC 7 July. Full barb is 5 ms-1.

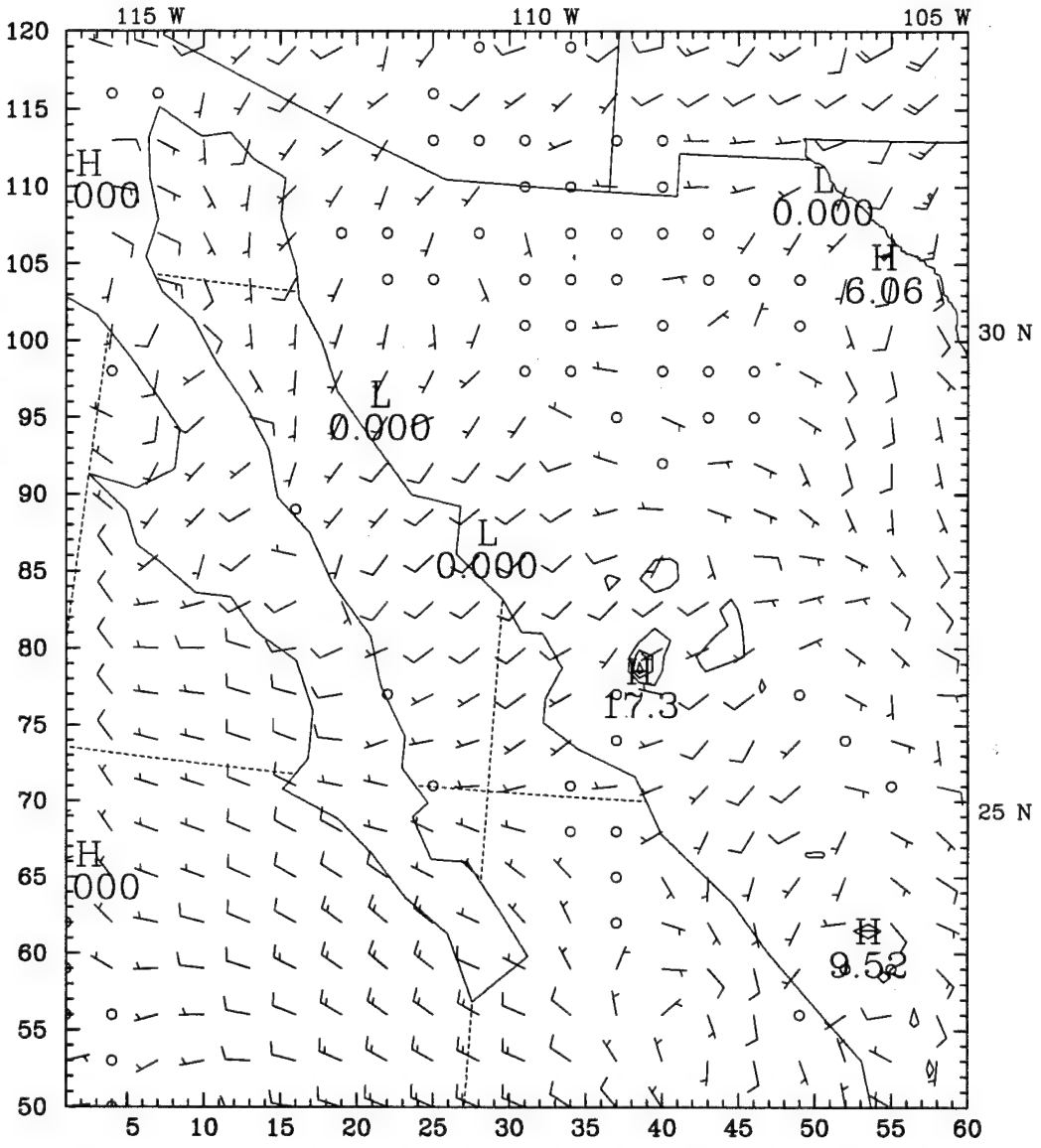

Figure 26b) Same as figure 26a, except at 1800 UTC 7 July.

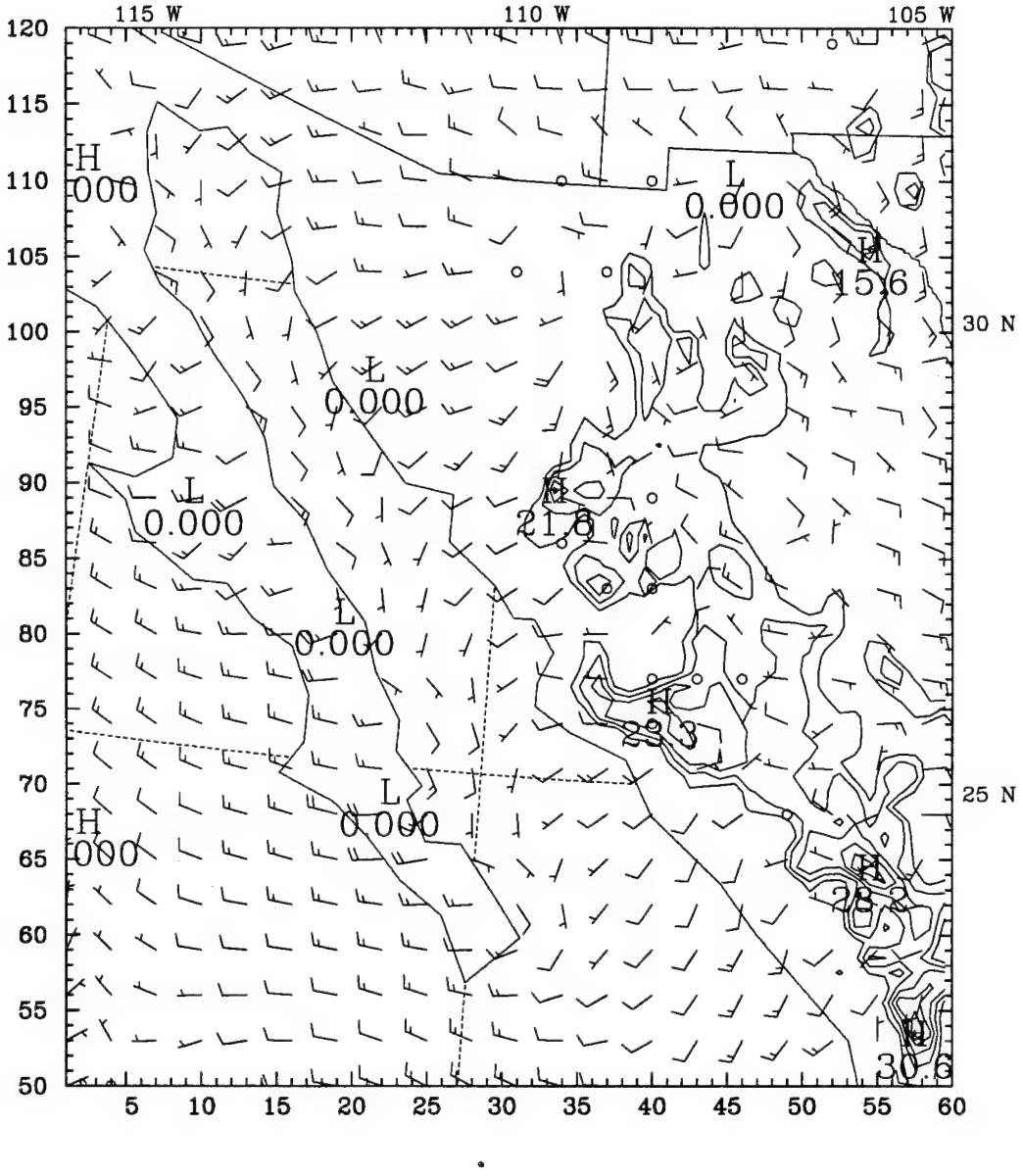

Figure 26c) Same as figure 26a, except at 0000 UTC 8 July.

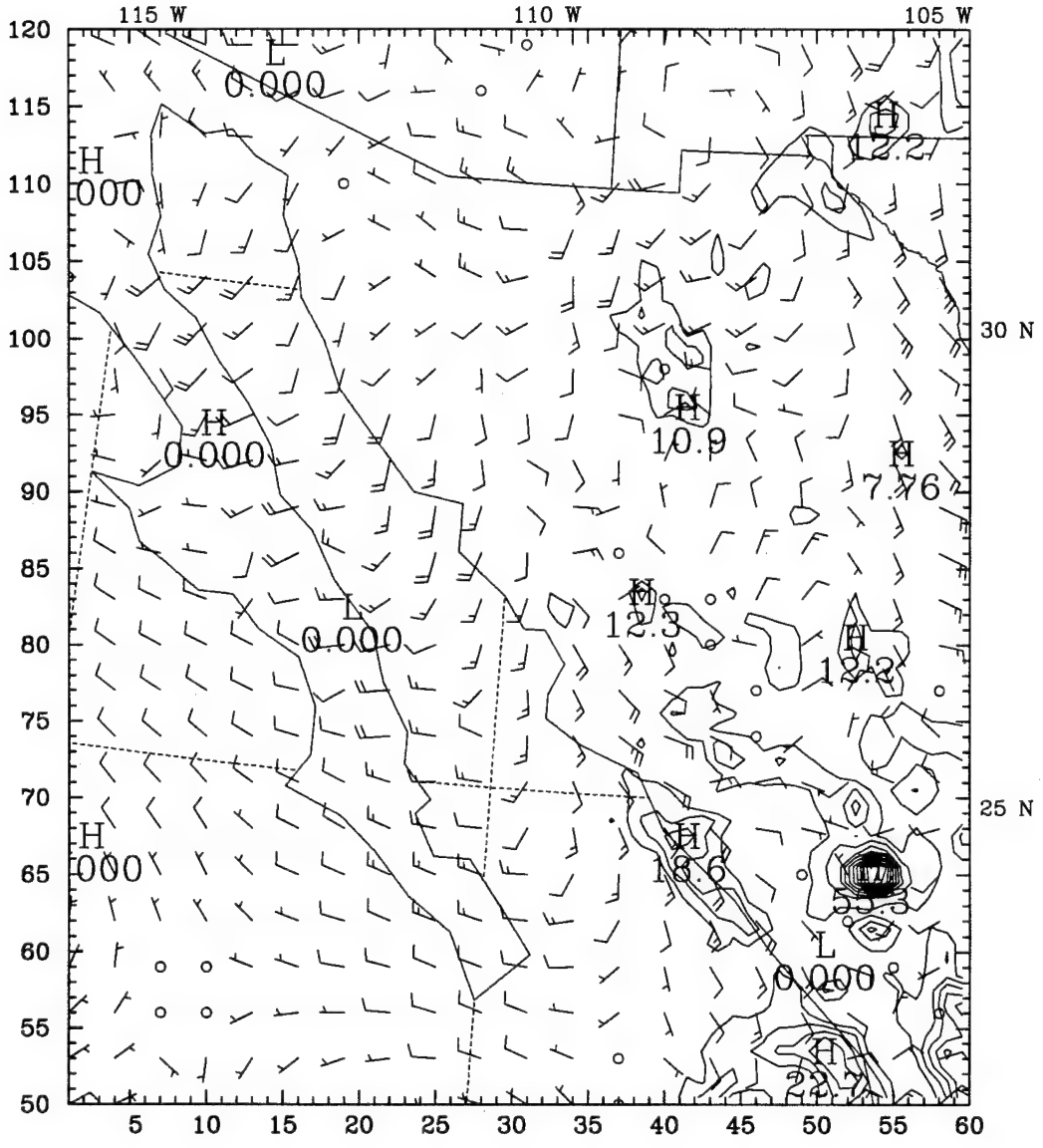

Figure 26d) Same as figure 26a, except at 0600 UTC 8 July.

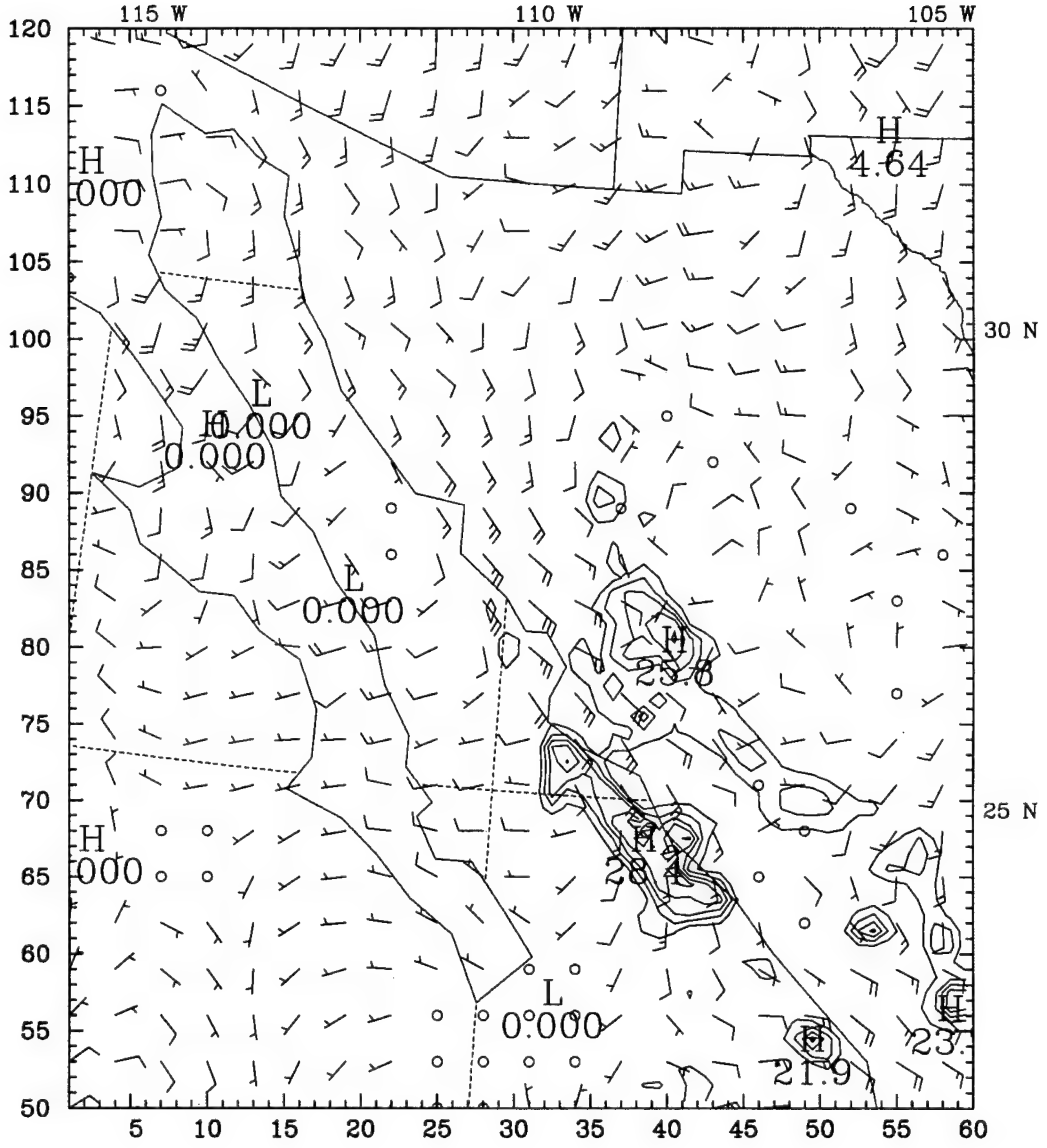

Figure 26e) Same as figure 26a, except at 1200 UTC 8 July.

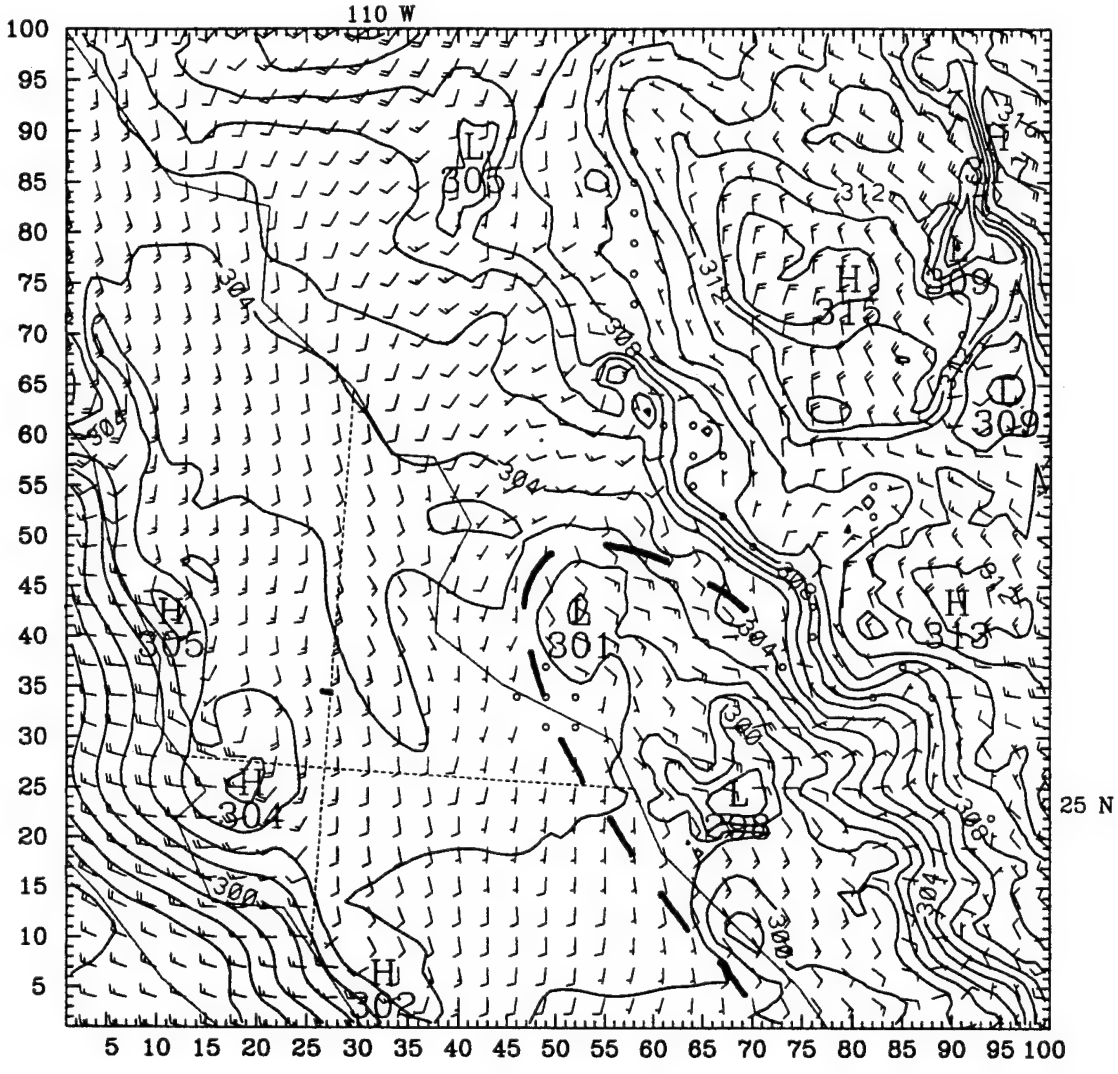

Figure 27a) MM5 nested grid sigma level 0.978 potential temperature contours (K) and winds at 0300 UTC 8 July. Full barb is 5 ms-1. Dashed line indicates position of leading edge of gulf surge.

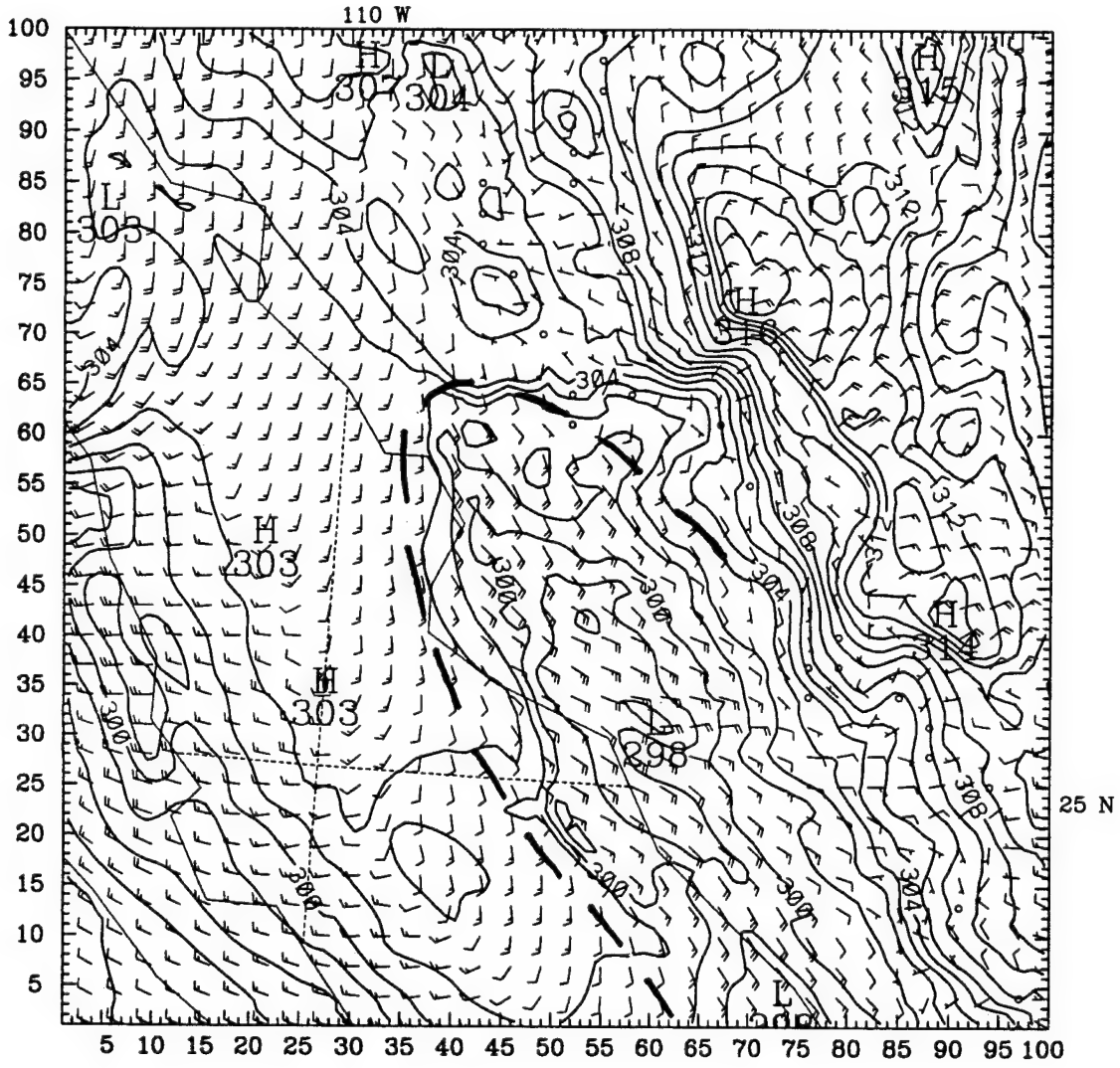

Figure 27b) Same as figure 27a, except at 0600 UTC 8 July.

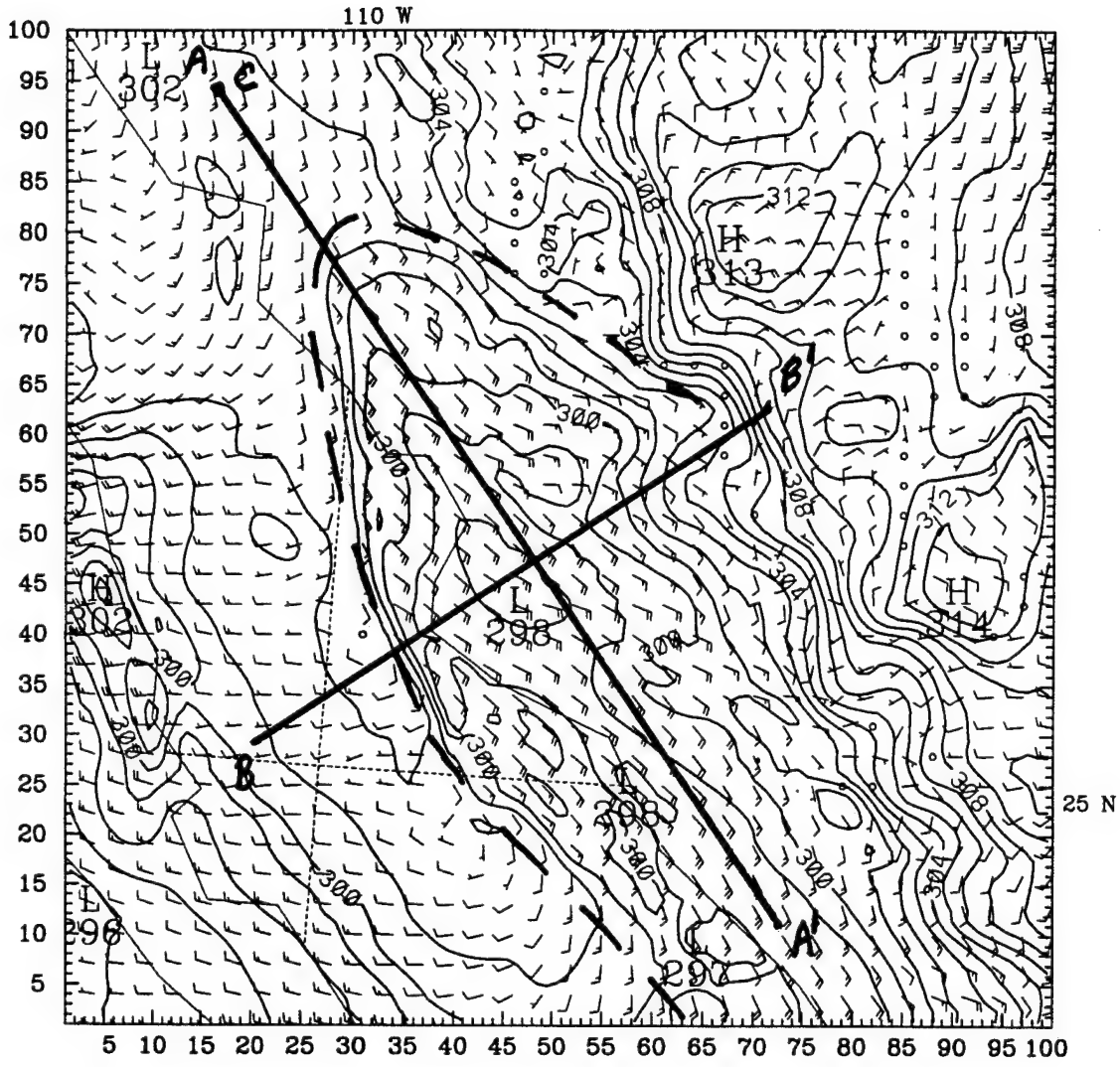

Figure 27c) Same as figure 27a, except at 0900 UTC 8 July. Additionally, thick lines indicate locations of cross-sections A-A' (figure 33), and B-B' (figure 34), and the location of a model sounding, C (figure 35).

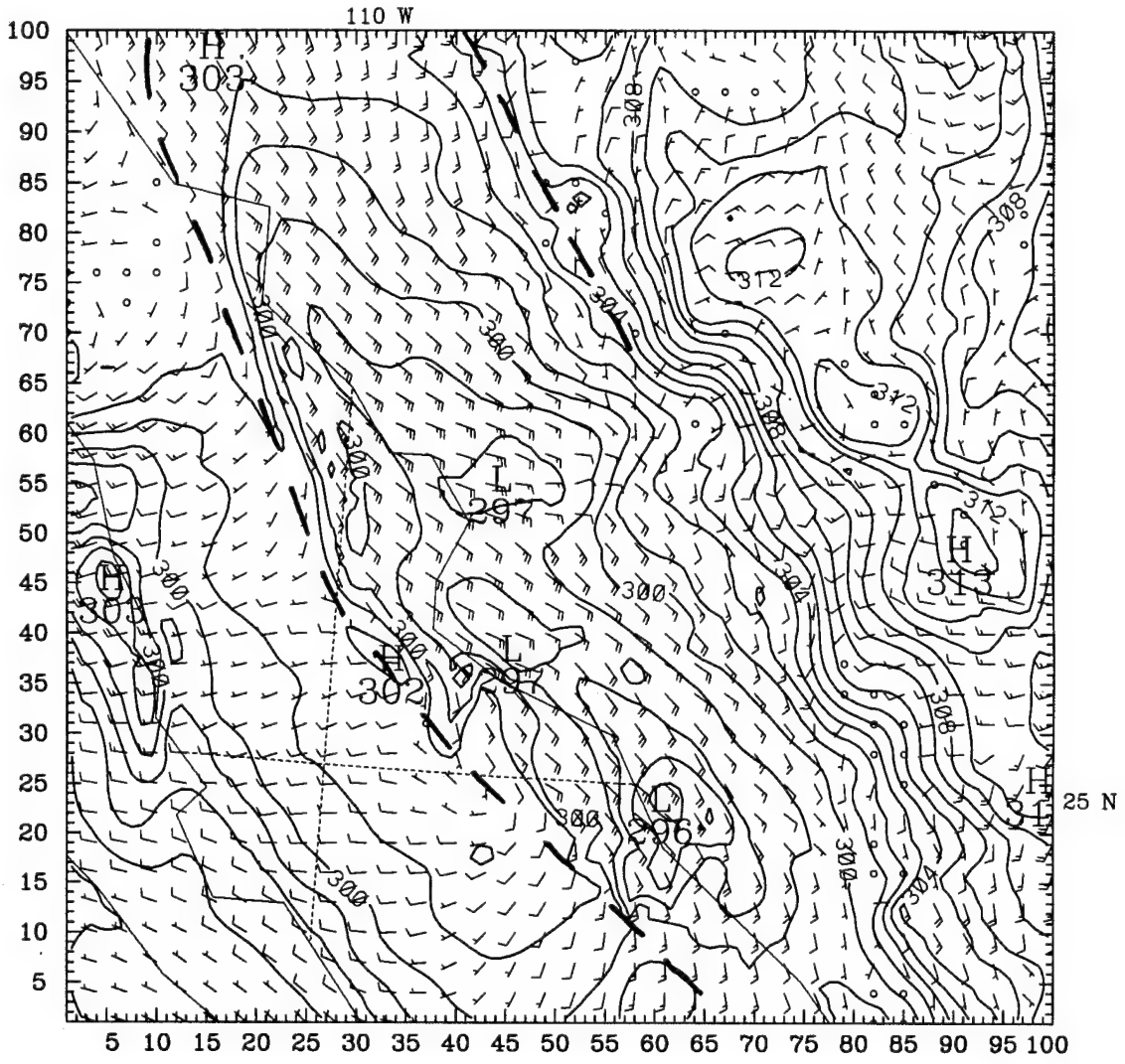

Figure 27d) Same as figure 27a, except at 1200 UTC 8 July.

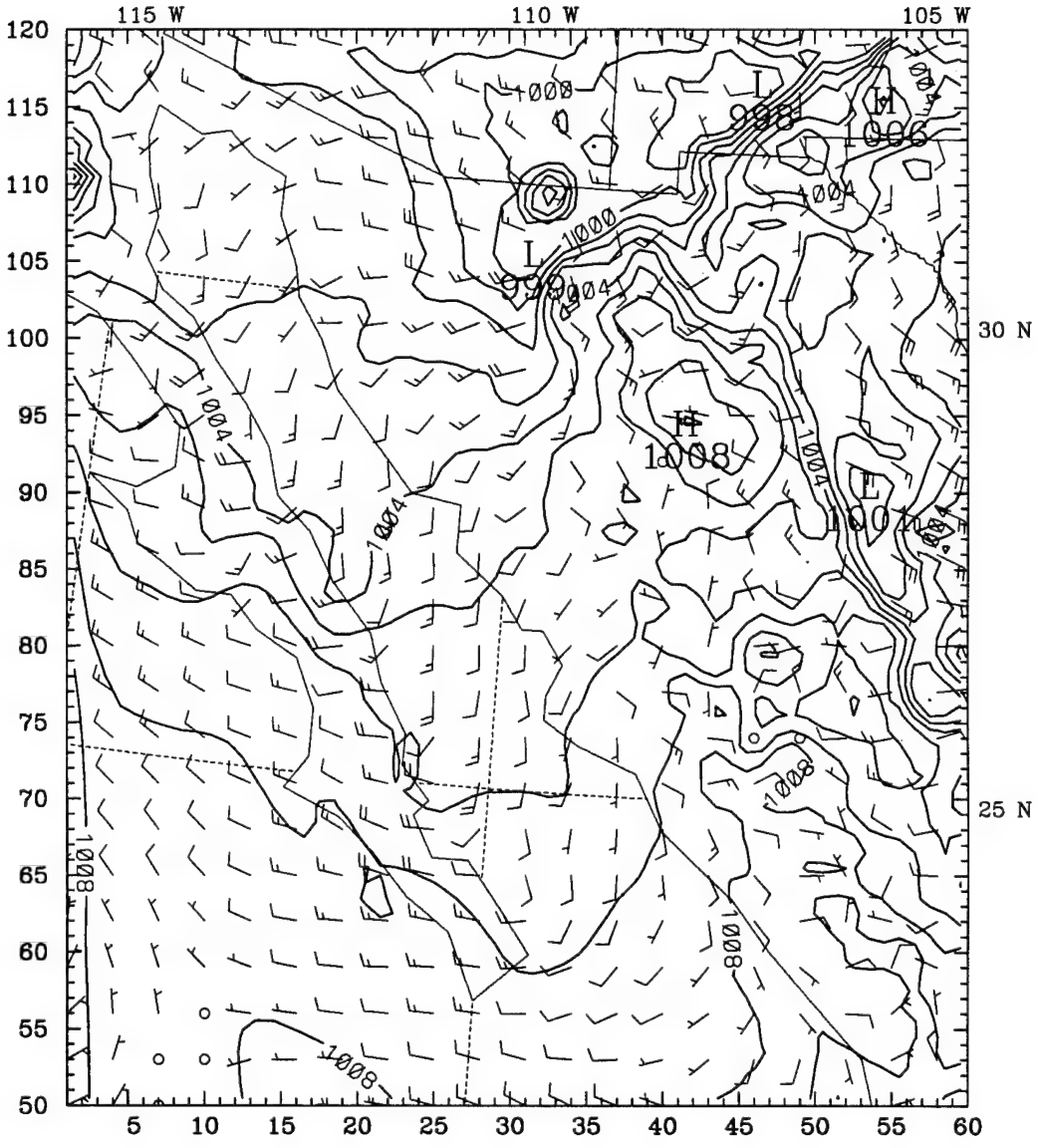

Figure 28a) MM5 coarse grid surface pressure reduced to sea-level (mb) and 980 mb winds at 0300 UTC 8 July. Full barb is 5 ms-1. Dashed line indicates position of leading edge of gulf surge.

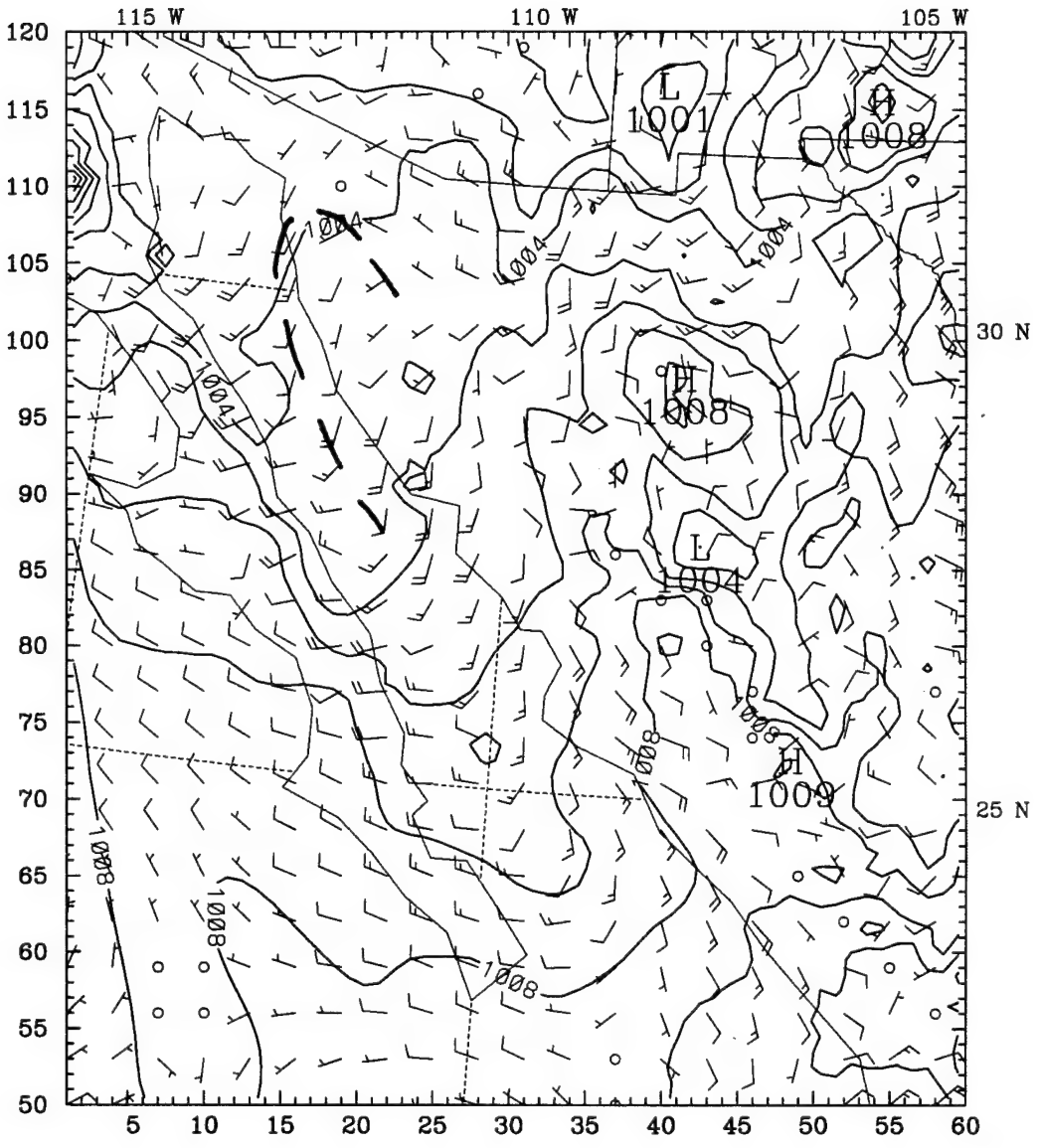

Figure 28b) Same as figure 28a, except at 0600 UTC 8 July.

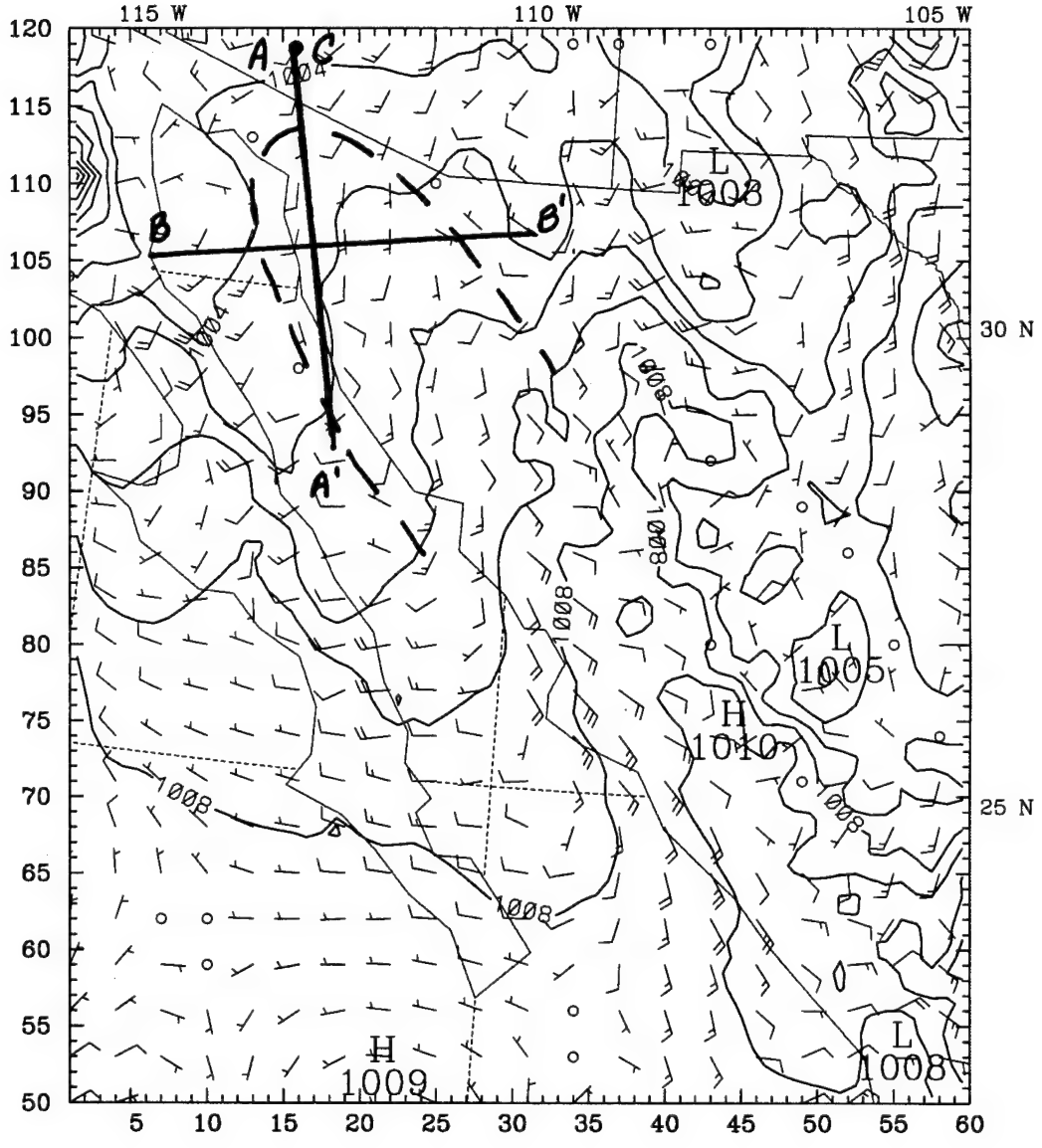

Figure 28c) Same as figure 28a, except at 0900 UTC 8 July. Thick lines indicate locations of model cross-sections, A-A' (figure 36), and B-B' (figure 37), and the location of a model sounding, C (figure 38).

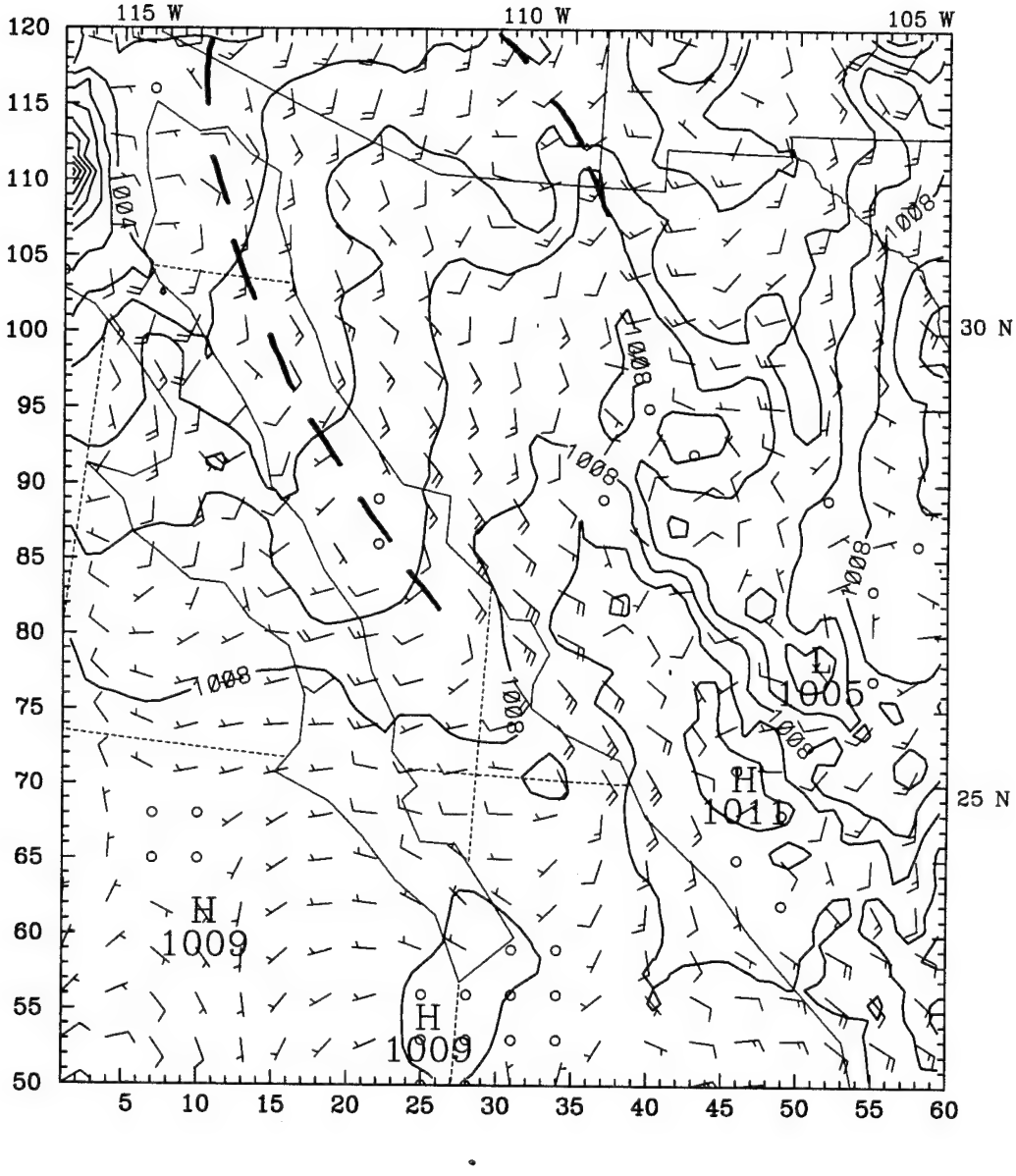

Figure 28d) Same as figure 28a, except at 1200 UTC 8 July.

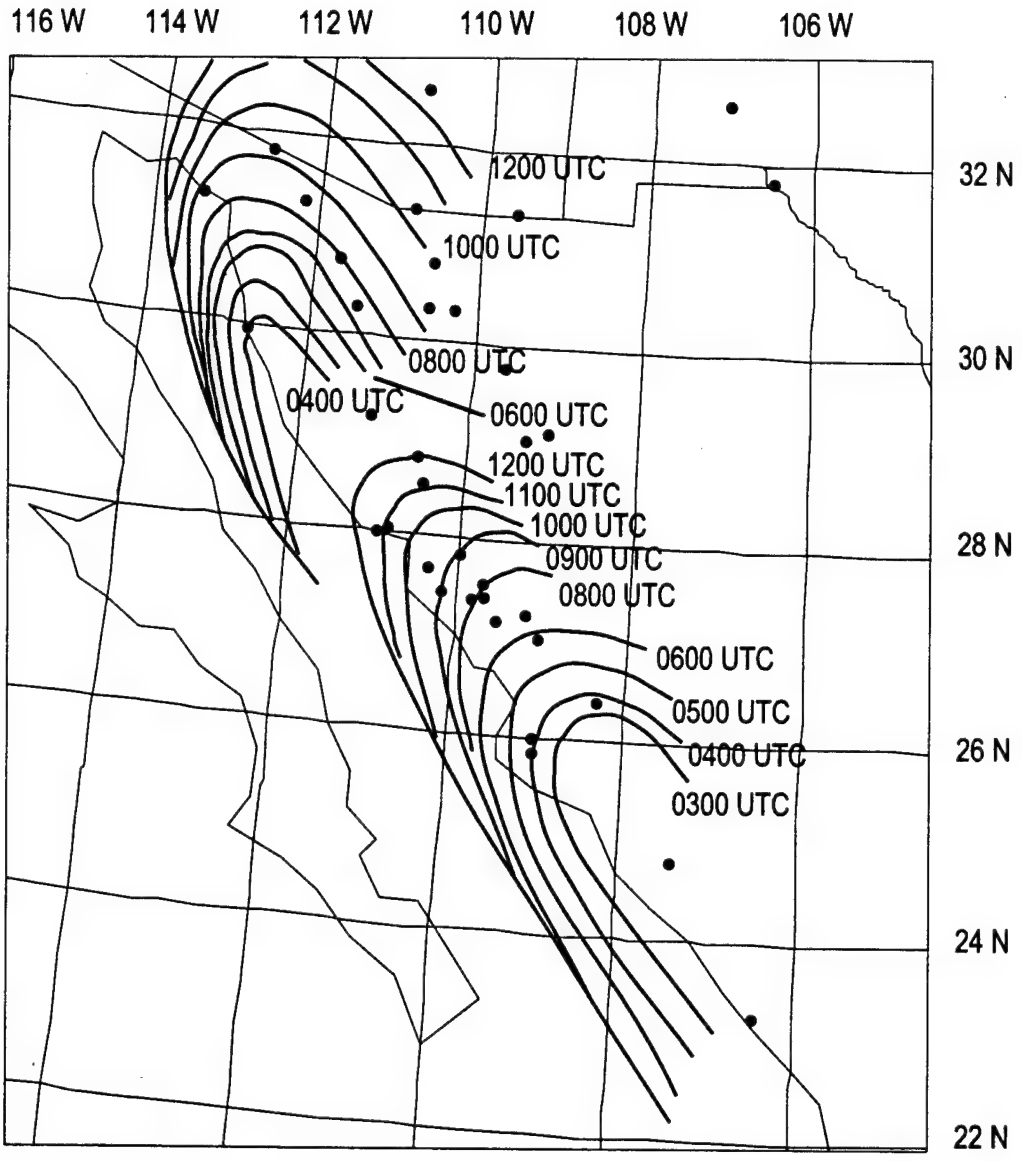

Figure 29) Isochrone analyses of leading edge of model surges on 8 July.

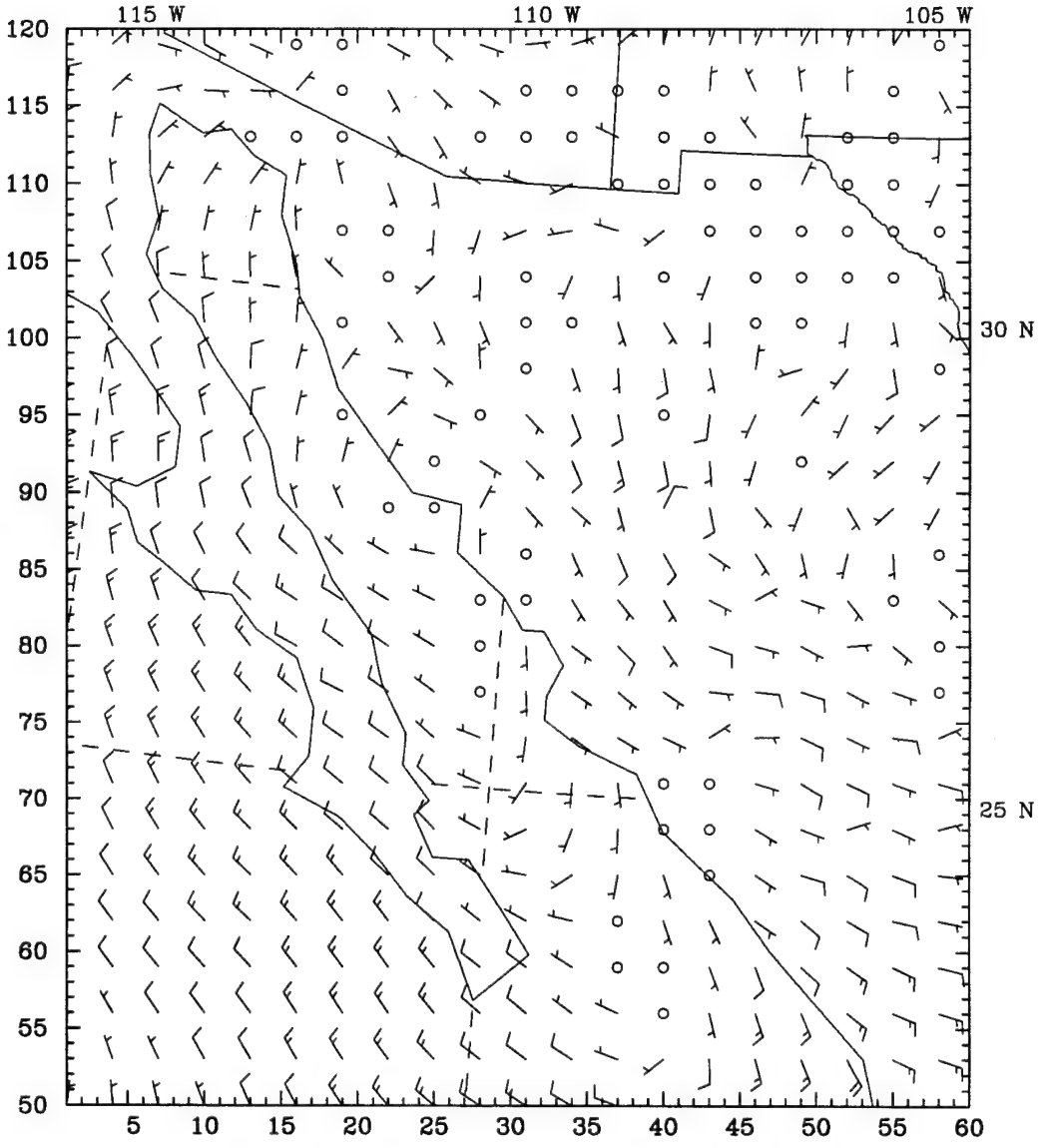

Figure 30a) MM5 coarse grid 6 hour convective and explicit precipitation amounts (mm 6h-1) and 970 mb winds at 1200 UTC 11 August. Full barb is 5 ms-1.

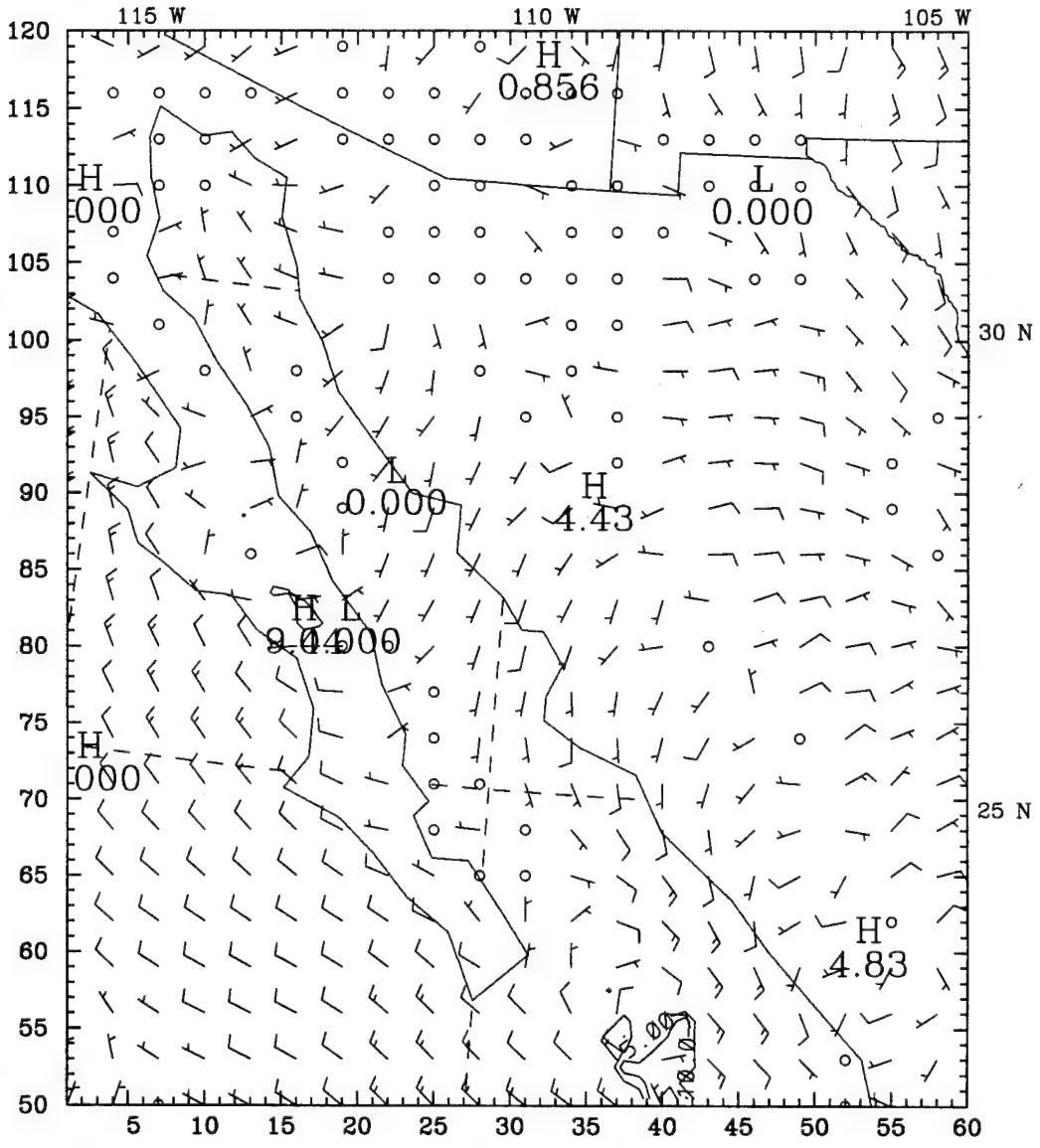

Figure 30b) Same as figure 30a, except at 1800 UTC 11 August.

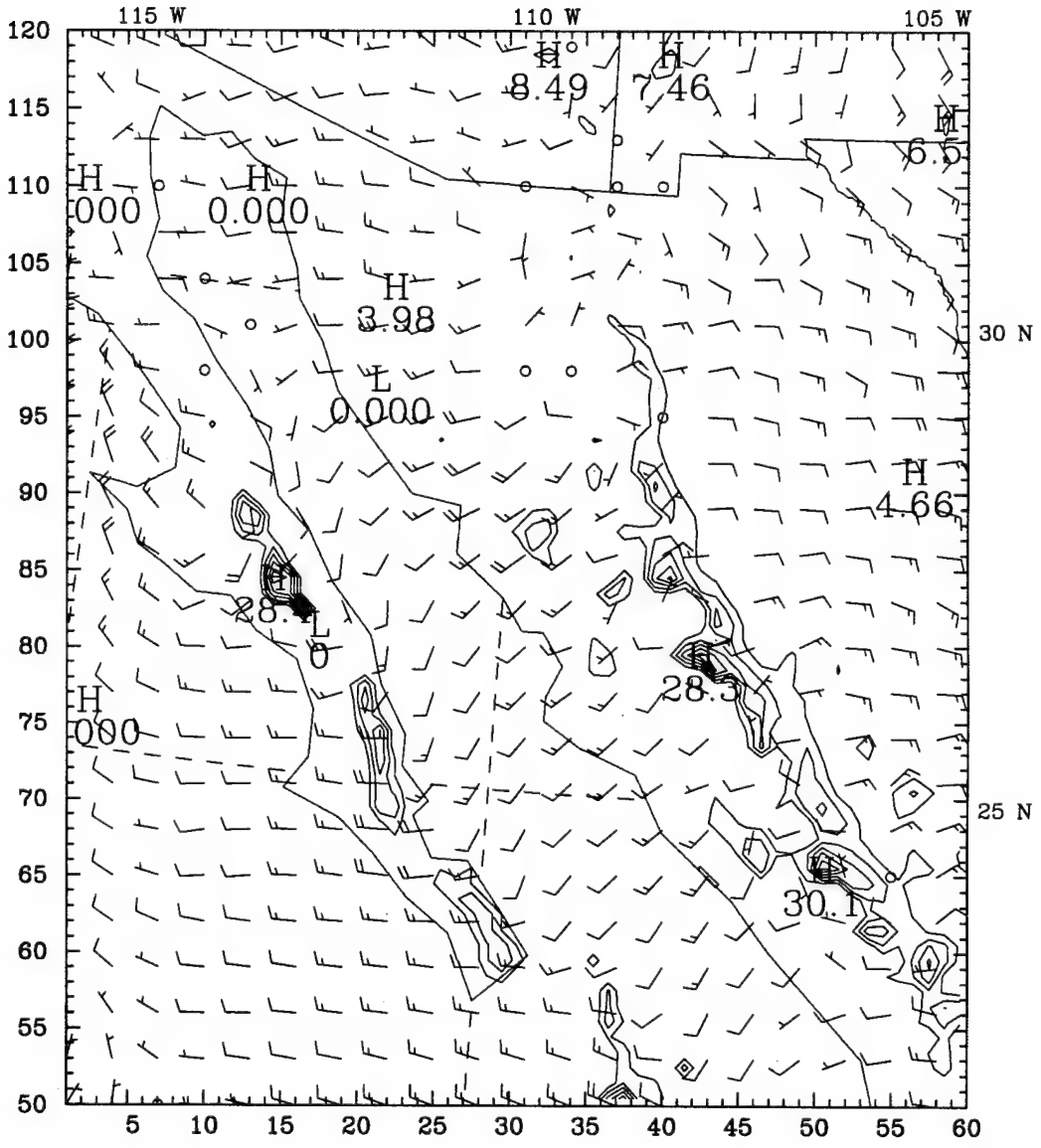

Figure 30c) Same as figure 30a, except at 0000 UTC 12 August.

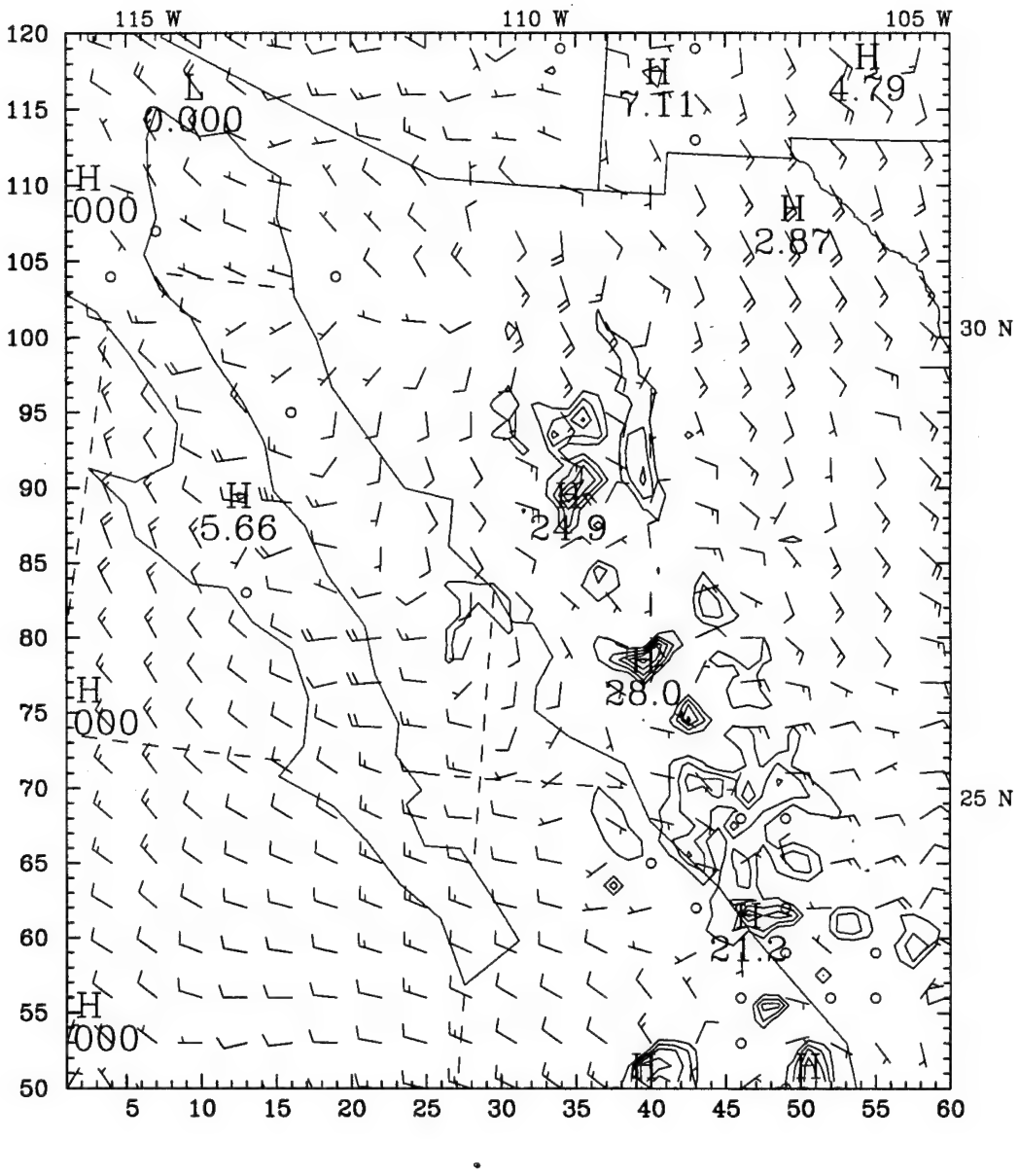

Figure 30d) Same as figure 30a, except at 0600 UTC 12 August.

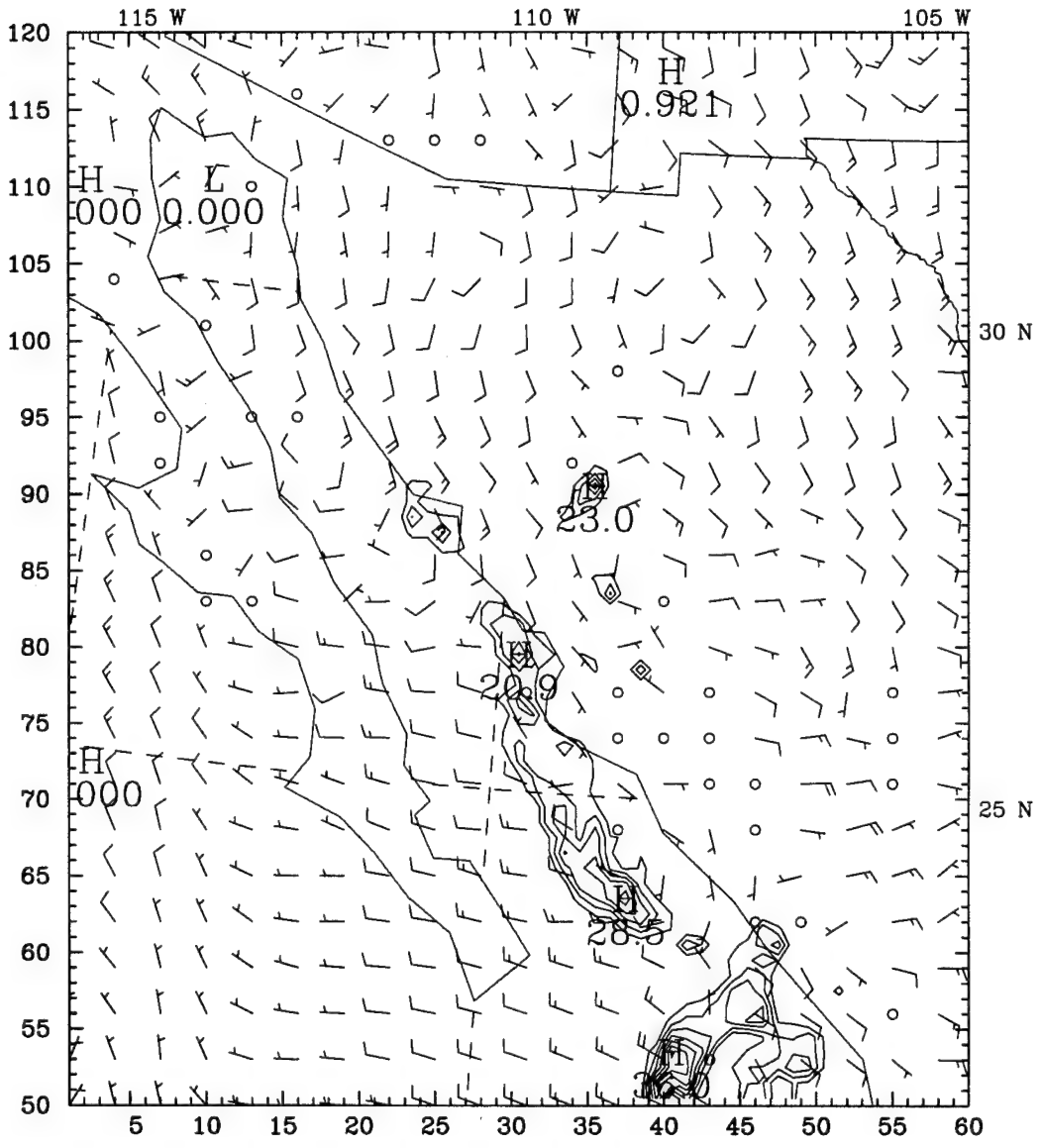

Figure 30e) Same as figure 30a, except at 1200 UTC 12 August.

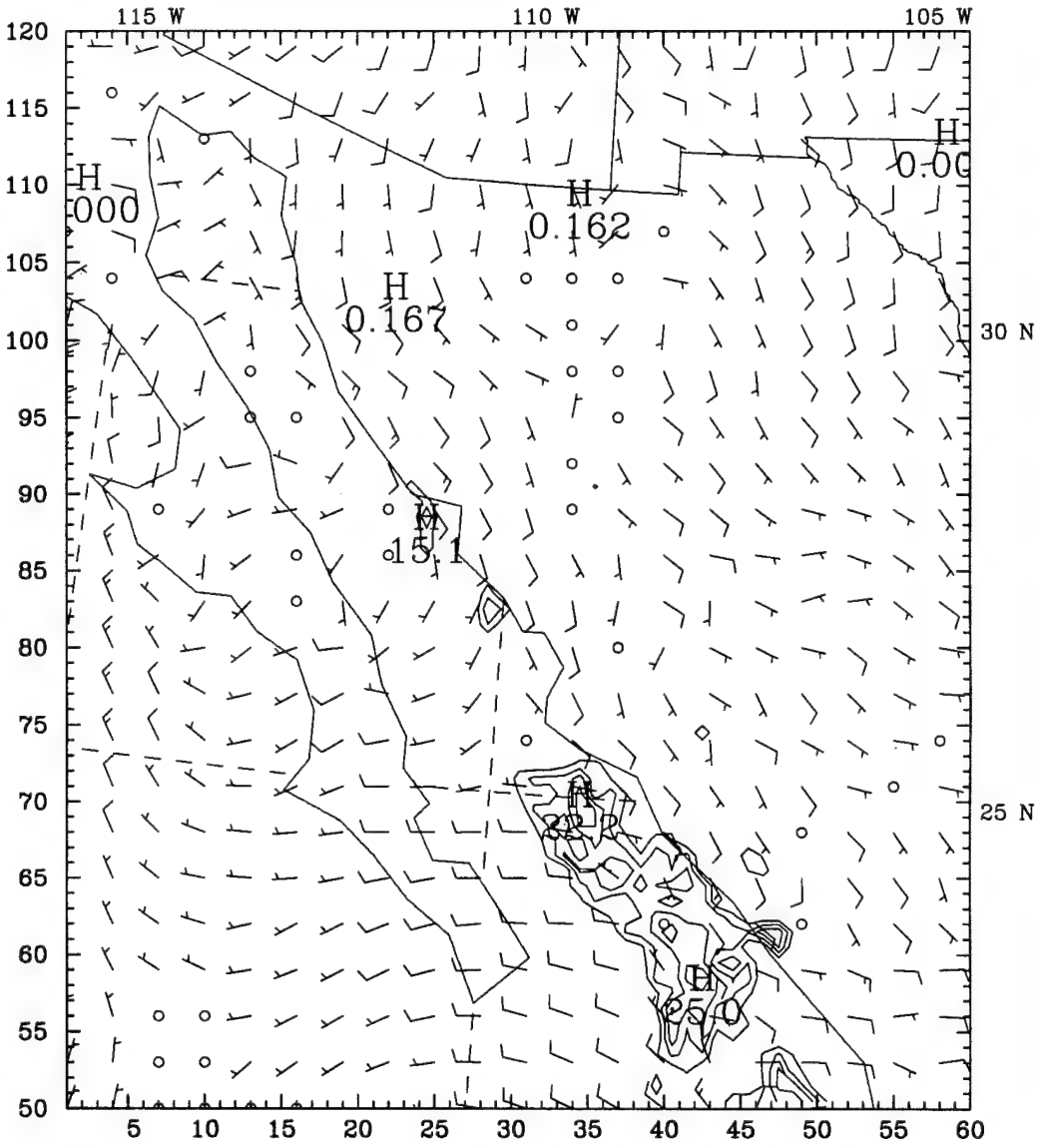

Figure 30f) Same as figure 30a, except at 1800 UTC 12 August.

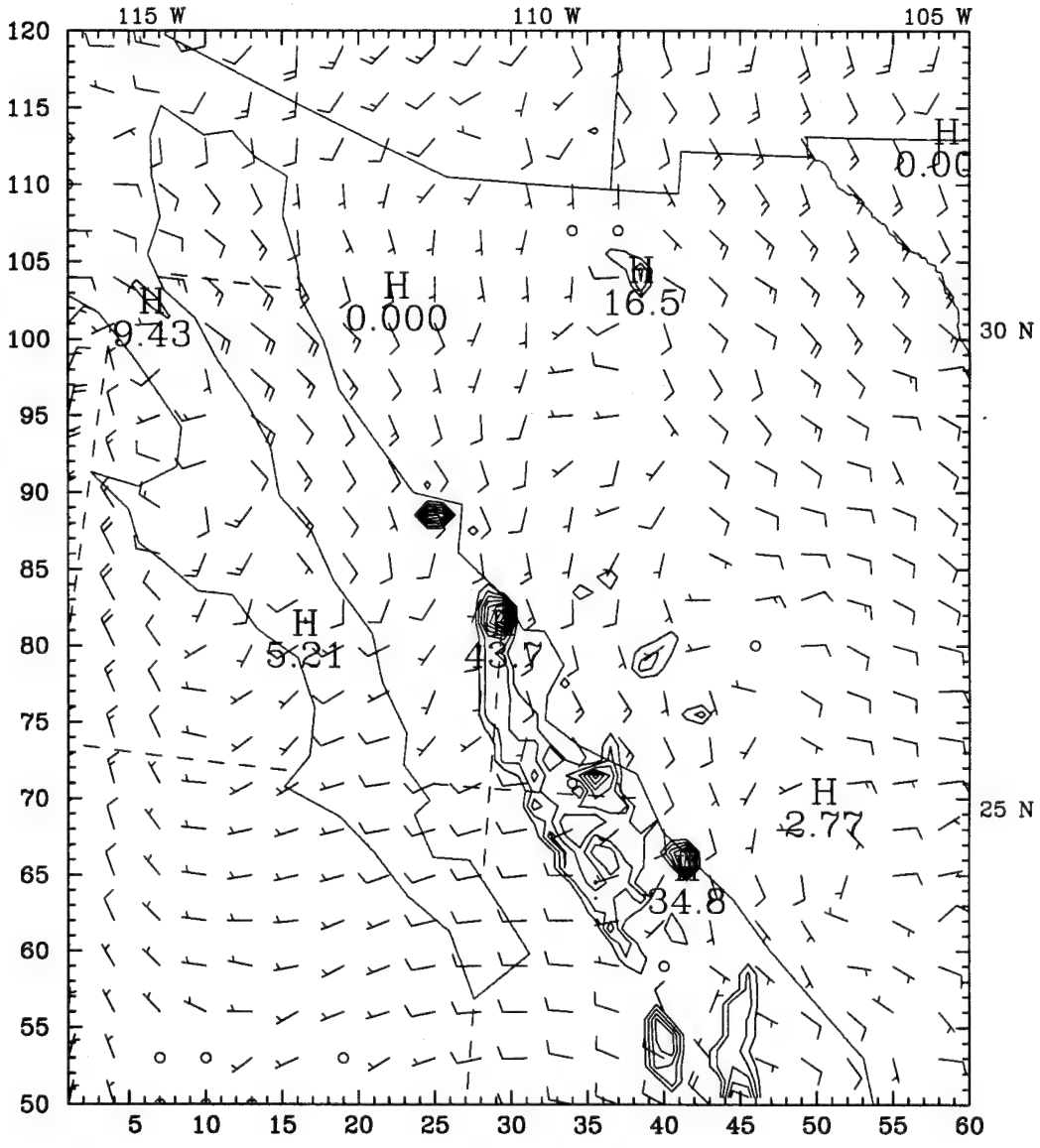

Figure 30g) Same as figure 30a, except at 0000 UTC 13 August.

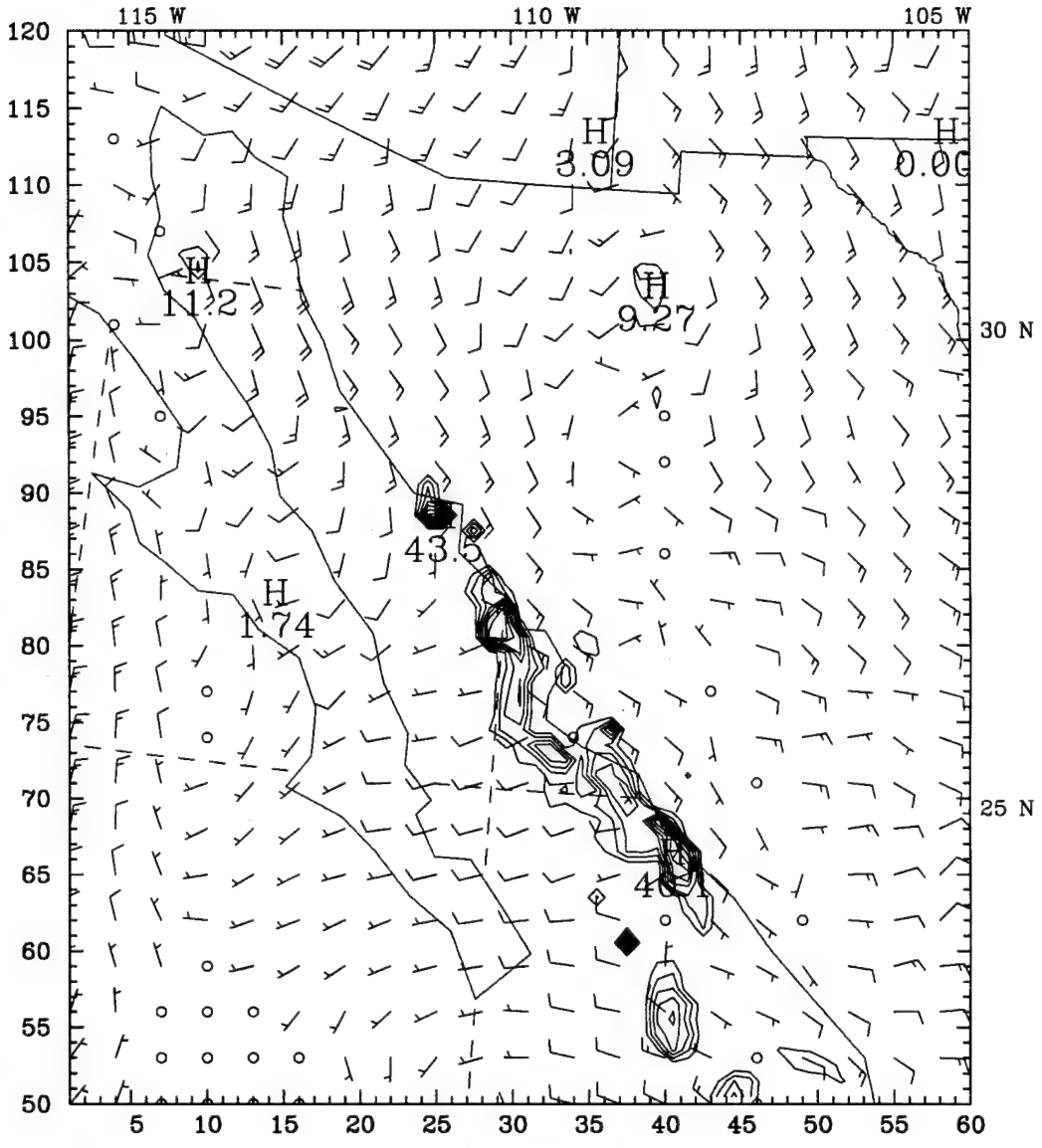

Figure 30h) Same as figure 30a, except at 0600 UTC 13 August.

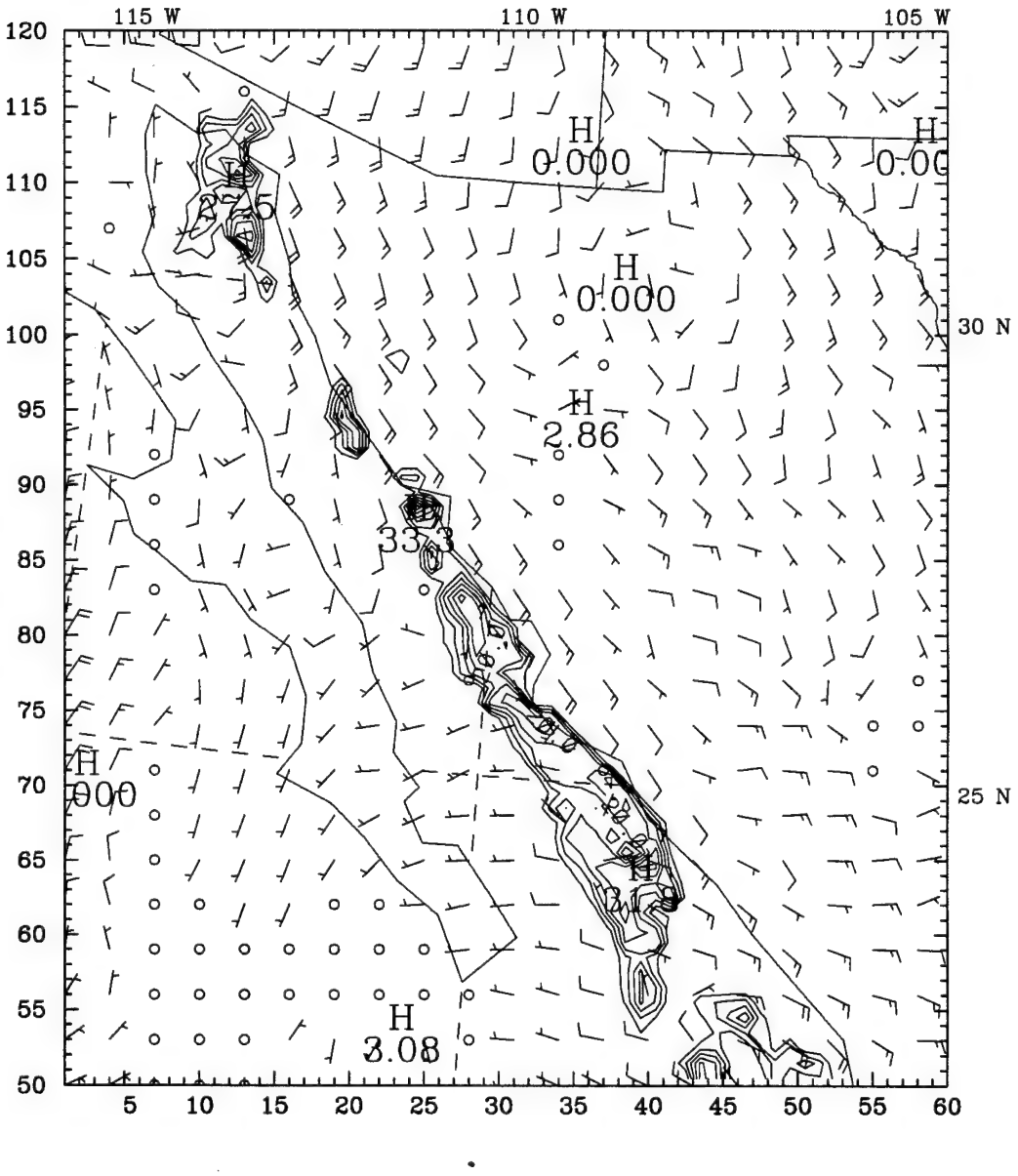

Figure 30i) Same as figure 30a, except at 1200 UTC 13 August.

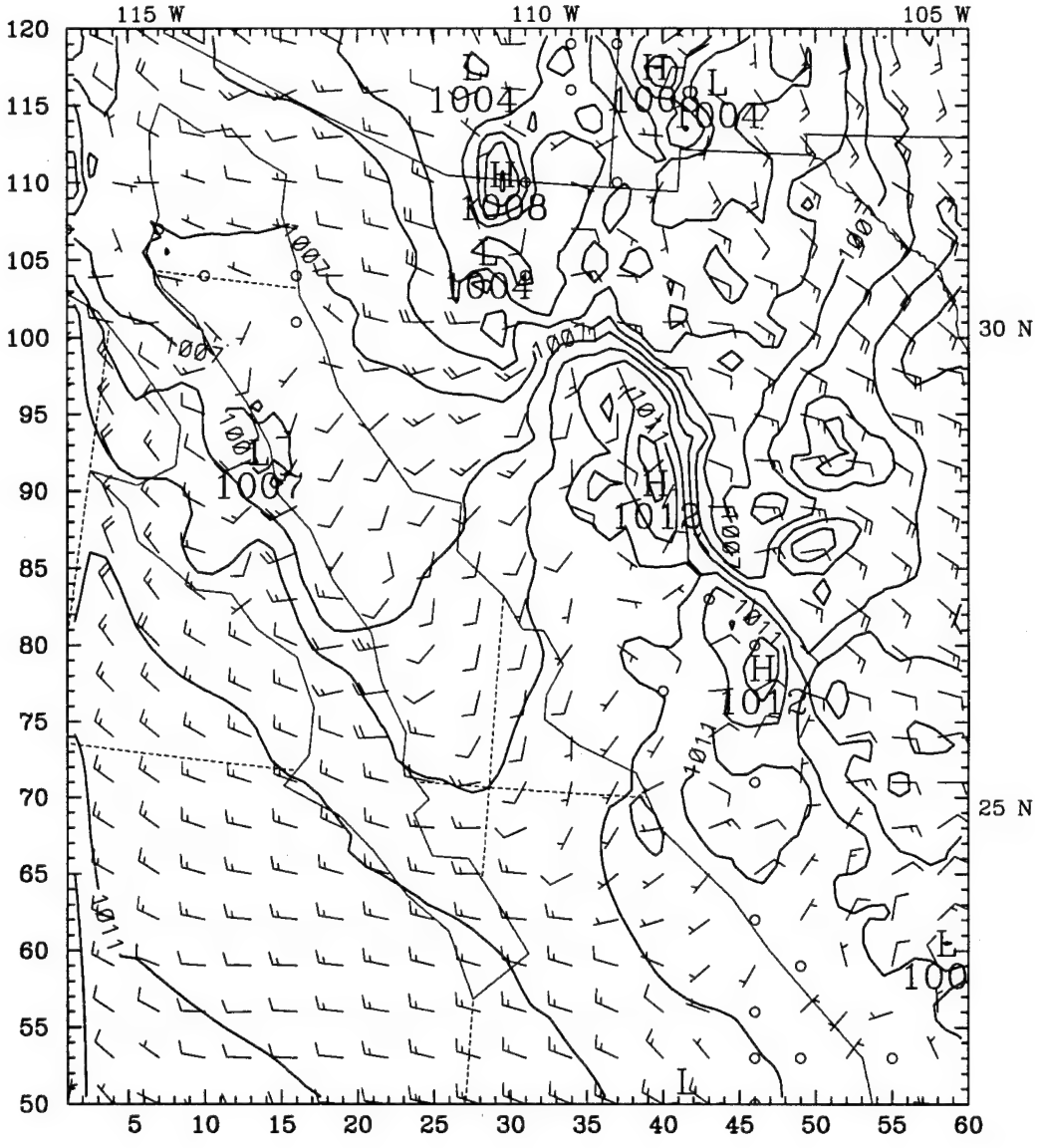

Figure 31a) MM5 coarse grid surface pressure reduced to sea-level (mb) and 980 mb winds at 0300 UTC 12 August. Full barb is 5 ms-1. Dashed line indicates position of leading edge of gulf surge.

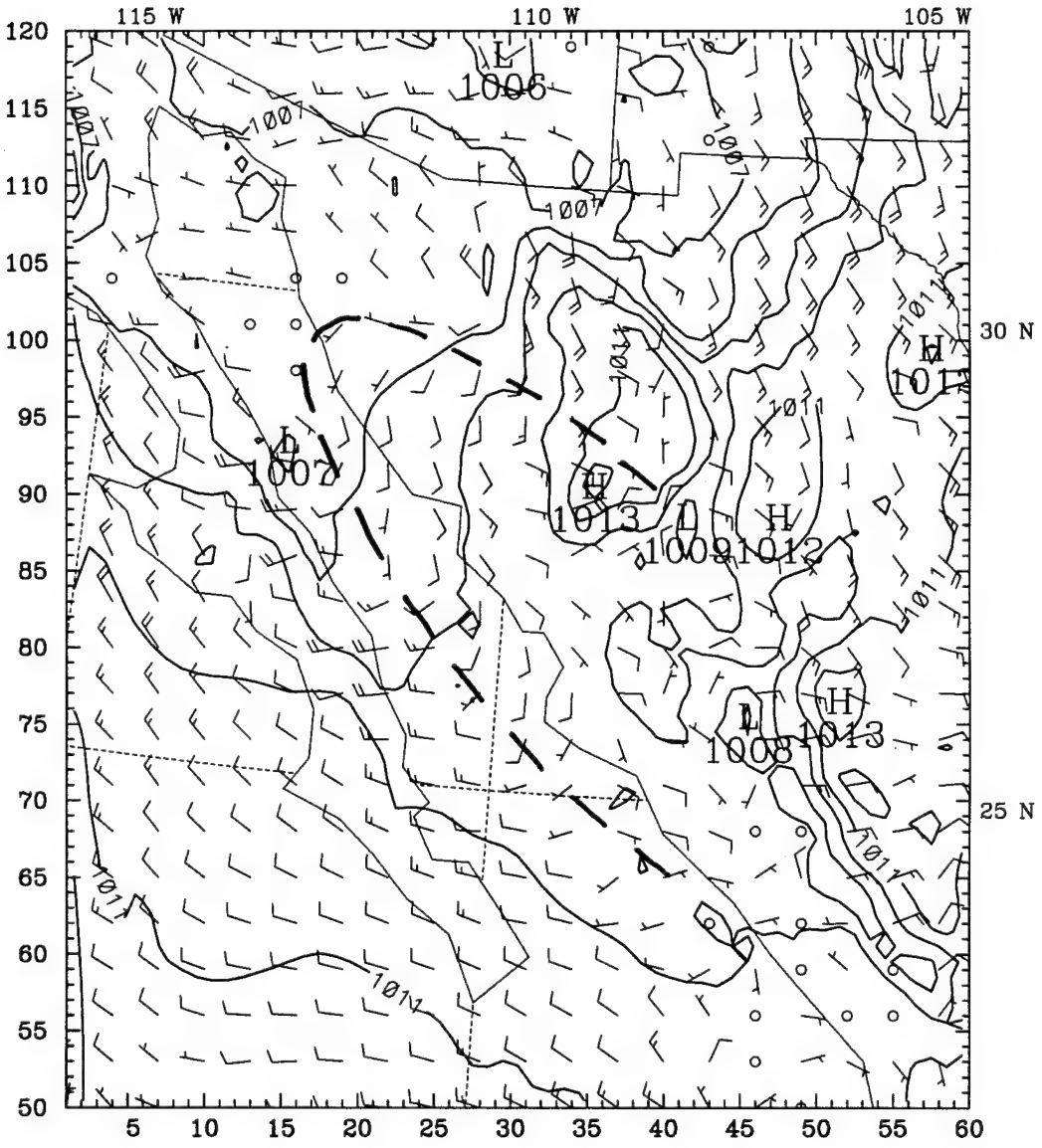

Figure 31b) Same as figure 31a, except at 0600 UTC 12 August.

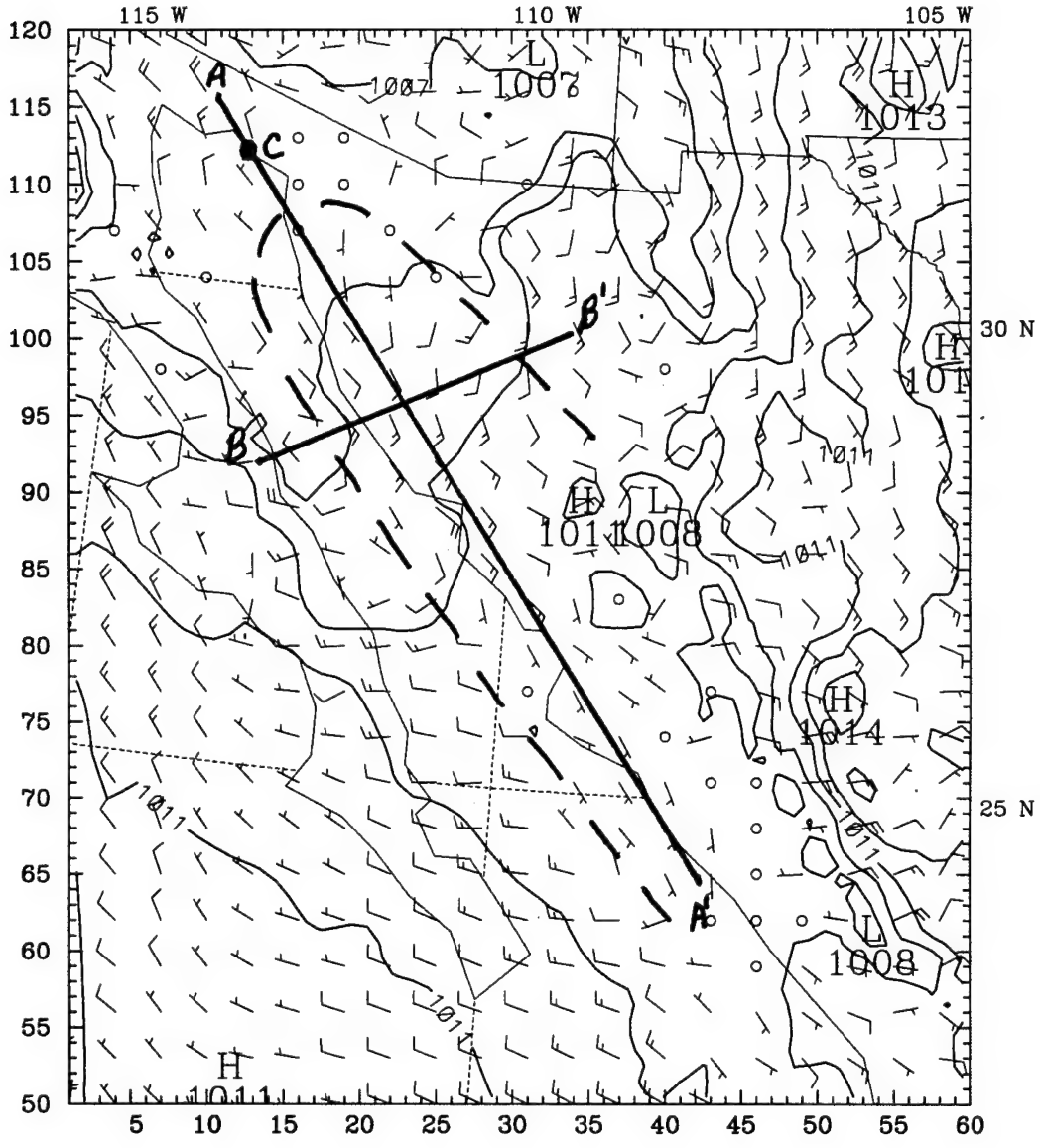

Figure 31c) Same as figure 31a, except at 0900 UTC 12 August. Thick lines indicate locations of model cross-sections, A-A' (figure 39), and B-B' (figure 40), and the location of a model sounding, C (figure 41).

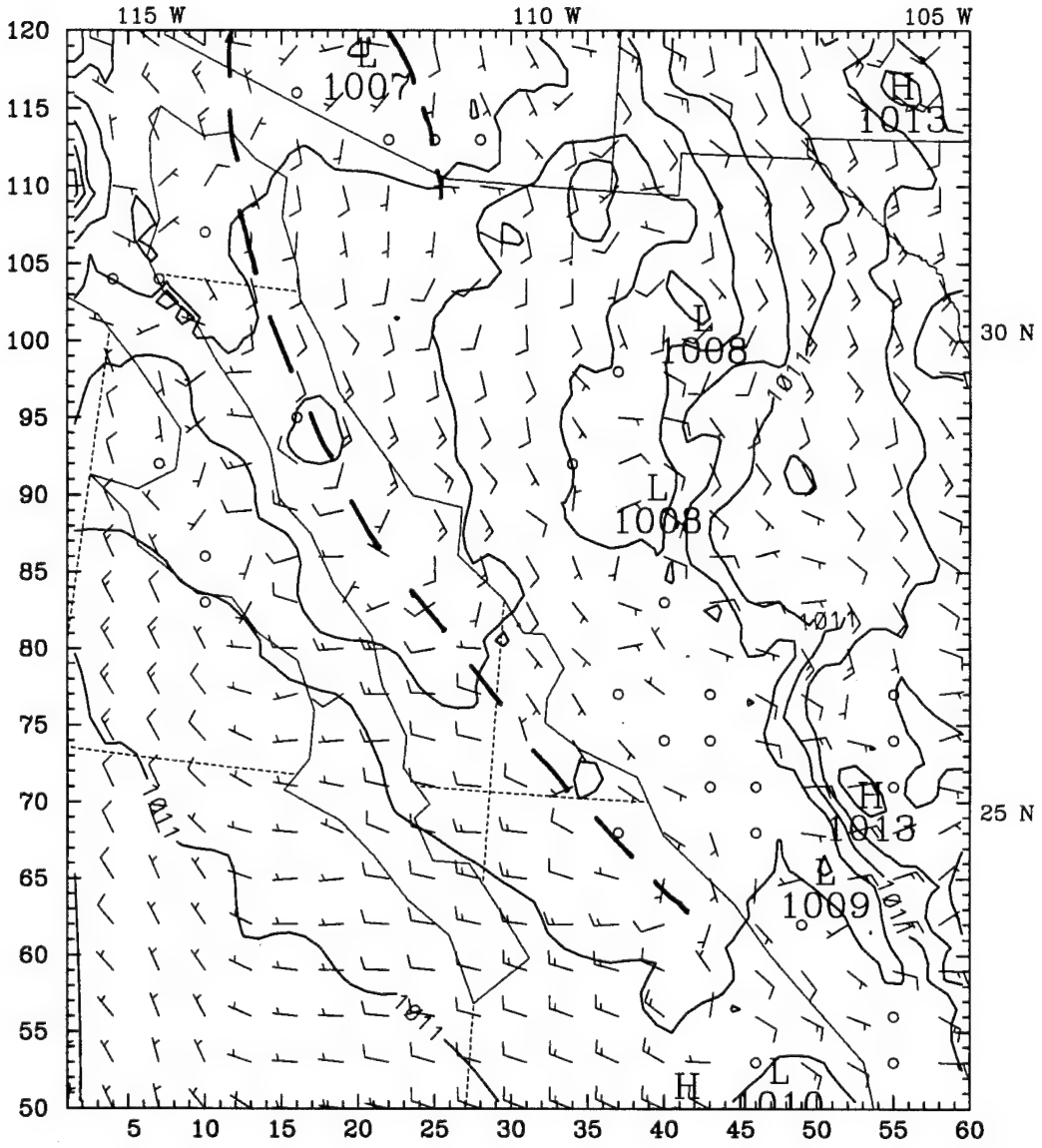

Figure 31d) Same as figure 31a, except at 1200 UTC 12 August.

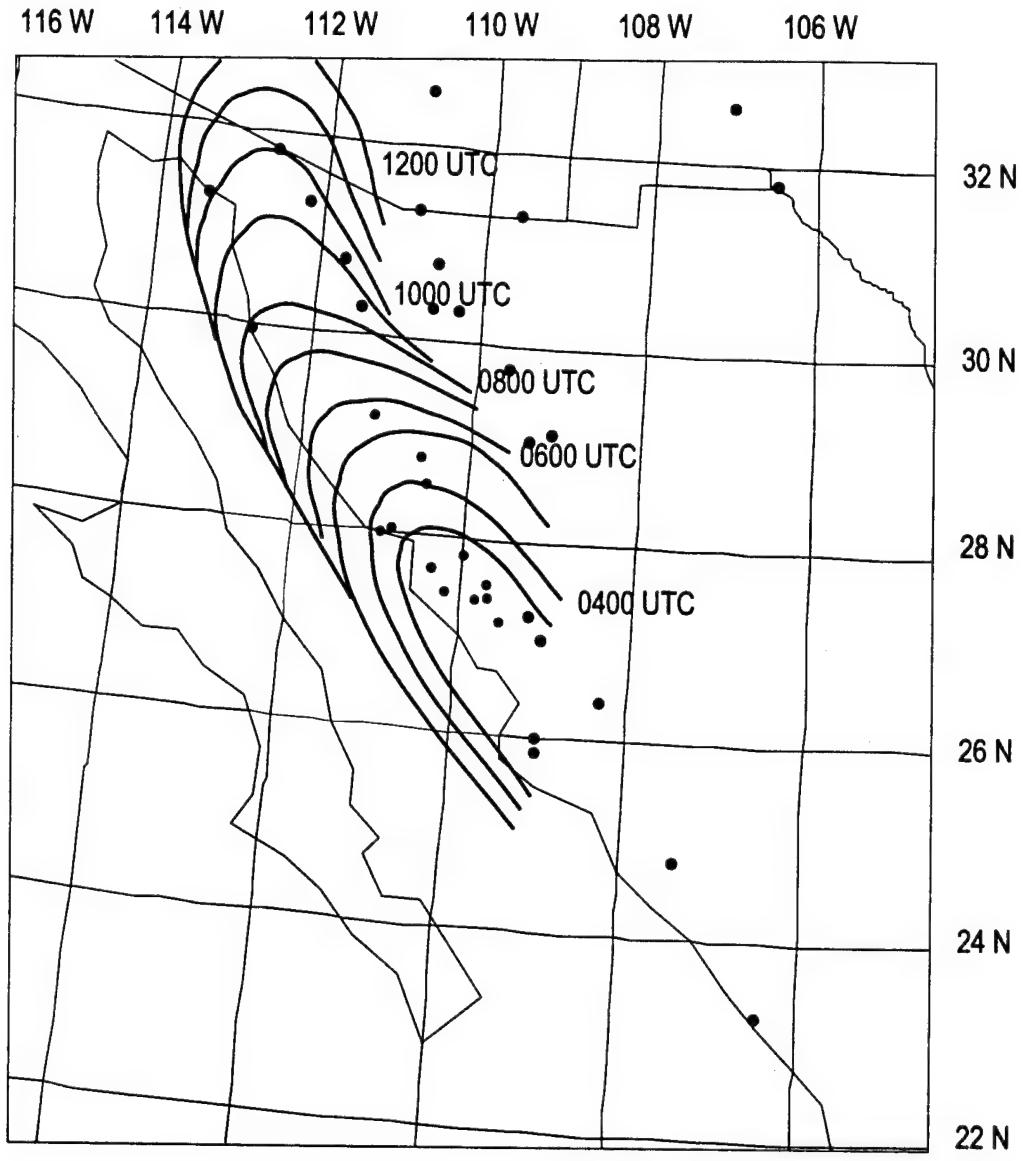

Figure 31) Isochrone analysis of leading edge of model surge on 12 August.

CHAPTER 7

Surge Mechanisms

Before an evaluation of the model data can be made to determine the characteristic of the surge, it is important to briefly review several types of wave and current phenomena that can be observed in the regional environment of the Gulf of California. Two specific wave phenomena that are not discussed are orographically trapped Rossby and shelf waves. While each of these may contribute to the Mexican monsoon, their propagation speeds are much slower than observed or modeled gulf surge events. Mechanisms of particular interest are Kelvin waves, density currents, bores, and ageostrophic downgradient flow.

7.1 Kelvin waves

The Gulf of California and the adjacent eastern shore are bounded by the high terrain of the Sierra Madre Occidental to the east. Since the typical monsoon flow is from the south or southeast, the higher terrain to the east of this Northern Hemispheric flow provides a boundary that can serve to trap Kelvin waves and allow them to propagate up the gulf. The warmer elevated residual layer that develops over the higher terrain in the afternoon and advects over the relatively cooler low-level morning temperatures of the eastern gulf coastline forms an inversion that serves as a waveguide for Kelvin waves. Once this waveguide is formed, southerly to southeasterly flow that moves through the gulf can be trapped by the mountains to the east of the flow due to the Coriolis force. Provided that a stable layer is maintained

throughout the day due to low-level cold advection or low-level cloud cover that diminishes typical solar heating, a Kelvin wave may continue to propagate up the gulf.

For the case of a linear, non-dispersive Kelvin wave, all of the flow within a Rossby radius of deformation is along the boundary with the Coriolis acting toward the higher terrain being balanced by the pressure gradient force acting toward lower terrain (Gill 1982). The wave speed of a linear, non-dispersive Kelvin wave in a stratified medium is

$$c = (g' H)^{1/2}$$

where g' is the reduced gravity, and H is the undisturbed depth of the moving fluid. Following the procedure of Reason and Steyn (1992), the reduced gravity is found by using the equation

$$g' = g \ (\theta_2 - \theta_1) / \theta_2$$

where θ_2 and θ_1 are the average potential temperatures of the upper and lower layers. The width of the linear, non-dispersive Kelvin wave is equal to the internal Rossby radius of deformation,

$$R = (g' H)^{1/2} / f$$

where f is the Coriolis frequency.

While this represents the case of a linear, non-dispersive Kelvin wave, most naturally occurring waves are not linear and propagation will result in dispersion, steepening, and in the development of a shock wave. As discussed by Gill (1982) and Reason and Steyn (1992) the effect of dispersion may be diminished, or even balanced, by frictional effects which result in either a slow steepening or none at all. In these cases an atmospheric solitary Kelvin wave may persist as long as the waveguide is present. When the nonlinear effects of steepening are balanced by the dispersive effects (Reason and Steyn 1992) then a solitary Kelvin wave is formed and will propagate at a speed of

$$c = [g' H (1 + \alpha)]^{1/2}$$

where α is the ratio of the amplitude of the solitary wave to the depth of the inversion layer. As described by Reason and Steyn, this type of wave can only develop if the dispersive effect of the along-shore mean flows are sufficient to balance the nonlinear steepening of the wave.

The propagation speed of a Kelvin wave in which the dispersive effects have resulted in the formation of a shock wave is

$$c = 1.45 (g' Hu)^{1/2}$$

where Hu is the fluid depth upstream of the shock (Reason and Steyn).

In order to examine the observed and model flow and determine whether a Kelvin wave is present it is important to note some of the characteristics these waves

in addition to their wave speeds. As described previously Kelvin wave move with higher terrain to the right in the Northern Hemisphere and with geostrophic flow behind the wave. The width of the wave is equal to the internal Rossby radius of deformation with the magnitude of the wave exponentially decaying away from the higher terrain. The wave propagates faster than the wind speeds behind the leading edge of the wave. The inversion that acts as a waveguide is higher behind the wave and the surface pressures will rise with the passage of the wave.

7.2 Density currents

Density currents occur as the boundary between a dense fluid and a less dense fluid moves toward the less dense fluid due to the contrast in the pressure gradient force between the two fluids, and the higher hydrostatic pressure associated with the dense fluid (Bluestein 1993). The boundary moves almost as a material surface as it advects the denser air into the region of less dense air. The speed of a density current is a function of the height of the dense air, the difference in pressure between the fluids and the speed of the less dense fluid. A simplified equation for the motion speed of a density current (Bluestein 1993) is

$$c = K[gH\frac{(\theta_{vw} - \theta_{vc})}{\theta_{vc}}]^{1/2} + 0.62u$$

In this formulation, K is typically 0.7 to 1.0 owing to the affects of friction and leads to some uncertainty in determining the precise speed of a density current, g is the Earth's gravitational constant, H is the height of the density current, θ_{vw} and θ_{vc} are the virtual potential temperatures of the warm and cold air, respectively, and u is the component

of the velocity of the air ahead of the dense fluid moving in the direction of the density current.

Density currents are frequently associated with thunderstorm outflows and have both a head and a wake associated with them as the dense air recirculates due to friction. Because of this recirculation pattern, the strongest wind speeds in the direction of movement will be immediately just above the ground and immediately behind the nose of the surge. Above the nose, the denser air will recirculate back behind the leading edge, move through the head, and into the wake region behind the density current (Goff 1976). As the density current moves and advects cooler air the pressures behind the leading edge will rise and the inversion layer will deepen.

7.3 Bores

A bore is a quasi-two-dimensional, propagating, step-like disturbance and is characterized by a sustained increase in the height of the streamlines and/or isentropes (Shreffer and Binkowski 1981; Clarke et al. 1981; Smith and Morton 1984; Fulton 1987). Bores are typically found in the boundary layer and only form under regions of high static stability. In contrast to a density current that indicates an almost material surface being forced ahead by the air behind it, a bore propagates through the air ahead of it.

Observational indicators of the passage of a bore are a sharp pressure rise, a wind shift, and surge in the direction of the bore. After the passage of a bore the elevated surface pressures stop rising and no cooling occurs. In contrast to a

density current, a temperature fall does not accompany a bore and the winds behind the bore are slower than the propagating bore.

7.4 Ageostrophic Downgradient Flow

Synoptic forcing that causes the development of a pressure gradient force parallel to higher terrain can cause ageostrophic downgradient flow (Overland 1984; Mass and Albright 1987; Overland and Bond 1993; Colle and Mass 1995). During ageostrophic downgradient flow, the pressure gradient force acts parallel to the barrier and accelerates the flow when friction is neglected. The only contribution of the pressure gradient normal to the barrier is that which balances the effect of the Coriolis force. A scale analysis by Overland and Bond (1993) shows that when the ratio of the cross-barrier length scale to the along-barrier length scale is small, and the Rossby number is approximately equal to or greater than one, then ageostrophic downgradient flow can occur. Ageostrophic downgradient flow has been associated with cold surges in the Himalayas (Nakamura and Murakami 1983), cold-air damming along the Appalachians (Bell and Bosart 1988), and cold surges along the Rocky Mountains (Colle and Mass 1995). For this mechanism, the alongshore flow is predominantly ageostrophic.

CHAPTER 8

Evaluation of Mesoscale Model Surge

Common gulf surge characteristics as defined by Hales (1972) and Brenner (1974) are an increase in southerly flow, decrease in temperature and increase in moisture near the surface. Surges also are related to increased thunderstorm activity in Arizona after the passage of a gulf surge (Hales 1974). Neither model simulation was run into the afternoon following each surge event surge to determine if afternoon convection formed in Arizona, but both of the simulations indicate a wind shift, moistening and slight cooling in the northern gulf. Further evaluation was performed in order to determine the mechanisms that contributed to these conditions in the northern gulf. It is important to note that the evaluation of the model surge is not meant to precisely explain the observed surge. In both cases MM5 produced surges that at best mimic the observations and at worst do not agree with the observed surge propagation speed. Nonetheless, by understanding the how MM5 develops these surges, it is hoped that future work can be done to more accurately model and observe them.

8.1 8 July 1993

On this day there is one observed surge and two model surges. The observed surge moves northwestward at 30 ms-1. The model surges move at speeds ranging from 10.3 to 15.1 ms-1. Although the surface observations do not provide enough information to accurately assess the actual type of surge mechanism, the model data do allow the determination of surge mechanisms.

The southern model surge develops in the southern gulf at 0300 UTC 8 July. Persistent heavy afternoon model convection approximately 150 km to the east of Los Mochis causes the development of a mesohigh and resulting outflow that initiates the surge. The surge is able to propagate up the gulf due to the well-defined inversion over coastal region at this time. While the surge moves up the gulf at 11.9 ms-1, the wind speed directly behind the leading edge of the surge are 10-15 ms-1 such that advection can replace the warmer fluid with a cooler one.

Using horizontal plots (figures 27 and 27), a cross-section along the surge (figure 30), a cross-section normal to the surge (figure 34), and a sounding ahead of the surge (figure 35) calculations are made to compare the southern model surge at 0900 UTC with various types of surge mechanisms. Since the model data indicate the southern model surge develops in response to strong convection and continues to propagate ahead of the convection, it is reasonable to consider the case of a density current. The depth of the southern model surge is 900 m and the specific gravity is 0.081 m s-2 yielding a density current relative speed of 8.5 ms-1. Accounting for the background wind speed component, the calculated speed of a density current is 13.5 ms-1 and is slightly greater than the 11.9 ms-1 speed indicated from the isochrone analysis (figure 29). The small difference in speeds can be attributed to estimation error. While this does not actually prove the southern model surge is a density current, conceptually the southern model surge is moving like a density current, with the strongest wind speeds behind the leading edge and stronger than the speed of the leading edge. Further analysis of the southern model surge indicates that the movement of the surge is not consistent with that of a Kelvin wave or a Bore, and the

synoptic scale pressures and temperatures along the gulf do not indicate conditions associated with ageostrophic downgradient flow.

A similar analysis is performed on the northern model surge at 0900 UTC 8 July (figures 36-38). In contrast to the southern model surge on 8 July, this surge develops significantly to the northwest of any model convection and organizes in conjunction with a zone of higher sea level pressures over the waters of the northeastern Gulf of California. The characteristics of this surge do not agree with that of a density current in that the winds behind the surge are slower than the propagation speed of the leading edge and only slightly cooler air is evident behind the surge. Neither does a bore phenomena explain the surge as surface pressures continue to rise after the passage of the surge. An examination of the low-level ageostrophic winds (figure 42) indicates the surge is moving normal to the direction of the ageostrophic flow and that the winds behind the surge are largely geostrophic normal to the terrain gradient. This indicates that the flow is not ageostrophic downgradient flow. A calculation of the speed of a linear Kelvin wave of the northern model surge with a depth of 850 m and a reduced gravity of 0.29 yields a theoretical speed of 15.8 ms-1 that agrees with the northern model surge speed of 15.1 ms-1. Solitary and shock Kelvin wave calculations result in higher theoretical speeds and do not agree with the speed of the model surge. While this does not clearly indicate that the model surge in the northern gulf is a linear Kelvin wave, the data do confirm that the surge is not a density current, a bore, or ageostrophic downgradient flow and that the behavior of the model surge is consistent with that of a Kelvin wave.

While the EMVER-93 and SWAMP-93 special observations do not permit the accurate computation of the speed of a density current or Kelvin wave given the lack

of data, MM5 provides a basis for estimating the type of wave involved. In the July case, the southern MM5 surge behaves as a density current. Cross-sections of the surge (figures 33 and 34) indicate the strongest winds are behind the surge and serve to advect cooler air to the northwest. The northern MM5 surge behaves much like a solitary Kelvin wave and the speed of the surge is actually greater than the winds immediately behind it. This indicates the surge is not advecting, but is propagating to the north. In this case, terming the boundary as a surge is somewhat erroneous since a surge by definition advects cooler and moister air. Despite this, the overall effect of the Kelvin wave is to turn the winds to the southeast, resulting in the advection of a cooler and moister air mass. In this manner, a Kelvin wave does fit the description of a surge in the sense that advection can follow its passage.

The 8 July observations indicate that a surge develops and progresses up the gulf at a speed of 30 ms-1. Provided the overall atmospheric conditions are similar to that of the model simulation, only solitary Kelvin waves and shock Kelvin waves can account for such high speed flow. This leads to the result that while the model is able to develop surges in this case, the resulting model surges move much more slowly than observed and are likely due to slightly different mechanisms. It is important to note that while the 8 July observations clearly describe one model surge, several stations hint at the possibility of two separate surges that develop near 1200 UTC in the central and southern gulf. A rough analysis using this two surge hypothesis gives a much slower surge speed of 20 ms-1 in the northern gulf that is closer to the northern model surge speed. Although this conclusion is speculative, it highlights the usefulness of high resolution models in determining the observational strategies for sampling coastally trapped phenomena in the future.

8.2 13 August 1993

MM5 only developed one surge in the August case that moves to the northwest at 16.7 ms-1 from 0300 UTC through 0600 UTC. After 0600 UTC the model surge accelerates to 20.0 ms-1 and its direction becomes more northward. As in the July case, horizontal plots (figures 30 and 31), a cross-sections along the surge (figure 39), a cross-section normal to the surge (figure 40) and a sounding ahead of the surge (figure 41) at 0900 UTC are used to dissect the model surge flow and determine a mechanism.

The behavior of this surge does not resemble a density current in that the winds behind the leading edge of the surge are too weak to advect the surge. Despite this, given the convection in the southern gulf it seems reasonable to examine whether or not the speed of the model surge corresponds with that of a density current. Computation of the speed of a density current a with a depth of 800 m and a reduced gravity of 0.081 m s-2 and a relative speed of 8.1 ms-1. The flow ahead of the surge is only about 2 ms-1 yielding a theoretical density current speed of 10.1 ms-1 that is much slower than the model surge speed of 20.0 ms-1. For this event the model surge is not a density current.

From an examination of the low-level ageostrophic winds and terrain (figure 43), it again appears that the ageostrophic winds are along the terrain gradient and normal to the surge movement such that the phenomenon is not ageostrophic downgradient flow. Furthermore, the surface pressures behind the MM5 surge leading edge continue to rise indicating the surge is not a bore. The remaining

mechanisms are the various forms of Kelvin waves. Ahead of the surge the depth of the inversion is 700 m with a reduced gravity of 0.23 m s-2 (figure 41). The theoretical speed of a linear Kelvin wave is 12.7 ms-1, too slow to account for the model surge speed. The speed of a solitary Kelvin wave is 17.9 ms-1, and the speed of a shock Kelvin wave is 18.3 ms-1 in agreement with the model surge speed of 16.7-20.0 ms-1.

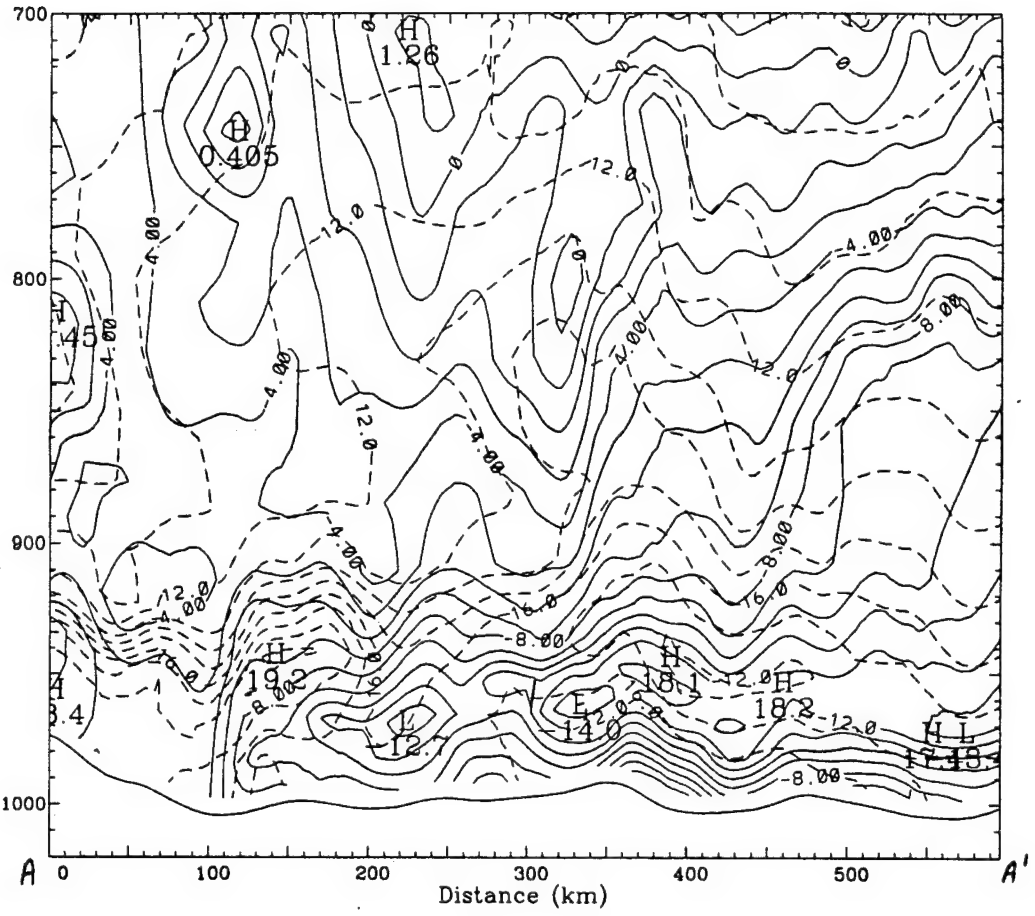

Figure 33) 0900 UTC 8 July MM5 nested grid cross-section along the central southern Gulf of California (location of cross-section shown as A-A' on figure 27c). Vertical coordinate is pressure (mb). Solid contours are wind speeds parallel to the coast (ms-1) with positive values from left to right (northwesterly). Dashed contours are mixing ratios (g kg-1).

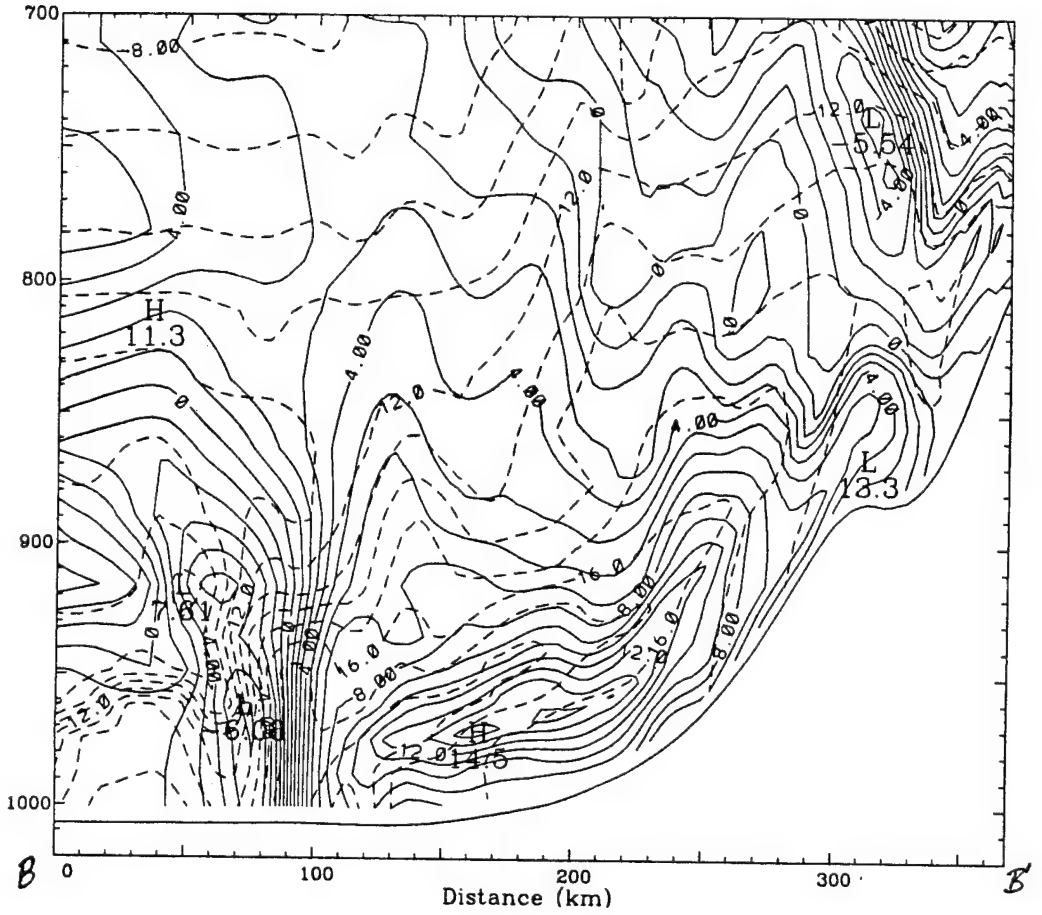

Figure 34) 0900 UTC 8 July MM5 nested grid cross-section perpendicular to the central Gulf of California (location of cross-section shown as B-B' on figure 27c). Vertical coordinate is pressure (mb). Solid contours are wind speeds parallel to the coast (ms-1) with positive values into the figure (southeasterly). Dashed contours are mixing ratios (g kg-1).

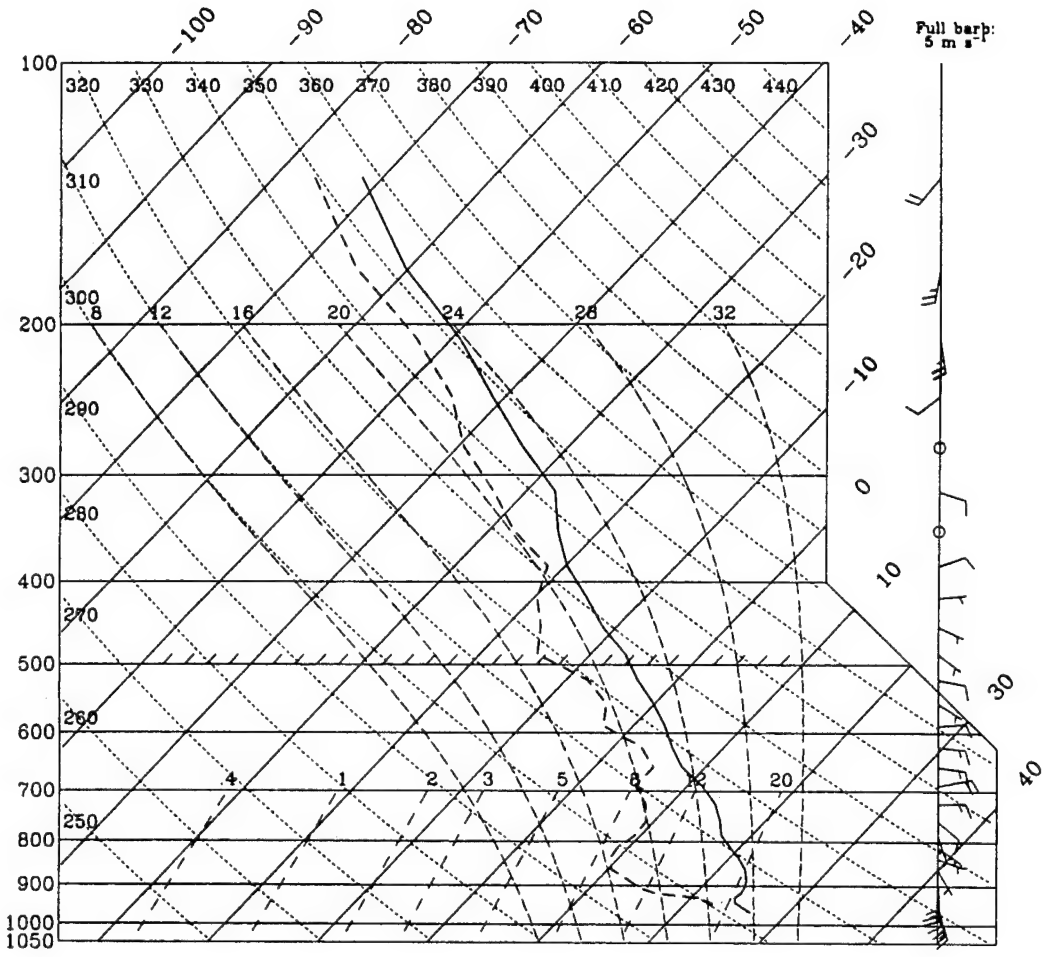

Figure 35) 0900 UTC 8 July MM5 nested grid sounding northwest of the southern mesoscale model surge (location of sounding shown as C on figure 27c). Full barb is 5 ms-1.

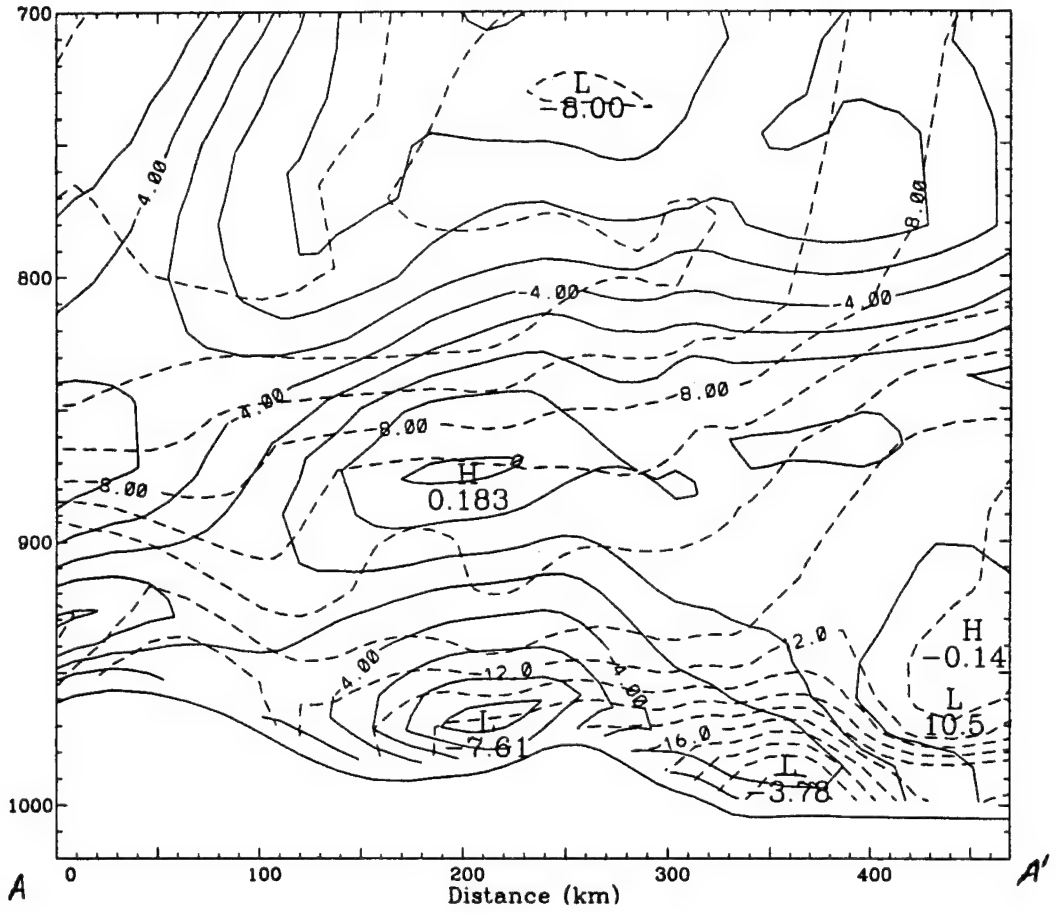

Figure 36) 0900 UTC 8 July MM5 coarse grid cross-section along the northern and central Gulf of California (location of cross-section shown as A-A' on figure 28c). Vertical coordinate is pressure (mb). Solid contours are wind speeds parallel to the coast (ms-1) with positive values from left to right (northwesterly). Dashed contours are mixing ratios (g kg-1).

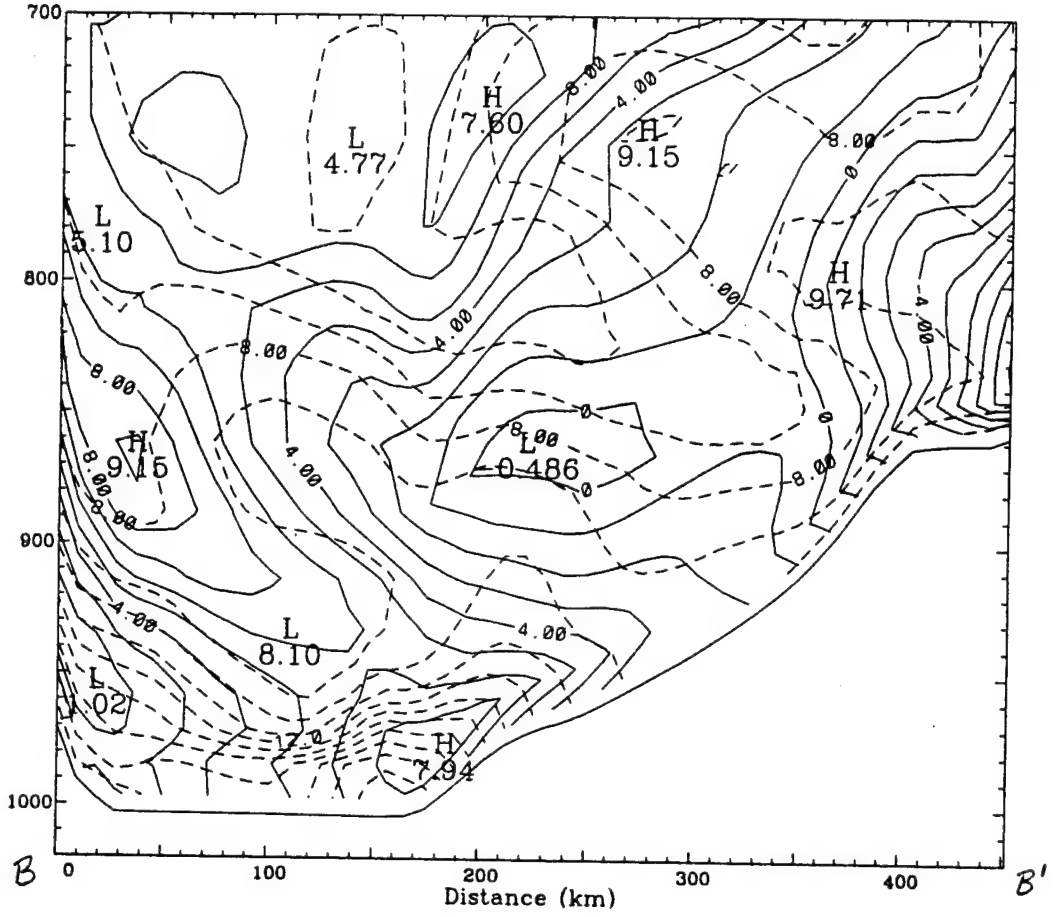

Figure 37) 0900 UTC 8 July MM5 coarse grid cross-section perpendicular to the northern Gulf of California (location of cross-section shown as B-B' on figure 28c). Vertical coordinate is pressure (mb). Solid contours are wind speeds parallel to the coast (ms-1) with positive values into the figure (southeasterly). Dashed contours are mixing ratios (g kg-1).

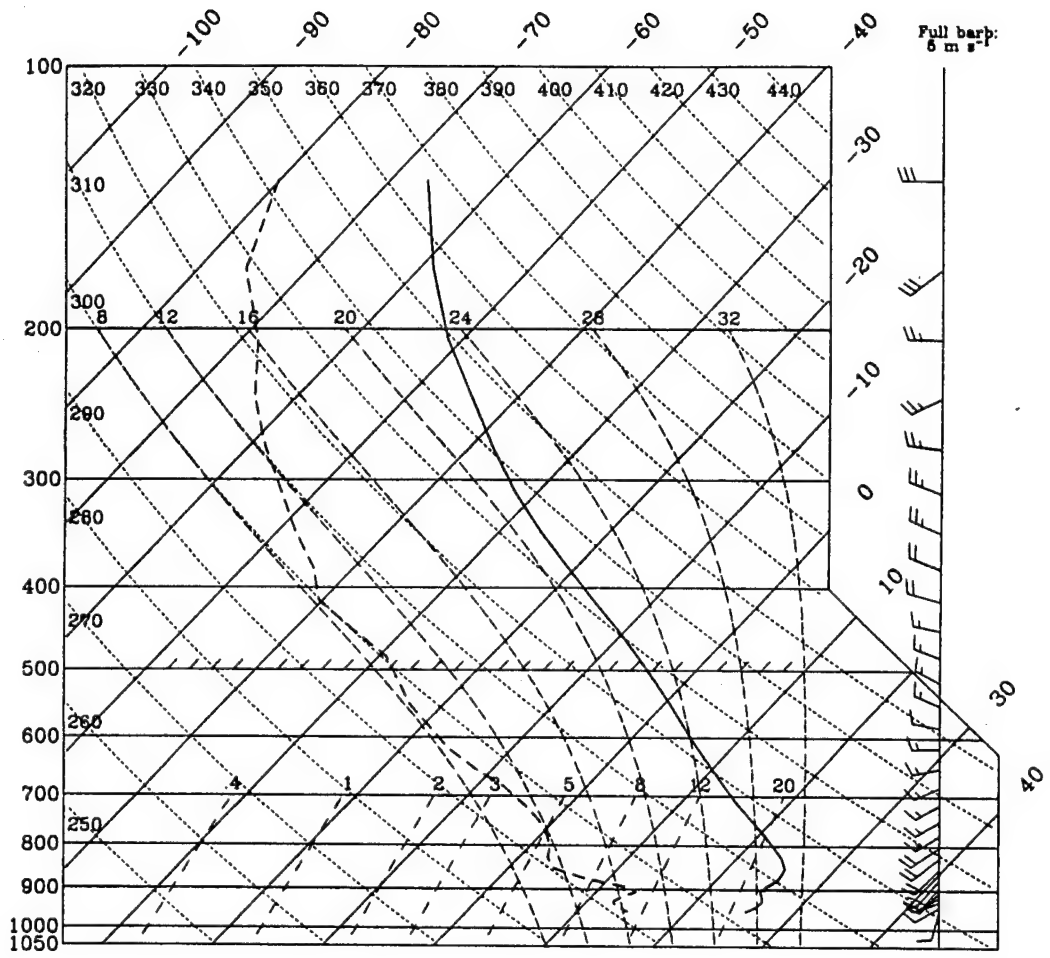

Figure 38) 0900 UTC 8 July MM5 coarse grid sounding northwest of the northern mesoscale model surge (location of sounding shown as C on figure 28c). Full barb is 5 ms-1.

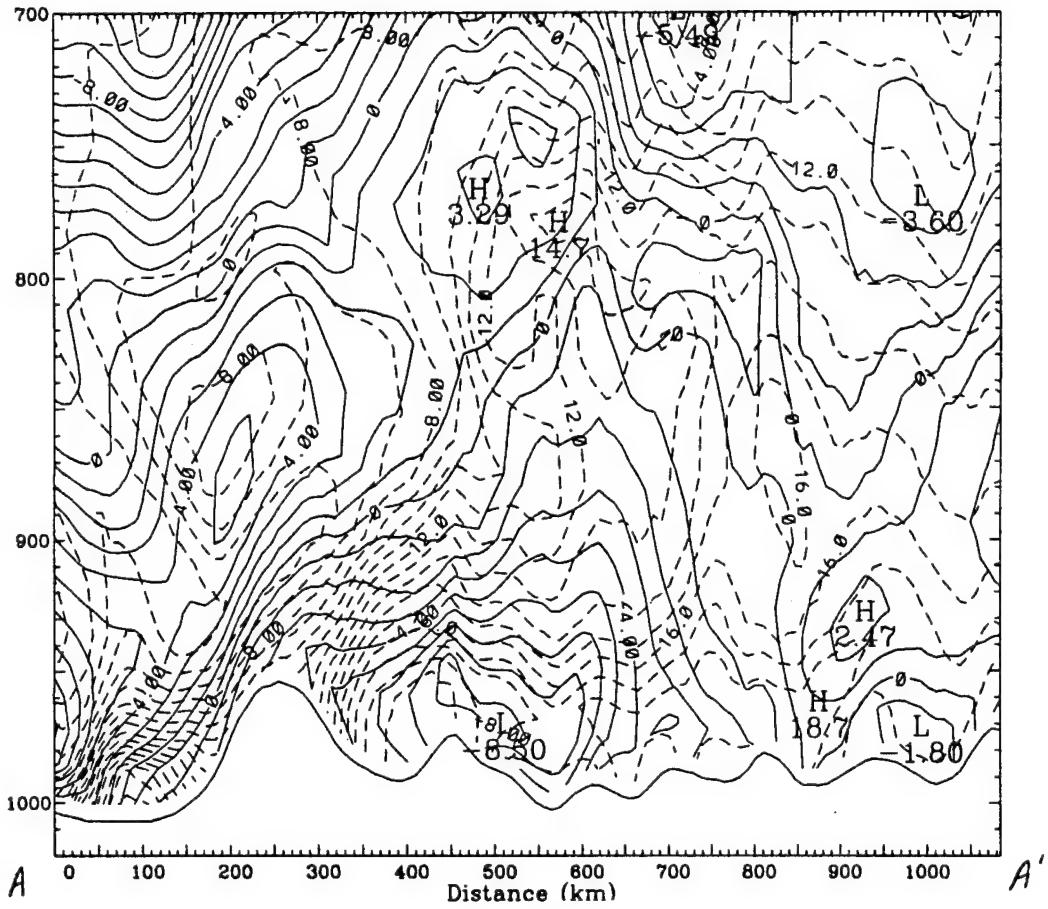

Figure 39) 0900 UTC 12 August MM5 cross-section along the northern and central Gulf of California (location of cross-section shown on figure 31c). Vertical coordinate is pressure (mb). Solid contours are wind speeds parallel to the coast (ms-1) with positive values from left to right (northwesterly). Dashed contours are mixing ratios (g kg-1).

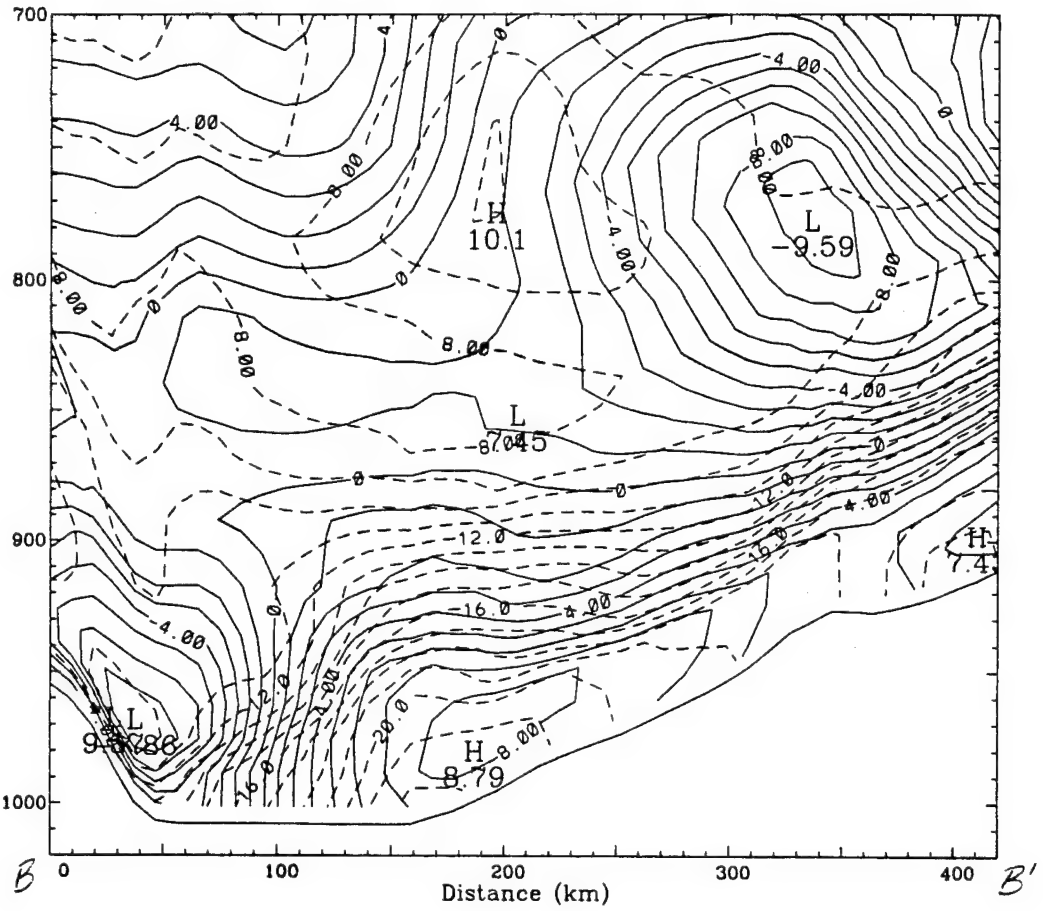

Figure 40) 0900 UTC 12 August MM5 cross-section perpendicular to the northern Gulf of California (location of cross-section shown on figure 31c). Solid contours are wind speeds parallel to the coast (ms-1) with positive values into the figure (southeasterly). Dashed contours are mixing ratios (g kg-1).

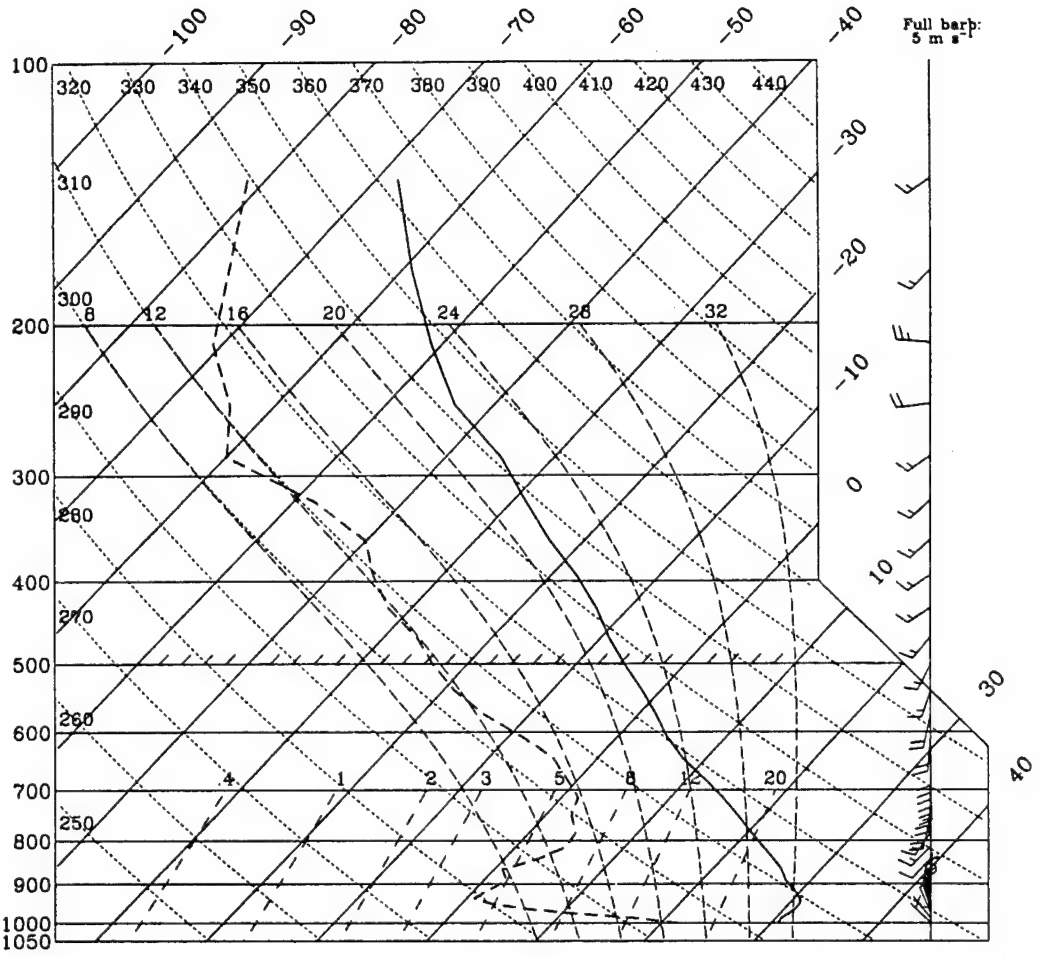

Figure 41) 0900 UTC 12 August MM5 sounding northwest of the mesoscale model surge (location of sounding shown on figure 31c). Full barb is 5 ms-1.

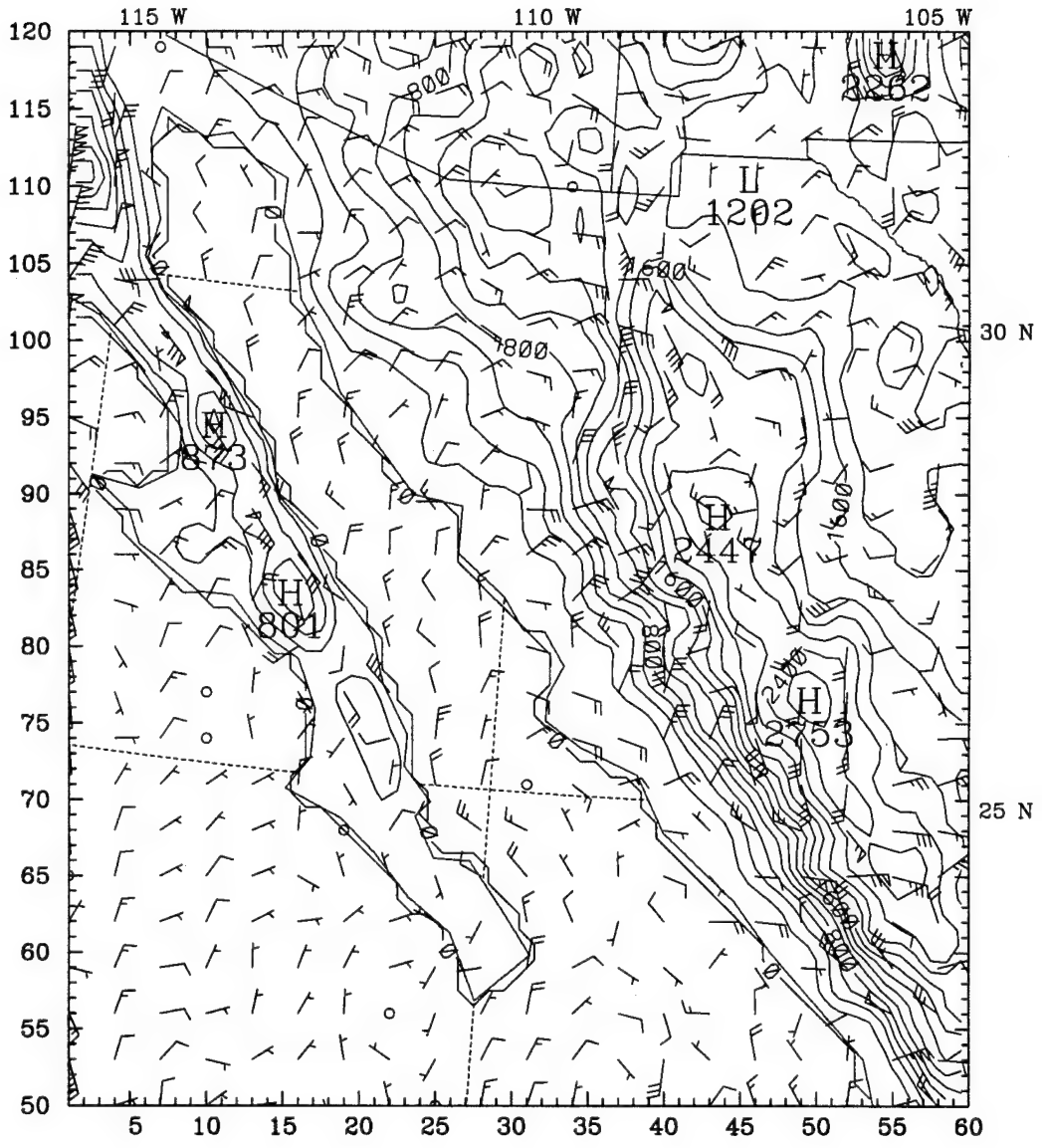

Figure 42) 0900 UTC 8 July MM5 coarse grid terrain contoured every 200 m and 970 mb ageostrophic winds. Full barb is 5 ms-1.

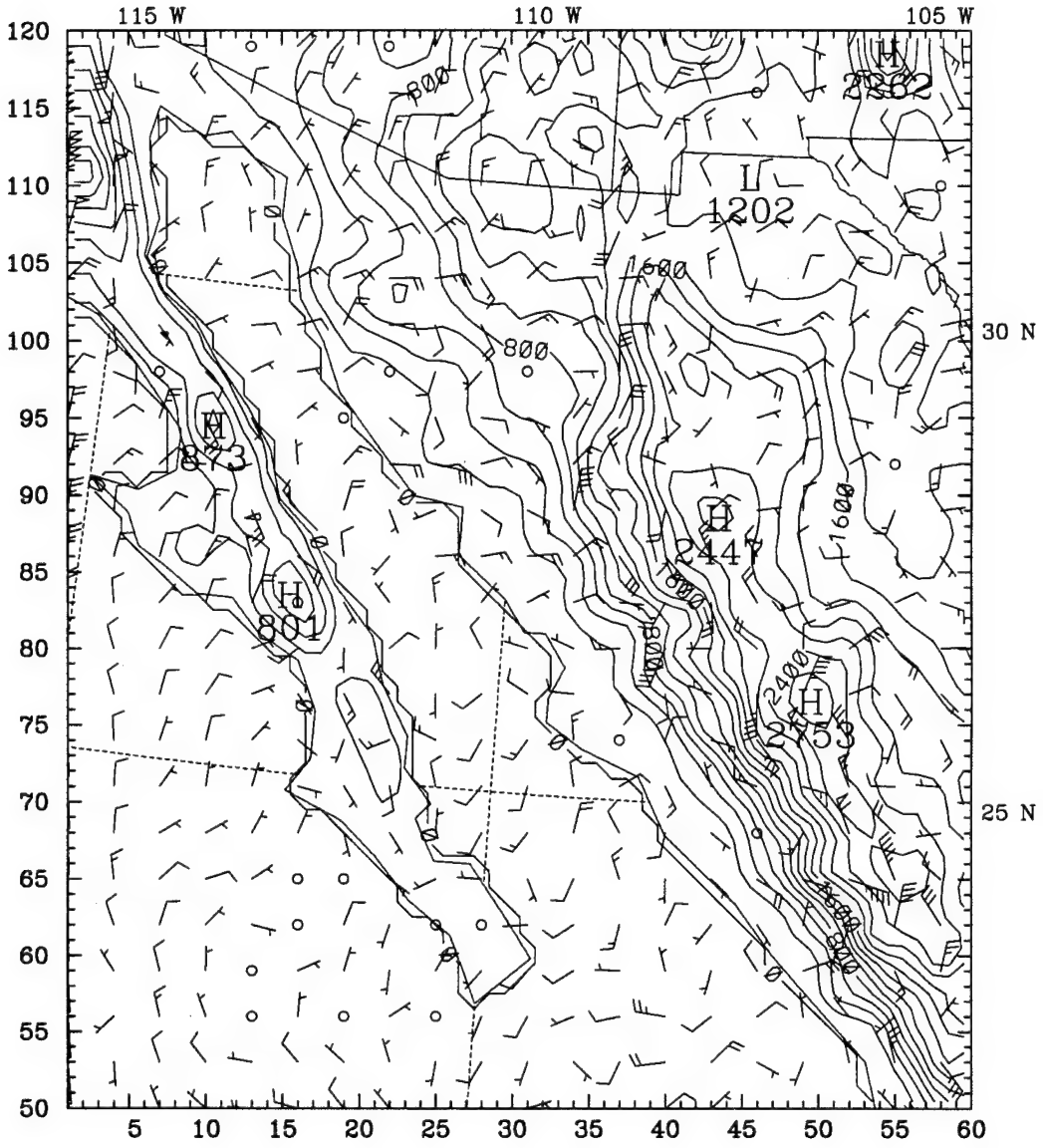

Figure 43) 0900 UTC 12 August MM5 terrain contoured every 200 m and 970 mb ageostrophic winds. Full barb is 5 ms-1.

CHAPTER 9

Summary

MM5 is used to simulate two gulf surge events that occurred during EMVER-93. The model is able to generate the strong southeast and southerly flow associated with each observed surge, and the model successfully advects moisture to the northern Gulf of California. Although the observational data was limited, the data that was obtained matched fairly well with the model results.

The model data from each simulation indicates the presence of Kelvin waves that propagate up the gulf. In the July case both a density current and a Kelvin wave move up the gulf during the morning of the observed surge. While observations are not sufficient to describe a surge mechanism, given the known conditions, and the model conditions throughout the region, it is reasonable to presume that the observed July surge is a solitary or shock Kelvin wave. For the August case, the model develops a Kelvin wave on the morning of the 12 August, 24 hours before the observed surge. For each case evidence supports the argument that surges develop in response to northward or northwestward propagating Kelvin waves that turn the low-level winds to the southeast and allow slightly cooler and much moister air from the gulf to advect northward. Additionally, the conditions in the gulf region must be stable enough to be allow the propagation of Kelvin waves. This agrees with the general proposal of the conceptual model of Stensrud et al. (1996).

A possible deficiency in this model simulation is that the Kain-Fritsch convective parameterization scheme used in this version of MM5 may be too

sensitive, generating more precipitation than can be accounted for in satellite imagery and observations. Although the inaccuracies in the initial conditions may have been the cause, further evaluation would be beneficial. The evolution of convection over western Mexico is particularly important to the forecasting of thunderstorms in the southwest United States since convection in the gulf can lead to the development of gulf surges as seen in the model simulations.

The operational ETA model has significant difficulty in predicting southeasterly or even southerly flow in the gulf for either of these two cases. During each simulation, the ETA model causes southwesterly to westerly flow over southern Arizona and does not even hint at the development of a surge. This strongly suggests that a new convective parameterization scheme is needed within the ETA model.

The conceptual model of Stensrud et al. (1996) also does not successfully predict either of these surge events. This indicates that surges can be produced via many routes, some of which were not seen during the 1990 monsoon season used by Stensrud et al. (1996). The complexity of the surges produced by the mesoscale model suggests that no simple conceptual model will work for all events. The only hope for forecasters trying to predict these events is in denser observations throughout the gulf and in the development of a robust operational model that incorporates all of the available Mexican and gulf data and uses a convective parameterization scheme known to be capable of reproducing at least the general evolution of deep convection associated with the monsoon.

The contributions of EMVER-93 and SWAMP-93 were crucial to this study, and it is hoped that continued work will be done to observe the characteristics associated

with gulf surges. Although the available observations agree fairly well with the model results in these two studied cases, there were insufficient observations to either determine surge mechanisms, or to precisely follow the actual movement of the gulf surge up the coast.

Bibliography

Adang, Thomas C., and Robert L. Gall, 1989: Structure and dynamics of the Arizona monsoon boundary. *Mon. Wea. Rev.,* **117,** 1423-1438.

Anthes, R. A. and T. T. Warner, 1978: Development of hydrodynamic models suitable for air pollution and other mesometeorological studies. *Mon. Wea. Rev.,* **106,** 1045-1078.

Anthes, R. A., E.-Y. Hsie, and Y.-H. Kuo, 1987: Description of the Penn State / NCAR mesoscale model version 4 (MM4). NCAR Tech. Note NCAR / TN-282+STR, 66 pp.

Bell, G. D. and L. F. Bosart, 1988: Appalachian cold air damming. *Mon. Wea. Rev.,* **116,** 137-161

Benjamin, S. G., and N. L. Seaman, 1985: A simple scheme for improved objective analysis in curved flow. *Mon. Wea. Rev.,* **113,** 1184-1198.

Bluestein, Howard B., 1993: *Synoptic-dynamic meteorology in midlatitudes, Volume II: Observations and theory of weather systems.* Oxford University Press, 594 pp.

Brenner, I.S., 1974: A surge of maritime tropical air - Gulf of California to the southwestern United States. *Mon. Wea. Rev.,* **102,** 375-389.

Bryson, R. A., and W. P. Lowry, 1955: Synoptic Climatology of the Arizona summer precipitation singularity. *Bull. Amer. Meteor. Soc.,* **36,** 329-339.

Carleton, Andrew M., 1986: Synoptic-dynamic character of "bursts" and "breaks" in the southwest U.S. summer precipitation singularity. *J. Climatol.,* **6,** 999-1014.

Carleton, Andrew M., Duane A. Carpenter, and Paul J. Weser, 1990: Mechanisms of interannual variability of the southwest United States summer rainfall maximum. *J. Climate,* **3,** 999-1015.

Colle, Brian A., and Clifford F. Mass, 1995: The structure and evolution of cold surges east of the Rocky Mountains. *Mon. Wea. Rev.,* **123,** 2577-2610.

Douglas, Michael W., 1993: Current research into the monsoon. *Sonorensis, Arizona Sonora Desert Museum Newsletter,* **13,** Num. 3,10-11

Douglas, Michael W., 1995: The summertime low-level jet over the Gulf of California. *Mon. Wea. Rev.,* **123,** 2334-2347.

Douglas, Michael W., Robert A. Maddox, Kenneth Howard and Sergio Reyes, 1993: The Mexican monsoon. *J. Climate,* **6,** 1665-1677.

Dudhia, Jimy, 1989: Numerical study of convection observed during the winter monsoon experiment using a mesoscale two-dimensional model. *J. Atmos. Sci.,* **46,** 3077-3107.

Dudhia, Jimy, 1993: A non-hydrostatic version of the Penn State-NCAR mesoscale model: validation tests and simulation of an Atlantic cyclone and cold front. *Mon. Wea. Rev.*, **121,** 1493-1513.

Dunn, Lawrence B. and John D. Horel, 1994a: Prediction of central Arizona convection, Part I: Evaluation of the NGM and ETA model precipitation forecasts. *Wea. and Forecasting,* **9,** 495-507.

Dunn, Lawrence B. and John D. Horel, 1994b: Prediction of central Arizona convection, Part II: Further examination of the ETA model. *Wea. and Forecasting,* **9,** 508-521.

Fritsch, J. M. and C. F. Chappell, 1980: Numerical prediction of convectively driven mesoscale pressure systems. Part I: Convective parameterization. *J. Atmos. Sci.,* **37,** 1722-1733.

Fulton, Richard, 1987: Observations of the interactions of a nocturnal thunderstorm outflow with a stable environment. M.S. Thesis, University of Oklahoma, 147 pp.

Gayno, George A., 1994: Development of a high-order, fog-producing boundary layer model suitable for use in numerical weather prediction. M.S. Thesis, Pennsylvania State University, 107 pp.

Gill, A. E., 1982: *Atmospheric-Ocean Dynamics.* International Geophysics Series, Vol. 30, Academic Press, 662 pp.

Goff, R. C., 1975: Vertical structure of thunderstorm outflows. *Mon. Wea. Rev.,* **104,** 1429-1440.

Grell, G. A., J. Dudhia and D. R. Stauffer, 1994: A description of the fifth-generation Penn State / NCAR mesoscale model (MM5). NCAR Technical Note, NCAR / TN-398+STR, 138 pp.

Guo, Y.-R., and S. Chen, 1994: Terrain and land use for the fifth-generation Penn State / NCAR mesoscale modeling system (MM5). NCAR Technical Note, NCAR / TN-397+IA, 114 pp.

Haagenson, P.L., J. Dudhia, G. A. Grell, and D. R. Stauffer, 1994: The Penn Sate / NCAR mesoscale model analysis for the Penn State / NCAR modeling system: Program DATAGRID and RAWINS. NCAR Technical Note, NCAR / TN-376+IA, 209 pp.

Hales, John E., 1972: Surges of maritime tropical air northward over the Gulf of California. *Mon. Wea. Rev.,* **100,** 298-306.

Hales, John E., 1974: Southwestern United States summer monsoon source - Gulf of Mexico or Pacific Ocean. *J. Applied Meteor.,* **13,** 331-342.

Janjic, Z. I., 1990: The step-mountain coordinate: Physical package. *Mon. Wea. Rev.,* **118,** 1429-1443.

Jurwitz, Louis R., 1953: Arizona's Two-Season Rainfall Pattern. *Weatherwise,* **6,** 96-99.

Maddox, Robert A., Darren M. McCullom, and Kenneth W. Howard, 1995: Large-scale patterns associated with severe summertime thunderstorms over central Arizona. *Wea. and Forecasting,* **10,** 763-778.

Mass, C. F., and M. D. Albright, 1987: Coastal southerlies and alongshore surges of the west coast of North America: Evidence of mesoscale topographically trapped response to synoptic forcing. *Mon. Wea. Rev.,* **115,** 1707-1738.

McCollum, Darren M., Robert A. Maddox and Kenneth W. Howard, 1995: Case study of a severe mesoscale convective system in central Arizona. *Wea. and. Forecasting,* **10,** 643-665.

Mesinger, F., Z. I. Janjic, S. Nickovic, D. Gavrilov, and D. G. Deaven, 1988: The step-mountain coordinate: Model description and performance for cases of alpine lee cyclogenesis and for a case of Appalachian redevelopment. *Mon. Wea. Rev.,* **116,** 1493-1518.

Moore, Thomas J., Robert L. Gall and Thomas C. Adang, 1989: Disturbances along the Arizona monsoon boundary. *Mon. Wea. Rev.,* **117,** 932-941.

Nakamura, H., and T. Murakami, 1983: Orographic effects on cold surges and lee-side cyclogenesis as revealed by a numerical experiment, Part II, transient aspects. *J. Meteor. Soc. Japan,* **61,** 547-567.

Overland, J. E., 1984: Scale analysis of marine winds in straits and along mountainous coasts. *Mon. Wea. Rev.,* **112,** 2532-2536.

Overland, J. E., and N. Bond, 1993: The influence of coastal orography: The Yakutat storm. *Mon. Wea. Rev.,* **121,** 1388-1397.

Rasmussen, Eugene M., 1967: Atmospheric water vapor transport and the water balance of North America: Part I. Characteristics of the water vapor flux field. *Mon. Wea. Rev.,* **95,** 403-426.

Reason, C. J. C. and D. G. Steyn, 1992: The dynamics of coastally trapped mesoscale ridges in the lower atmosphere. *J. Atmos. Sci.,* **49,** 1677-1692.

Ripa, P., and S.G. Marinone, 1989: Seasonal variability of temperature, salinity, velocity, vorticity, and seal level in the central Gulf of California, as inferred from historical data. *Quart. J. Roy. Meteor. Soc.,* **115,** 887-913.

Sellers, W. D., and R. H. Hill, 1974: *Arizona Climate. 1931-1972,* The University of Arizona Press, 616 pp.

Smith, Walter P. and Robert L. Gall, 1989: Tropical squall lines of the Arizona monsoon. *Mon. Wea. Rev.,* **117,** 1553-1569.

Stensrud, David J., Robert L. Gall, Steven L. Mullen, and Kenneth W. Howard, 1995: Model climatology of the Mexican monsoon. *J. Climate,* **8,** 1775-1794.

Stensrud, David J., Robert L. Gall, and Mel K. Nordquist, 1996: Surges over the Gulf of California during the Mexican monsoon. *Mon. Wea. Rev.,* in review.